Aston University

Some pages of this thesis may have been removed for copyright restrictions.

If you have discovered material in AURA which is unlawful e.g. breaches copyright, (either yours or that of a third party) or any other law, including but not limited to those relating to patent, trademark, confidentiality, data protection, obscenity, defamation, libel, then please read our Takedown Policy and contact the service immediately

VIBRATION ANALYSIS OF A PRINTED CIRCUIT BOARD

Geok Hian Lim

Doctor of Philosophy

Aston University

March 2000

This copy of the thesis has been supplied on condition that anyone who consults it is understood to recognise that its copyright rests with its author and that no quotation from the thesis and no information derived from it may be published without the author's prior, written consent.

ASTON UNIVERSITY

VIBRATION ANALYSIS OF A PRINTED CIRCUIT BOARD

Geok Hian Lim

Doctor of Philosophy March 2000

ABSTRACT

The reliability of the printed circuit board assembly under dynamic environments, such as those found onboard airplanes, ships and land vehicles is receiving more attention. This research analyses the dynamic characteristics of the printed circuit board (PCB) supported by edge retainers and plug-in connectors.

By modelling the wedge retainer and connector as providing simply supported boundary condition with appropriate rotational spring stiffnesses along their respective edges with the aid of finite element codes, accurate natural frequencies for the board against experimental natural frequencies are obtained. For a PCB supported by two opposite wedge retainers and a plug-in connector and with its remaining edge free of any restraint, it is found that these real supports behave somewhere between the simply supported and clamped boundary conditions and provide a percentage fixity of 39.5% more than the classical simply supported case.

By using an eigensensitivity method, the rotational stiffnesses representing the boundary supports of the PCB can be updated effectively and is capable of representing the dynamics of the PCB accurately. The result shows that the percentage error in the fundamental frequency of the PCB finite element model is substantially reduced from

22.3% to 1.3%. The procedure demonstrated the effectiveness of using only the vibration test frequencies as reference data when the mode shapes of the original untuned model are almost identical to the referenced modes/experimental data. When using only modal frequencies in model improvement, the analysis is very much simplified. Furthermore, the time taken to obtain the experimental data will be substantially reduced as the experimental mode shapes are not required.

In addition, this thesis advocates a relatively simple method in determining the support locations for maximising the fundamental frequency of vibrating structures. The technique is simple and does not require any optimisation or sequential search algorithm in the analysis. The key to the procedure is to position the necessary supports at positions so as to eliminate the lower modes from the original configuration. This is accomplished by introducing point supports along the nodal lines of the highest possible mode from the original configuration, so that all the other lower modes are eliminated by the introduction of the new or extra supports to the structure. It also proposes inspecting the average driving point residues along the nodal lines of vibrating plates to find the optimal locations of the supports. Numerical examples are provided to demonstrate its validity. By applying to the PCB supported on its three sides by two wedge retainers and a connector, it is found that a single point constraint that would yield maximum fundamental frequency is located at the mid-point of the nodal line, namely, node 39. This point support has the effect of increasing the structure's fundamental frequency from 68.4 Hz to 146.9 Hz, or 115% higher.

Key Words: Vibration; Modal Sensitivities; Printed Circuit Board; Finite Element; Edge Support; Point Support.

ACKNOWLEDGEMENTS

This thesis was written during the period while the author was employed as a Senior Lecturer, School of Mechanical and Production Engineering, Nanyang Technological University, Singapore. The author would like to express his sincere thanks to Dr. J.E.T. Penny, who was the project supervisor for his guidance, encouragement and support during this period of research.

The author would also like to take this opportunity to thank Assoc. Prof. Ong Jor Huat for his invaluable advice and support in making this research successful.

The author would also like to thank the Nanyang Technological University for allowing him to make use of the laboratory and computing facilities in conducting this research.

TABLE OF CONTENTS

LIST OF FIGURES

Chapter 5

Chapter 6

LIST OF TABLES

Chapter 6

NOMENCLATURE

$\{\ \}$ denotes a column vector

$[\ ]$ denotes a matrix

$[\ ]^T$ transposition of a matrix

$[\ ]^{-1}$ inverse of a matrix

$[M]$ mass matrix

$[K]$ stiffness matrix

$[L]$ lower triangular matrix

$[M_a]$ analytical mass matrix

$[K_a]$ analytical stiffness matrix

$[S]$ eigensensitivity matrix

λ_i ith eigenvalue

$\{\phi\}_i$ mass normalised eigenvector

$\{\phi_a\}_i$ ith eigenvector of analytical model

$\{\phi_e\}_i$ ith eigenvector of experimental model

$(\lambda_a)_i$ ith eigenvalue of analytical model

$(\lambda_e)_i$ ith eigenvalue of experimental model

$\{\Delta p\}$ vector representing the change in structural parameters

$\{\Delta\xi\}$ vector representing the change in eigenvalues/eigenvectors

a length of plate (mm)

b width of plate (mm)

c length of wedge retainer (mm)

h plate or beam thickness (mm)

D plate flexural rigidity

$$D = \frac{Eh^3}{12(1-\nu^2)} \text{(Nmm)}$$

E Young's modulus (N/mm^2)

c length of wedge guide (mm)

f frequency (Hz)

ω circular frequency (rad/s)

t time (s)

A cross-sectional area (mm^2)

G shear modulus (N/mm^2)

x,y plate spatial coordinates

I moment of inertia

ρ density of plate or beam (kg/mm^3)

ν Poisson's ratio

W transverse deflection of plate (mm)

λ^2 dimensionless frequency parameter

$$\lambda^2 = \omega \text{ a b } \sqrt{\rho h / D}$$

α rotational spring stiffness for wedge retainer (Nmm/rad)

β rotational spring stiffness for 96-pin plug-in connector (Nmm/rad)

R_1 rotational spring factor for wedge retainer (mm/rad)

R_2 rotational spring factor for connector (mm/rad)

CHAPTER 1

INTRODUCTION

1.1 OVERVIEW

In current engineering practice, the emphasis placed on reliability, performance and safety of structural systems are becoming more and more demanding due to the continuous challenges from real life operating and environmental conditions. Structural vibration problems nowadays present a major hazard and design limitation for a very wide range of engineering products. In the aircraft industry, for example, there are a number of components or assemblies on an aircraft, whose structural integrity is of paramount concern, and whose vibration directly affects performance, either by virtue of causing temporal malfunction under excessive motion or by creating discomfort, such as high intensity noise.

Increasingly, more electronic equipment are designed and built for use on board aircraft, ships and land vehicles. Since the purpose of an electronic system is to work electrically, it is logical that most of the time and money go into the electronic circuitry. However, shock and vibration have been found to be the major causes of electronic equipment failures. Markstein (1987) reported that shock and vibration failures in electronic equipment are second only to failures due to temperature. Therefore, unless the electronic assembly is designed for its dynamic environment, there can be problems occurring subsequently which may require an extensive amount of redesign.

Continuous vibration may lead to fatigue failure of the PCB as a result of cyclic stresses. Steinberg (1988) found that vibration induced failures include the cracking of solder joints, breaking of component leads, loosening of screws and damage to connectors. Failures of PCBs can be avoided by understanding the nature of vibration, i.e., evaluating the dynamic response characteristics and stress levels. This involves the determination of natural frequencies and displacements. Since the dynamic displacements and stresses can be evaluated from the natural frequencies, the determination of the natural frequencies of the PCB is of fundamental importance during the design stage.

1.2 ANALYTICAL MODELLING

Generally, for real life engineering structures, their dynamics can be described by partial differential equations of motion. Analytical solutions are readily available to these equations for simple structures such as beams, shafts, shells and plates. However, due to the complexity of most engineering structures, analytical solutions are often impossible to obtain (if they exist at all) and numerical approximations have to be pursued.

The requirement for a more generalised method of modelling dynamic characteristics of large and complicated structures with either homogenous or heterogeneous physical properties has brought about the development of finite element (FE) analysis. Due to the advances achieved in numerical methods and the advent of more powerful computers, FE analysis has become one of the most popular techniques in structural dynamics analysis.

1.2.1 FE Modelling

In FE analysis (Zienkiewicz and Taylor, 1989), a continuous structure such as a plate, a beam or a shell is divided into many 'small' elements (called 'finite elements'). Since an element has small geometrical size, its physical properties can be assumed to be homogenous over the whole element. Therefore, the mass, stiffness and possibly damping matrices of the element can be easily obtained based on the theory of dynamics (e.g., Newton's law, Lagrange's equation) and mechanics of deformable bodies (e.g., strain-displacement equations, stress-strain relations). The global mass, stiffness and possibly damping matrices of the structure can then be assembled using these element matrices by considering physical connectivities between elements and boundary conditions. Once a mathematical model (spatial model in terms of mass, stiffness and possibly damping matrices) has been established, the next step is to solve the differential equations of motion by using various numerical algorithms to obtain a description of the dynamic behaviour of the structure.

An analytical model established using FE analysis can be used to perform many types of structural analysis such as response and load prediction, stress and stability analysis, life time prediction, structural modification and optimisation, etc. As such, FE modelling is a very powerful tool for structural designs. With this tool, some deficiencies in the design of a structure can be identified at early design stages and modifications to improve design can be made accordingly and at much lower cost than in later stages.

1.2.2 Inaccuracies and uncertainties in FE Analysis

The FE analysis method has matured over the past three decades to an extent where design, meshing, analysis and post-processing are highly integrated and automated. However, in view of the ever increasing complexity of structural design nowadays, there is a need to know the limitations of the method as well as to examine critically the results obtained in applying FE analysis method to structural dynamics.

There are many potential uncertainties in FE analysis, which can be related to one of the following types: modelling uncertainties; physical properties uncertainties; analysis uncertainties; analysis mistakes.

Each FE must be described in terms of element type and formulation. Using alternative element types or formulations used will in general lead to different analysis results. Another uncertainty of this type is related to geometrical representation of structures and mesh density. Mesh distortion can lead to erroneous stiffness and mass terms. Low mesh density will mostly imply high degree of geometrical simplification and thus lead to inaccurate results. There should be a trade-off between mesh density and computer CPU time. Another uncertainty related to modelling is that the structure designed and dimensioned on a blueprint or sketch might differ from the structure that has been tested due to fabrication tolerances or errors.

After a model has been created, the analyst must define element properties like material constants, shell thickness, etc. Which properties must be defined depends on the element

type and on the material that is used. Physical element properties also include boundary conditions, spring stiffness and lumped mass properties. Uncertainties may arise from the choice of the physical properties of the structural materials used, the approximation of boundary conditions, the classical lumping of distributed parameters (whose solutions are never unique), and the inadequate modelling of structural joints and couplings (Friswell and Mottershead, 1995). In addition, many physical effects are not always correctly modelled, such as non-linear effects, damping, etc.

Uncertainties related to the analysis method may also exist. Some analysis methods provide options capable of obtaining results faster while maintaining adequate accuracy. Eigenvalue extraction, for example, can be done with a reduced set of degree-of-freedom (called the master degrees-of-freedom) instead of the complete set (Bath and Wilson, 1972), lumped mass matrices can be used instead of consistent mass matrices, etc. However, the effect of these simplifications on the analysis outcome needs to be estimated.

Mistakes like program bugs, typing errors, wrong units, incorrect boundary conditions, etc. can always happen even though most FE pre-processors provide tools to reduce the risk of making these mistakes. Unless they have an important effect on the analysis results, identification of these errors can be very difficult.

Due to these inaccuracies or uncertainties that may be present in an FE model, there is a need to carry out dynamic testing of the actual structure modelled in order to confirm the validity of the FE model established before it is used for its intended applications.

1.3 EXPERIMENTAL MODELLING

Apart from the aforementioned analytical approach which can be employed for modelling dynamic characteristics of a structure, another approach is to establish an experimental model of the structure by performing vibration tests and subsequent analysis on the measured data, this later process is known as Modal Testing.

1.3.1 Modal Testing

In modal testing (Ewins, 1984), a structure to be analysed is vibrated with a known excitation under closely-controlled conditions so that appropriate vibration data in forms of frequency responses or time responses can be obtained for further analyses to extract modal parameters (e.g. natural frequencies, damping and mode shapes) of the structure. There are two main excitation approaches, i.e., single-input excitation and multiple-input excitation. By the single-input excitation approach, a single force is applied to excite a test structure and the ensuing responses are measured at those co-ordinates of interest. The excitation can be either a deterministic or banded random signal, depending on test conditions and a trade-off between cost and desired accuracy of test. The single-input excitation approach works well for small structures, and has gained much popularity because it is fast and easy to perform and is cheap to implement. In use of single-input excitation, however, there exists a possibility of exciting a structural system at a node or nodes of one or several of its modal vectors. Improper location of the excitation may lead to the missing of a mode in later modal parameter estimation. Also, a single-input excitation is often ill-suited for large structures. This is because response signals

measured at those points far from the excitation location may become very weak due to energy dissipation in the transfer path of the excitation. The multiple-input excitation approach attempts to excite a test structure using multiple forces applied simultaneously at different locations so that balanced response information can be obtained (Allemang and Brown, 1986). Multiple-input excitation is well suited for large and complex structures, and has many successful applications in aerospace and automotive industries. For measurement using such an excitation approach, however, it is required that all response and/or input signals be measured synchronously. Due to this synchronisation requirement, multiple-input excitation is more difficult, time consuming and expensive to implement in practice than single-input excitation.

The test data from which modal parameters are identified can be in forms of frequency response function, impulse response function or free response function. Basically, there are two ways for estimating frequency response function. One is to simply divide the Fourier transforms of the response signals by the transform of the input force. Another is to calculate the ratio between auto- and cross-spectrums of input and output signals with any of the equations derived under different assumptions of where the noise enters the measurement problem. Impulse response functions are obtained from inverse Fourier transform of frequency response functions. Free response function is the free decay of a system generated either by the release of initial displacement and/or velocity conditions or by the termination of initial excitation.

Modal parameter estimation is a special case of system identification where a priori model of the system is known to be in the form of modal parameters. Therefore,

regardless of the form of input-output data measured, the form of the model used to represent the experimental data can be stated on a modal model either in the time, frequency or Laplace domains using temporal and spatial information. Modal analysis methods can generally be classified as frequency domain methods or time domain methods. Frequency domain methods work on a set of frequency response functions (FRFs). Modal parameters can be identified by performing further analysis (such as curve-fitting analysis) on a modal model established using a set of FRFs. Time domain methods directly operate on measured free-responses or impulse responses. Modal parameters can be computed from a mathematical model established using time response data.

During the last two decades, modal testing has developed rapidly both in theory and in practice (Allemang, 1993). Many techniques have been developed in order to extract more reliable modal parameters of structures from test data. These techniques have been fruitful largely due to the introduction of the fast Fourier transform (FFT) algorithm and the development in recent years of powerful multiple-channel FFT analysers as well as to fast data acquisition equipment. The availability of computer-controlled measurement and special-purpose analysis software has reduced the measurement time and human effort, and improved the reliability and accuracy of measured data and the modal properties extracted from them.

After years of continued improvement in measurement equipment and development of modal estimation techniques, there has been a general agreement up to date that the measured response data or experimentally-derived modal data are reckoned as more

'correct' than their counterparts obtained from FE analysis, provided sufficient care is given to the experimental and identification procedures. The most significant application of modal testing is perhaps to compare and eventually to validate an analytical model using measured vibration data. Also, modal testing can be used to construct dynamic models of the components of a structure (such as joints and couplings) whose accurate dynamic characteristics are too difficult to be modelled analytically.

1.3.2. Assumptions and Limitations in Modal Testing

There are three basic assumptions made of any structure upon which experimental modal analysis is to be undertaken (Allemang and Brown, 1986). First, the structure is assumed to be linear. This means that the response of the structure to any combination of forces simultaneously applied is the sum of the individual responses to each of the forces acting alone. For a wide variety of structures, this is a very valid assumption. The behaviour of a linear structure can be characterised by a controlled excitation experiment in which the forces applied to the structure have a form convenient for measurement and parameter estimation. For some structures, however, the assumption of linearity is not valid and it is hoped in these cases that linear models can provide reasonable approximation of their dynamic behaviour.

The second basic assumption is that a structure under test is time invariant. This essentially means that the parameters to be determined are constants. If the dynamic characteristics of a structure that is being tested change with time, then measurements

made at the end of the test period would determine a different set of modal parameters as compared with those from measurements made at the beginning of the test period.

The third basic assumption is that a structure under test is observable. This means that input-output measurements can result in sufficient information to establish an adequate behavioural model of the structure. This is not true for some cases. For example, structures or machines which have loose components, or more generally, which have the degrees of freedom of motion that are not measurable, are not completely observable.

In addition to those assumptions made above, there are nowadays some limitations present in practice of modal testing such as,

1) Some types of degree of freedom, such as rotational or internal ones, cannot be readily measured with present technology;

2) The frequency range of test data is also limited; thus confining the range of identified modes;

3) Some modes of the structure under test may not be excited in a test or, if excited, may not be identified in the modal parameter extraction process.

Due to the aforementioned assumptions and limitations in modal testing, dynamic characteristics of a structure cannot be completely and accurately represented by a mathematical model established purely based on the experimental data obtained from modal test.

1.4 STRUCTURAL DYNAMIC MODELLING IN DESIGN PROCESS

In a typical engineering design process, both analytical prediction and experimental modal testing procedures are involved in an interactive way (Mitchell, 1988). They have complementary roles for the complete description and understanding of the dynamic behaviour of a structure and one cannot be substituted for the other.

At the design stage, an analytical model (normally a FE model) can be used to predict the dynamic behaviour of a new structure and to modify the design of that structure if any deficiencies are found before the structure is constructed. At a later stage, when a prototype of the structure has been constructed, a modal test can be performed to establish an experimental model using test data. Because of the aforementioned uncertainties, assumptions and limitations involved in the two modelling approaches, none of the established FE model and experimental model can be assumed to be perfect. Therefore, analysts and experimentalists must confront with the problem of reconciling the two dynamic databases for the same structure.

Test data are often considered as more accurate and thus often used as a reference to judge the quality of an established FE model. If analytical predictions of the FE model are not in good agreement with test results, the analytical model should be updated by correlating the analytical model with test data. The purpose of analytical model updating is to make use of the advantages of the models derived from the two modelling procedures and overcome their respective disadvantages. As the updated analytical model combines all the advantageous features of the original FE model and experimental

model, it can give a more detailed and accurate description of the dynamic characteristics of the structure, and thus can be used for further analysis such as response prediction, structural coupling, life time prediction, or structural integrity assessment, etc.

There are two analytical tools that are involved in structural design and dynamic modelling. One is Sensitivity Analysis, which studies how the dynamic characteristics of a structure vary with changes of structural physical parameters. The other is Modification Prediction (Re-Analysis), which addresses how to efficiently and accurately predict the dynamic characteristics of modified structures. At the conceptual design stages, modifications to a structural design are often needed if any deficiencies in the design are found. Also in the model updating procedure, modification to the analytical model is sought. For such cases, it is necessary to perform structural dynamic sensitivity analysis and modification prediction. Results from the sensitivity analysis can be used to find out the most effective modification, given the desired changes or adjustments of dynamic characteristics. By application of the modification prediction, the computational cost involved in the required re-analyses of dynamic characteristics can be reduced. The roles of these two analytical tools - Sensitivity Analysis and Modification Prediction - in the design process and structural dynamic modelling are depicted in Figure 1.1.

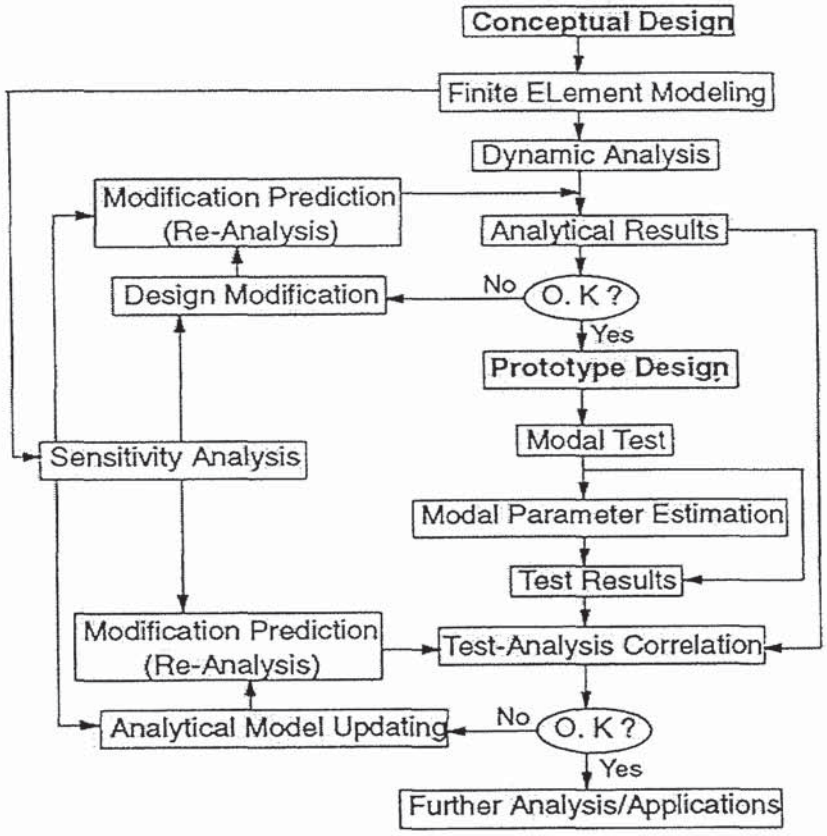

Figure 1.1 Structural dynamic modelling in a typical design process

1.5 OBJECTIVES OF THE THESIS

FE methods can provide valuable information to the design engineer during product development. The reliability and performance of PCB assemblies used onboard aircraft, ships and land vehicles are of increasing importance. This thesis applies the FE method to determine the effects of system variables on edge support conditions, such as wedge retainers and plug-in connectors, and the locations of point supports that could affect the dynamic characteristics of the PCB assemblies. Modal testing to verify the FE models developed is also conducted.

1.6 PREVIEW OF THE THESIS

In the following text, a brief introduction will be given to each of the remaining chapters, in which the research work is presented.

Chapter 2 presents a review of the vibration testing of engineering structures. First, some background to vibration testing is briefly presented and the need to improve the reliability of hardware that are subjected to vibration environments. Secondly, vibration test methods aim at subjecting the test item to real dynamic environment is introduced and the difference between sine testing and random vibration testing is discussed. Also included is a discussion on the types of shaker system and control system integration necessary to perform the environmental stress testing, including the excitation devices, types of excitation, accelerometers and analysers.

Chapter 3 provides a comprehensive literature review on stresses in solder joints. It is shown that temperature cycling and vibration loading are two of the main causes of PCB failures. It further discusses as to how the fatigue life of many types of components can be controlled by controlling the printed circuit board resonant frequency. An FE model of a PCB supported on two wedge retainers and a plug-in connector is developed and its dynamic characteristics is obtained. Fine-tuning of the boundary conditions of the supporting edges was then conducted so that there was good agreement with experimental tests.

Chapter 4 deals with the eigensensitivity analysis of the PCB and discusses the implementation of modal sensitivities to model tuning. It is shown that the rotational stiffnesses of the boundary supports can be updated effectively. The following case studies are provided: Case 1 - PCB with assumed clamped edges; and Case 2: PCB with in-service support conditions.

Chapter 5 is concerned with the study of introducing point constraint to the beam structure with a view to maximising its fundamental frequency. Starting from the mode shapes of a cantilever beam, it considered the likely locations to introduce a point support so that the percentage increase in natural frequency may be optimised. Three case studies were presented, namely, a clamped-simply supported beam, a clamped-simply-simply supported beam and a beam with two simple supports and the results were discussed to validate the proposed methodology in choosing support locations to maximise the natural frequency of vibrating beam structures.

Chapter 6 provides a methodology for maximising the fundamental frequency of a vibrating plate which is applicable to the vibrating PCB assembly. The technique is simple and does not require any optimisation or sequential search algorithm in the analysis. Numerical example using a plate with four simply supported points is provided to confirm the validity of the proposed approach. The validity of the approach is further tested by investigating the effect of a point constraint on a PCB, which is supported on its three edges by two wedge retainers and a plug-in connector, as seen in a typical electronic box.

Finally, Chapter 7 summarises all the main results presented in this thesis and indicates the direction for possible further studies.

CHAPTER 2

REVIEW OF VIBRATION TESTING

2.1 INTRODUCTION

This chapter briefly reviews the vibration testing of engineering structures. It involves some background to vibration testing, the test methods normally used to improve the reliability of engineering structures subject to vibration environments. Several textbooks are referenced which may be used for further review of the subject in more detail (Rao, 1995, Thomson, 1993). It also discusses the types of shaker systems and the integration of a digital computer controlled system normally used in environmental stress testing.

2.2 DEVELOPMENT OF VIBRATION TESTING

Vibration testing grew out of the need to improve the design and reliability of hardware subjected to vibration environments. The first environment was sine wave excitation from energy producing devices running at constant speeds or at varying speeds but having at all times a single frequency forcing function. Later, with the introduction of high energy jet engines and rockets led to the development to provide random excitation to simulate the energy inputs from these sources (Tustin & Mercado, 1984).

In addition to the above approaches for testing another sine-type test called resonance dwell has been, and continues to be used to determine the fatigue characteristics of structures. Resonance dwell tests are typically run for periods of time to duplicate the

expected service life of the equipment and induce a similar number of stress reversals on the hardware to insure that it will survive its service life. These tests are primarily related to a sine excitation environment.

At the start, very little real life information was available. Tape recorders were introduced long after the start of vibration testing therefore, little field data was available to record the loads on various parts of a structure in a service environment. Similarly, the design engineers had very little loading information on which a new structural design or the redesign of an existing structure is based.

As technology progressed, and more in-service loading information became available, test specifications were generated based on the latest information available, as measured or predicted on existing structures, on ground or air type vehicles. From this initial base of information the military standards have been revised over the years until the present time where we now have a new MIL-STD-810E. There has been a constantly growing set of specifications developed as a result of experience. The present military standards or IEC standards represent the best accumulation of information that can be used when designing a new product or device.

It is obvious that in designing a new structure that has never been built before, there is a lack of specific details about its behaviour under a set of as yet unknown forcing functions. The engineer has to design it to meet a MIL-STD which is the best set of information available. Military Standards are intended to provide initial guidelines for designers in the absence of real life environments.

They have another function in that by using a Military Standard, suppliers will test all hardware that eventually ends up in a given vehicle in a similar manner so that the overall testing programme need not be conducted in a single laboratory but can be conducted at various geographical locations with some feeling of confidence that the stresses imposed are uniformly applied to all pieces of the total vehicle. Finally by using some standard, tests are repeatable.

One of the great dangers of such test programmes is that by using arbitrary forcing functions, many elements of the system may be subjected to extremely high test conditions over what it will see in real life. The net result is that products may be over designed and become very high cost and in many cases far too heavy.

Over the years there have been many changes and refinements to MIL-STD specifications. For instance, aircraft type testing environments have been broken into many sections depending upon the location of the hardware, i.e., whether it is mounted on the wing, forward fuselage, rear fuselage, or tail section. This is an attempt to bring realism into the testing programme and prevent over-design and over-testing.

One of the most significant improvements has been that transmissibility characteristics of the airframe have now been used to modify the input to hardware located at some distance from the main source of vibration (Soong & Grigoriu, 1993). Figure 2.1 indicates such a condition and provides a typical modified profile to which hardware can be tested. This materially reduces the design requirements on the hardware in frequency regions which have low excitation and strengthens the design in the areas of heavy stress loading. In general, MIL-STD specification testing may have little

relevance to the development of commercial products unless the products are intended to live in a military environment, or unless the military environment is expected to be similar to the commercial environment.

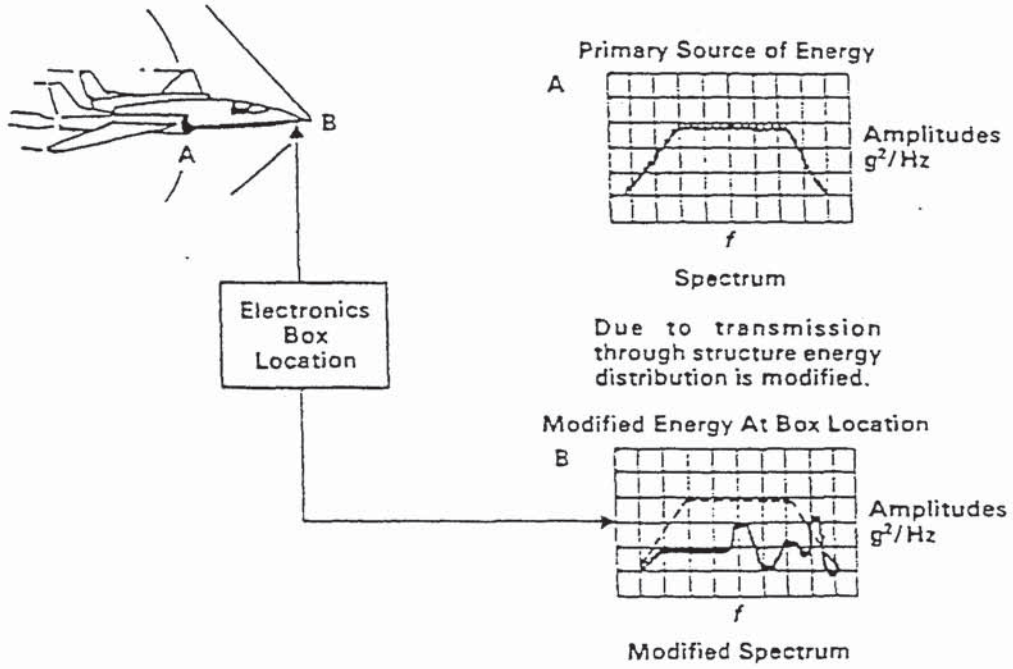

Figure 2.1 A typical modification of MIL STD 810 specification

The most recent expansion of vibration testing has been the combination of vibration with temperature variations at the same time to simulate a more complex environment. The reason for this particular combination is that over the years of accumulating data it had been found that vibration coupled with the hot and cold environments tended to produce the largest number of failures on items that had passed both the vibration or temperature tests separately, but when performed together it was found that numerous other failures occurred. This refinement of the testing technique is aimed more at

improving the reliability of the product rather than being related to the initial design of the product.

The name CERT stands for "Combined Environment Reliability Testing". As the name clearly states reliability is the primary goal of these types of tests. There are a number of ways in which this test programme is executed. There is a large increase in "screening" tests. These tests are used early in the assembly process of hardware to find faults well before a completed box is delivered for final test. The goal is to eliminate as many failures as possible due to components, connectors, and solder joints, etc., before a sub-assembly is put into final test.

There will be a series of sub-assembly tests as they are put together with other sub-assemblies which eventually form a final product. The first application of MIL-STD 781C has been to all of the latest design fighter aircraft production programmes and to all missile programmes of recent generation. In addition, all new development programmes now have this requirement. This is true of both the Air Force and Navy, and the Army is now introducing combined environment reliability testing as well.

Many of these systems control from two to ten shakers from a single vibration control system which was designed to be expandable for multi-shaker control in an effort to reduce the investment required for control. This programme is commonly referred to as "Multi-Shaker Control" and the system was designed primarily to allow its expansion to provide for lower cost test control in such situations. On the other hand the system is a very high performance system that can be dedicated to engineering or qualification testing as the situation dictates.

2.3 VIBRATION TEST METHODS

The true intention of vibration testing is to subject a test item to the real environment that it will live in. If the test item is to live in a sine forcing environment, then it should be tested by a sine forcing input; and if the test item is to live in a random environment, then it should be tested by a random input. An excellent reference book on vibration testing is given by McConnell (1995).

2.3.1 Sine Testing

Sine testing grew out of the propeller driven aircraft needs to determine the damaging effects of products which were subjected to forcing functions as a result of the vibration of the motors propelling the aircraft. In addition to the simulation of its environment, sine testing has other advantages in that it can provide a very accurate representation of the resonant responses that can be executed in a structure, to obtain information on the magnification (or Q) factor and in many cases can be used for modal type investigation of a structure.

During sine testing the test item is forced by sine-wave energy at a single frequency which is swept across the frequency band of interest for a number of cycles as required by a given test. This means that any resonant condition in the test item is excited as the sine-sweep passes its frequency. It also means that each resonance is excited one at a time.

2.3.2 Random Testing

In broadband random testing, energy at all frequencies is introduced over the entire frequency range being excited by the random forcing energy. This means that all resonant frequencies in the test item will be excited simultaneously.

It is this characteristic which provides the very important features in a random test because it is the excitation of a multiple number of resonances at the same time which frequently causes malfunction or failure of the device under test. The most important thing to do when designing a test procedure is to ensure that the type of test is selected to simulate the real life environment of the product.

2.4 SHAKER SYSTEM AND CONTROL SYSTEM INTEGRATION

Two types of transducers are required to form a typical shaker system. They are shakers and accelerometers. The shakers convert electrical energy into mechanical energy of motion whereas the accelerometers convert mechanical energy of motion into electrical energy.

2.4.1 The Shaker System

The two types of shakers currently used in environmental testing are hydraulic and electrodynamic. As is indicated by the name, one is driven by a hydraulic pumping system and the other by a power amplifier. A hydraulic ram versus an amplifier/loudspeaker is one way of comparing the two systems, except the

"loudspeaker" has no cone to couple the voice coil to air - instead of the items being fastened to the voice coil.

Shaker systems vary in size over a large range of ratings depending upon the application, and costs vary accordingly. When planning to install a system, there are a number of factors to consider in making a choice. It is frequently necessary to use more than one system to fit the anticipated applications.

The first consideration is usually related to deciding if the test jobs can all be done on either a hydraulic or an electrodynamic shaker so that only one system is needed. The hydraulic actuator is normally classed as a displacement generator and the electrodynamic as a force generator. The reason for this differentiation may not be apparent at first; however, it is important to realise that the hydraulic system must produce an actual placement in a test item in order to impart force into the test item mounted on the shaker head.

The electrodynamic shaker, on the other hand, has a moving armature that is, in fact, suspended in space and not driving against ground. This characteristic permits the armature current to generate a force which is passed into the test item but, in the event response characteristics of the test item do not want to permit movement in the given direction, the item can respond reactively against the armature even though the force is being applied, but may not necessarily move in the direction the force.

Under these conditions, the electrodynamic exciter actually induces force to a specimen and permits it to respond in a natural manner, whereas the displacement generator must

create force by movement and, therefore, in certain instances is more prone to break the test article. This means that in certain applications, the electrodynamic exciter would be a proper selection, whereas in other applications, the hydraulic exciter could be more appropriate.

Looking at the reality of an application is the most important thing to do. For instance, if we are primarily concerned with large objects, such as shipping containers, and testing them for operation in a transportation environment which is related directly to displacement, a hydraulic system would be a good choice for the application. On the other hand, if we are dealing with a space vehicle which is not living in a displacement environment, it is much more appropriate to use electrodynamic exciters to create the force input which then induces motion in the test item and permits it to respond in its natural manner, probably with less possibility of damage.

Another consideration is related to the displacement capability of the two types of exciters. Electrodynamic shakers typically are restrained to +/- 12 mm (certain shakers can go to +/-25 mm), whereas hydraulic shakers can have strokes up to 120 mm if the hydraulic pumping system is sized correctly. This again relates to the application and the levels to be induced into the test article. For instance, in transportation and low frequency type tests requiring operation as low as 1 Hz and an acceleration of 0.26 G peak sine, a displacement of 120 mm would be required. Such displacements are not obtainable on electrodynamic shakers and, therefore, a hydraulic shaker appears to be the best selection.

Another selection criteria is frequency range of operation. Hydraulic systems have historically been used for very low frequency, large stroke testing but, because of the nature of the servo valves required to modulate the oil flow, the upper frequency ranges are typically limited to about 500 Hz. Newer developments indicate possibilities of operating these shakers at higher frequencies. On the other hand, the electrodynamic exciter, because of its displacement limitations, is typically not too useful for very low frequency tests. Once the test range gets to approximately 5 Hz and up, the exciters are very useful because they can easily control up to 2 to 5 kHz depending upon the shaker size.

Test item size is also a matter to be considered in selecting shakers. In general, large, heavy packages tend to be good candidates for low frequency testing and, in many cases, moving tables to handle large dimensions can be handled very nicely by hydraulic systems using more than one shaker actuator. Electrodynamic shakers can also be used in multiples; however, heavy static loads need to be supported by external suspension systems to take the loading off the armature flexures to maintain it at approximately zero displacement before vibration is started. This sometimes complicates the test set-up but, depending upon the nature of the test article, may require electrodynamic shakers because of the application involved. The electrodynamic shaker is ideally suited for many applications because of its flexibility and application to small and medium test items and versatility for chaining axis of vibration. This can be very important in some applications.

Both types of shakers exhibit resonant conditions which cause some problems in control - the hydraulic systems typically have an oil column resonance that is rather

severe in the 200 to 300 Hz region, and shaker armatures typically have resonances in the 1,500 to 3,000 Hz region. These resonances are frequently high in dynamic range.

The modern digital vibration control systems, such as the SD1200 Series, which is used in conducting vibration testing in this research, can readily cope with this condition provided they have sufficient dynamic range. Control of 72 dB or more dynamic range is available with the SD1200 Series. Dynamic range is a major consideration in buying a control system because it is these resonances and other package, fixture, and coupling resonances which give rise to the need for automatic control systems. Since the resonance conditions shift due to non-linear responses in test items is unpredictable, automatic control is essential for conducting test operations rapidly. This need brought about development of equalizing systems for random control and servo control systems.

2.4.2 Rating a Vibration System

Factors that need to be considered in selecting the size of a shaker system for random control are the desired acceleration and the total moving mass (include the test specimen, test fixture and armature). Having decided upon the maximum acceleration level from a system and the frequency range over which it must operate, we add up the total weight of the test item, the attachment fixture and mounting hardware that couples the test item to the shaker armature, and add the armature mass to come up total moving mass. This is then multiplied by the acceleration to give us the rating for the system.

2.4.3 Displacement Limits

Ratings start to be limited in the low frequency end because of displacement limits in electrodynamic shaker design. A new, 50 mm double amplitude flexure system in the Ling Dynamic Systems shakers has significantly improved the ability to test large displacement at lower frequencies on some of the electrodynamic shakers. Hydraulic shakers typically have much greater displacement capability, but pumping requirements can be expensive.

Once we have obtained the Sine rating it would appear that we can convert that rating to RMS and multiply by 3 to obtain the peak rating for random, normally listed as being with a load equal to armature mass for electrodynamic systems. This is not necessarily true.

Because of the variation in the "E" and "I" requirements of different shakers, the above "simple" conversion will not hold in most instances and, because of the wide band power requirement and peak power needs for 3 signal performance, the actual application should be discussed thoroughly with the suppliers of shakers and associated power amplifiers to insure that the dynamic testing job can be accomplished at a reasonable price with the system selected.

2.4.4 Velocity Limits

Another item of concern in rating a system is the velocity limit of the system. This limit is a function of both the power amplifier and shaker design. Electrodynamic shakers

have velocity limits that relate to design of their flexures as well as PA/shaker matching. Hydraulic shakers have limitations on horsepower and pumping capability. Your shaker manufacturer can help you understand these limitations and keep you out of trouble in meeting the needs of your application.

2.4.5 Mass Controlled System

Most experienced test engineers advise that the best situation is when we have a "mass controlled system", meaning that, if the armature mass exceeds test package mass significantly, the reactive forces from the test package tend to be less of a problem than would otherwise exist. This consideration sometimes leads to the buying of a large electrodynamic shaker with a smaller amplifier to do a job that could be done by a small amplifier and a smaller shaker; however, the mass of the moving element in the bigger shaker tends to make table mounting simpler and control easier.

One of the most common mistakes is to buy a system that has only enough capability to barely do a job. This allows no error in estimating the fixture weight and variation in package weight and should be avoided at all cost. It is much better to buy a system that is larger than the exact need because one seldom knows what the future requirements will be. Do not buy a marginal system for an application.

2.4.6 Accelerometers

The accelerometer is the most common class of transducer used for measuring motion. is a signal sensor measuring one parameter of motion. There are displacement and

velocity transducers as well as strain gauges, all of which are capable of sensing motion. There are a large number of transducers available to the testing laboratory various applications and the accelerometer is the most common device now in use.

There are literally hundreds of different accelerometers available. The reason is that transducers, as a class, whether they are force generating or signal detecting devices, have characteristics which can be modified to optimise the ability of the device to suit specific applications is true in either shaker or accelerometer design. Accelerometers are designed with trade-offs between frequency range, sensitivity, cross axis motion, thermal sensitivity, and base strain to name a few. Accelerometers, just like shakers, must be selected for the job they are to perform in the environment that exists. Some are sensitive to magnetic fields, some are not. The selection of accelerometers for control purposes is very important. One of the more important characteristics is the resonance frequency of the moving element. If it is not high enough, it can contaminate the response data from the shaker head and give erroneous information to the controller which does not know of this problem.

2.4.7 Ground Loops

In addition, the mounting of the transducer is particularly important with respect to the measurement being taken. Alignment of its axis must be coincident with the need formation in that direction. Insulation of the accelerometer circuit from the shaker or test package is usually very desirable so as not to induce a ground loop into the signal control system.

The introduction of around loops is frequently one of the most difficult problems in a testing laboratory. Isolation of AC grounds from signal grounds is absolutely essential. This requires close attention to the grounding circuits used in both AC and signal branches of the system and, over the years, has proven to be the biggest problem arising in laboratories with respect to good data acquisition.

Unfortunately, when a laboratory has been installed and is very clean with respect to ground loops, the installation of one new item into a system in many cases can completely upset the signal ground conditions for the whole system. This, then, destroys all the previous hard work put into cleaning up the grounds. This is an item that should be continually watched in every laboratory.

2.4.8 Analysers

The function of the analyser is to measure the various signals developed by the transducers in order to ascertain the excitation force and response levels. Analysers are sophisticated data acquisition devices complete with signal processing and on-line analysis. There are different types of analyser available and the choice will depend on the type of excitation which has been used. Digital devices are most common. The two most common devices are Frequency Response Analyser and Spectrum Analyser.

The Frequency Response Analyser is used purely for sinusoidal excitation. The analyser generates the sinusoidal excitation signal at the desired frequency. The input, signals from the force and response transducers are correlated with the output signal in such a way that only component at the frequency of the output signal is present. This

permits an accurate measurement of the component of the transducer signals at the current frequency of interest.

The Spectrum Analyser can be used with almost any form of excitation: random, transient, and periodic. It can measure simultaneously all the frequency components present in a signal using the Fast Fourier Transform (FFT). Its output consists of a spectrum, a discrete one containing a finite number of components, describing the relative magnitudes of a whole range of frequencies present in a signal.

CHAPTER 3

COMPUTER MODELLING OF PCB

3.1 INTRODUCTION

More electronic equipment are designed and built for use onboard aircraft, ships and land vehicles. Since the purpose of an electronic system is to work electrically, it is logical that most of the time and money go into the electronic circuitry. However, shock and vibration have been found to be the major causes of electronic equipment failures. Markstein (1987) reported that shock and vibration failures in electronic equipment are second only to failures due to temperature. Therefore, unless the electronic assembly is designed for its dynamic environment, there can be problems occurring subsequently which may require an extensive amount of redesign.

Continuous vibration may lead to fatigue failure of the PCB as a result of cyclic stresses. Steinberg (1988) found that vibration induced failures include the cracking of solder joints, breaking of component leads, loosening of screws and damage to connectors. Failures of PCBs can be avoided by understanding the nature of vibration, i.e., evaluating the dynamic response characteristics and stress levels. This involves the determination of natural frequencies and displacements. Since the dynamic displacements and stresses can be evaluated from the natural frequencies, the determination of the natural frequencies of the PCB is of fundamental importance during the design stage.

When the PCB resonant frequency is excited, the plate structure is forced to bend back and forth. When displacement amplitudes are high, then the relative motion between the components and PCB are high, which often results in cracked solder joints and broken lead wires. The fatigue life of these components can often be increased by reducing the dynamic displacements of the PCB. As the displacements can be controlled by the resonant frequency, it follows that the fatigue life of many types of components can be controlled by controlling the PCB resonant frequency.

With the natural frequency information, it is possible to determine the fatigue life of the components, the solder joints and the PCB and hence achieve high reliability of the PCB assembly. Steinberg (1988) has proposed a simple rule of thumb for designing PCB in a vibration environment based on his own personal experience and not on a stress analysis program. Sloan (1985) provided techniques to evaluate the dynamic response of the electronic equipment design due to vibration and explored the relationship between the fundamental frequencies and the stresses and forces experienced by an electronic assembly.

3.2 LITERATURE REVIEW

Lau and Rice (1985) reviewed various publications presented for solder joint fatigue in surface mount technology (SMT), such as solder joint reliability, testability of the SMCs, and component/substrate thermal management issues. Yamada (1987) proposed an approach to the fracture analysis of solder joints by replacing the plastic zone at the crack tip with a uniformly distributed load. Further, Yamada (1991) believed that understanding the crack behaviour in solder joints is the first step toward

achieving higher reliability of an electronic package. He further stated that the fatigue life of a solder joint is dependent on the frequency as well as the number of cycles.

Two types of components are used in SMT. One contains no leads and is known as a leadless component. The interconnections between the leadless components and the substrate are solders that had received wide attention as reviewed earlier. The second type of component is leaded. The leaded components contain leads that are adhered, by adhesive materials, to the substrate. Since the leads serve as mechanical supports, they are expected to provide the necessary compliance. For electronic packages, the solder joint fatigue is a significant factor resulting in the failure of a device. Burgess et al. (1984) investigated solder fatigue of power packages. Four main reasons causing solder fatigue were reported. First, plastic deformation dominates solder fatigue since soft solders can never have high stresses. This is an important point for the avionic industry because the deformation is large due to the difference in the coefficient of thermal expansion of the component leads and the PCB. Secondly, stress concentration occurs at the chip corners and solder voids resulting in rapid fatigue. Thirdly, intermetallic formation prevents the reheeling process of a crack thus accelerating fatigue damage. Finally, the residual flux from the manufacturing process is a major contributor to solder fatigue. The IEEE Computer Committee formed a Compliant Lead Task Force to evaluate the "J" leads of a chip carrier. Landis (1985) submitted his report to the IEEE and reported two dilemmas. Firstly, the stiffness of the leads were too high and secondly, the leads had gone through overstressed bending that resulted in fractured and overstressed leads.

Among the researchers in the area of SMT reliability, Engelmaier (1984) is considered to be one of the pioneers in this field. He raised issues that received significant concern in the functional reliability of surface mount attachment technology. These issues were: (1) complex thermal situation, (2) cyclic strains due to in-plane expansion mismatch, cyclic warpages and transient conditions, (3) complex, non-uniform solder joint geometries, (4) constituent material properties with nonlinear dependence on temperature and cyclic frequency, (5) solder fatigue behaviour that is dependent on both temperature and time due to the stress relaxation phenomenon and (6) complex solder joint metallurgy due to intermetallics. Although the thermal issue on solder joint reliability was fully discussed, the vibration problem was not mentioned.

Engel et al. (1984) investigated the stresses in the solder joints caused by the difference in thermal expansion coefficients. Vibration effects were acknowledged, but no study was conducted. It was suggested that distributing the pins over the package reduces the loads on the corner pins more effectively than a circumferential distribution. Two points were highlighted in the paper: (1) corner pins are critical, and (2) lead height effect was investigated and longer leads were recommended. Lau et al. (1988) presented their experimental results on PLCC solder joint reliability and found the fatigue mechanism in solder joints. The solder joint fatigue cracking starts near the tip of the outer solder fillet and propagates along the interface between the J-lead and the solder joint. Fatigue lives of the samples used in the study were characterised in terms of the isothermal test results.

Subrahmanyan et al. (1989) tested the solder joints under both isothermal and thermomechanical environments and stated that the kinetics of damage during

isothermal and thermomechanical fatigue of solder joint may be the same. A governing equation for stress at the leads was derived and used for the damage integral calculation. Isothermal tests on leadless chip carriers were conducted by Solomon (1989). He used load drop and electrical resistance change to determine the fatigue life of solder joints. For a given displacement, as the cracks progress, the load required drops and the resistance increases. The thermal strain caused by the mismatch between the solder joints and the PCB was simulated by mechanical cycling between -55°C, and 150°C corresponding to different displacement levels. The failure mode was found to be when the cracking starts below the chip carrier and extends into the fillet of the solder joints. Four methods for determining solder joint failure were listed by Frear (1989). They are: (1) visual inspection, (2) electrical discontinuity, (3) electrical resistance increase, and (4) continuous continuity monitoring. He proposed a test method which introduced strain to the joints mechanically. The specimens were placed in a temperature chamber for thermal cycling. The joints were monitored by an event detector. When 15 events were detected, the joint was labelled as failed. An event was an intermittent or transient resistance fluctuation that exceeded 5,000 ohm and had a duration of at least 0.2 microsecond.

To determine the influence of lead type on solder joint reliability during thermal cycling, Engelmaier et al. (1989) examined "J" lead and "hinged S-bend design" clip leads. He concluded that the latter provided higher compliancy and the failure mechanism for both lead designs was cracks due to thermal expansion mismatch between the solder and the leads. The temperature profile was reported to be an important factor affecting fatigue lives. Two papers mentioned the vibration effects on solder joint reliability. However, no study was conducted to investigate the vibration

effect in either paper. Hagge (1989) reviewed some basic mechanical design approaches available to assure reliable interfaces within and between packaging levels in the chip, package, and PCB assemblies. While Caruso (1990) proposed a process for translating aircraft mission profiles into laboratory temperature-altitude-humidity tests.

Emphasising the vibration effects on solder joint reliability, Lau et al. (1990) studied four types of SMCs, namely 160-pin quad flat pack, 132-pin plastic quad flat pack (PQFP), 68-pin plastic leaded chip carrier (PLCC) and 84-pin PLCC. The study included both in-plane and out-of-plane vibration tests and a 3-dimensional FE analysis of the components under thermal cycling. A complicated equation was derived for the natural frequency of a PCB with a component attached at the centre of the board. Reliability design charts for the solder joints of the components were provided from the shock and vibration tests. The thermal FE analysis provided agreement with Solomon (1989) experimental data. Although both the thermal and vibration environments were considered in the paper, no attempt was made to combine the two effects to simulate a practical and realistic case. The vibration sources were characterised by Collins (1986). They are shipping, handling and internal (such as unbalanced fan) vibrations. These are low frequency sources. A design guideline was provided at the end of the paper. Nevertheless, high frequency vibrations, such as gun firing or missile operations, are important factors for avionics that were not mentioned.

For high frequency vibration problems, Markstein (1987) revealed that 20% of the mechanical failures in airborne electronics were due to vibration and shock, while the remaining 80% was related to thermal problems. He applied information provided by

Steinberg and presented an equation for the desired PCB resonant frequency, allowing the solder joints of SMCs to survive 20 million stress reversals. Markstein (1989) showed an example calculation emphasising the importance of design experience in making high reliability electronics. The combined thermal and vibration stresses were pointed out to be necessary to expose flaws in design or production. However, only vibration problems were discussed. He highlighted that random vibration causes simultaneous resonances. However, the largest displacement occurs at the centre of the PCB and at the fundamental resonant frequency which is of concern. In turn, it is the fundamental resonant frequency that induces the largest amount of stresses and strains. Hence, efforts on solder joint and PCB reliability should be focussed on the system's fundamental natural frequency response. At the chassis level, he emphasised that the resonance of the chassis and the PCB should be sufficiently separated by at least one octave in order to avoid the amplification effect. One octave is defined as a doubling of the resonant frequency.

According to the observation of Szmkowiak et al. (1981), the largest displacement was developed at the centre of the board, leading to the principal failure mode of the board system, i.e., fracture of the component leads at the component or board surface. The corner leads of the component were found to be critical during vibration process, while the shorter leads resulted in higher stresses than the longer leads. Roberts & Stillo (1991) published their theoretical analysis and experimental tests on random vibration analysis of component-board systems. They used the FE method in the theoretical analysis. The component-board systems were tested in a chassis during a two-hour experiment. The discrepancy in the first mode natural frequencies between the theoretical and experimental results was justified by the fact that the wedge locks of

the board support does not provide clamped edge conditions as assumed in the theoretical analysis. In addition, large components adjacent to the component of interest were assumed to increase the system stiffness.

Wong et al. (1991) applied modal testing and structural modification techniques to predict the modal parameters of a PCB with a single SMC. It was found that accurate identification of the properties of an SMC was difficult. These SMCs contributed both mass and stiffness to the PCB assembly and affected the system natural frequencies. Pitarresi & Di Edwardo (1993) investigated how the fundamental natural frequency may be raised through the use of various point supports, arbitrarily located under the PCB. Their approach requires the use of an iterative search algorithm but the solution may still not be exhaustive enough for the optimum. Abrate (1995) studied the vibration of laminated composite plates with point supports by using Rayleigh-Ritz method and Lagrange multiplier to enforce the zero displacement constraints at the support locations. The plates were studied with the constitutive equations expressed in terms of four lamination parameters. These four parameters covered all possible distributions of fiber orientation and layer thickness through the thickness of the laminate. His approach showed that optimum design was not unique since many laminates had the same combination of lamination parameters even though fiber orientations and ply location through the thickness were different.

Ham & Lee (1996) developed an automated fatigue testing system to study the integrity of electronic packaging subjected to mechanical vibration. They highlighted the fact that failures always occur in the leads rather than in the solder joint for the spider gullwing type lead under vibration loading.

3.3 FINITE ELEMENT MODELLING OF PCB

The finite element method plays an important role in the dynamic analysis and design of engineering structures. Zienkiewicz (1977) and Zienkiewicz & Taylor (1989) have reviewed the subject in detail. The modern electronic systems normally encompass an equipment chassis and a plug-in PCB assembly. The PCB assembly is supported on its three edges by two opposite wedge lock retainers and a plug-in connector. This type of configuration is widely used because of its ease of removal for servicing. Epoxy fiberglass is the most common material used and the rectangular board is the most common shape used by the electronic industry.

The manner in which the PCB assembly is supported at the edges can considerably affect its natural frequencies. When the PCB is subjected to vibration, it will experience excessive displacement, particularly at resonant frequencies. Also, when subjected to a shock, the same phenomenon will be observed albeit for a transient period. Failures due to lead wires, connectors, solder joints or other structural members may occur and consequently the whole electronic equipment may malfunction or fail.

The mathematical modelling of the PCB structure by FE method plays an important role in the vibration analysis and design of the structure. An accurate FE model of the PCB is necessary so that reasonable frequency predictions are possible. As the PCB assembly is being regarded as a flat rectangular plate structure, the idealisation of the stiffness and mass matrices of the structure can be achieved with very high accuracy. The error in the idealisation lies in the difficulty of modelling the boundary

conditions. In practice, the PCB assembly is normally supported by edge retainers along its two opposite edges, along the bottom edge by a plug-in connector and with the remaining edge free from any support.

Under vibration loading, the PCB can be analysed as a rectangular thin plate and its natural frequencies and mode shapes determined. The method by Rayleigh (1877) provides a good approximation to the fundamental natural frequency of the PCB. Leissa (1973) and Gorman (1982) have studied the free vibrations of rectangular plates and provided analytical solutions. However, in these analytical methods, it is common to assume that the edges of the plate provide the classical boundary conditions, i.e. free, simply supported or clamped conditions.

There exist 21 distinct cases that involve all possible combinations of classical boundary conditions for rectangular plates (Leissa, 1973). In reality, the edge retainers and connectors do not behave as classical supports and the assumptions of such boundary conditions will lead to either the under-estimating or over-estimating of the system natural frequencies. It has been considered by the Warburton & Edney (1984) that an elastically supported edge behaves somewhere between a clamped and simply supported boundary condition, and they used a combination of corresponding mode shapes for beams as the assumed plate deflection function and applied the Rayleigh-Ritz method to determine the natural frequencies for rectangular plates with elastic supports.

3.3.1 PCB Mesh Generation

The natural frequencies and mode shapes of a vibrating PCB have been studied using Algor (1991), a commercially available FE package. The FE model of PCB was modelled using a four-node plate element with 110 elements (10 x 11 mesh). The FE mesh generation and its associated node numbering is shown in Figure 3.1. Table 3.1 shows the material properties of the PCB used in this study. The two wedge retainers were modelled as simply supported with constrained rotational springs along their respective edges. The plug-in connector was also modelled as simply supported with constrained rotational springs along its edge.

3.3.2 Model Tuning

Fine-tuning of the FE model was required so that the natural frequencies obtained under simulation would compare closely with the experimental frequencies. Simulation runs were conducted initially with the PCB simply supported at the three supported edges and with the remaining edge free. Varying the rotational stiffnesses along the two wedge retainers were then considered. This was followed by introducing the connector with varying rotational stiffnesses along the bottom edge. Simulation runs were also conducted by assuming that the three edges were simply supported and clamped supported respectively and with the remaining edge free, namely, SSSF Case and CCCF Case respectively. The simulated simply supported and clamped supported edges cover the lengths of the wedge retainers and connector on the board. In other words, the SSS and CCC do not represent the boundary conditions over the full edges of the PCB. The frequencies for the first five modes are tabulated in Table 3.2. Figures 3.2 and 3.3 show

the variations of the spring stiffnesses of the wedge retainers and connector respectively upon the natural frequencies of the PCB structure. The first five modes of the fine-tuned model is shown in Figures 3.4a to 3.4e.

Material	Epoxy fiberglass FR-4
Young's modulus	1.7×10^4 N/mm^2
Poisson's ratio	0.12
Density	1.87×10^{-6} kg/mm^3

Table 3.1 Material properties of PCB used

Mode No.	Algor FE CCCF(Hz)	Algor FE SSSF(Hz)
1	93.7	51.3
2	141.9	108.2
3	239.8	178.0
4	257.4	234.1
5	318.3	238.5

Table 3.2 Characteristic frequencies for classical supports

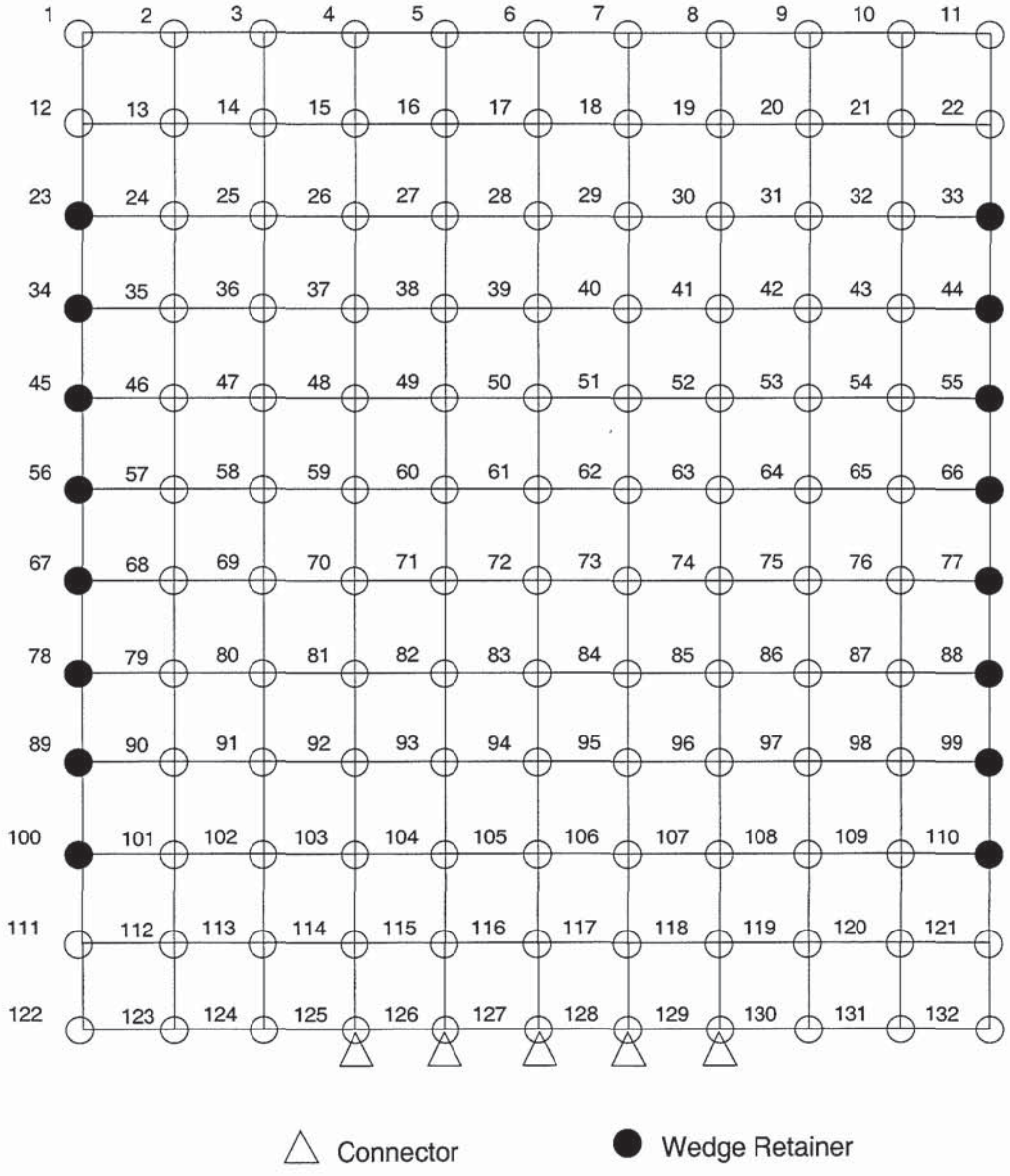

Figure 3.1 Finite element mesh generation of 110 elements for the PCB

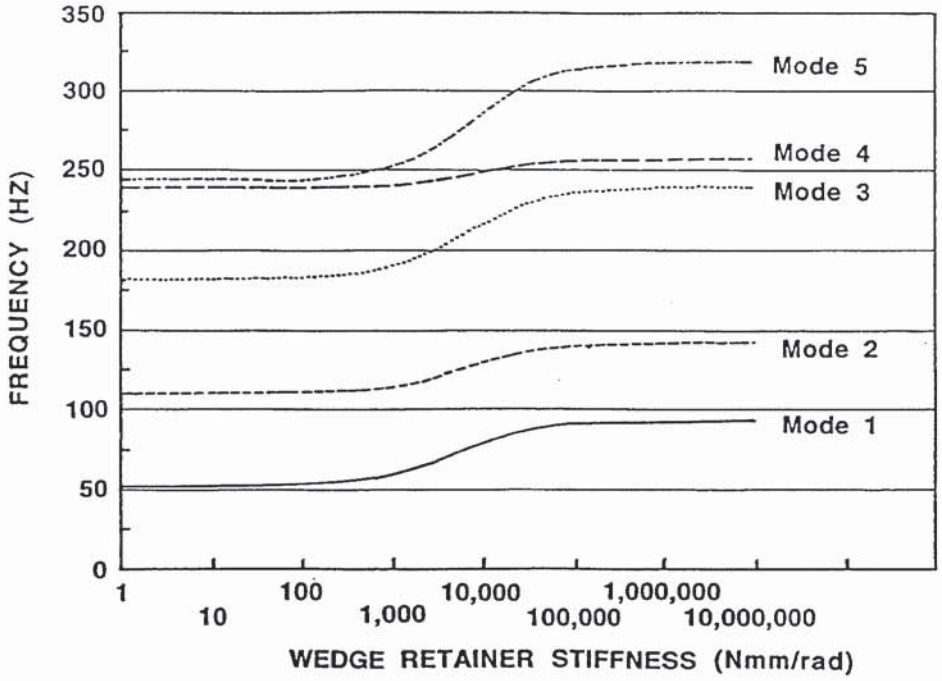

Figure 3.2 Variation of frequency against wedge retainer spring stiffness

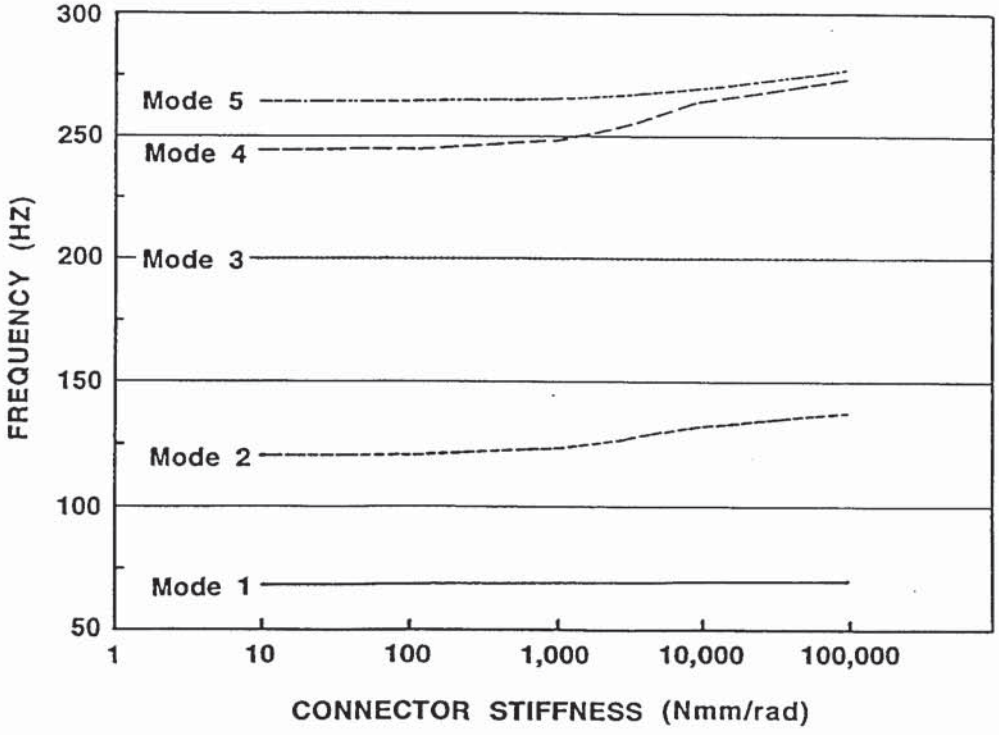

Figure 3.3 Variation of frequency against connector spring stiffness

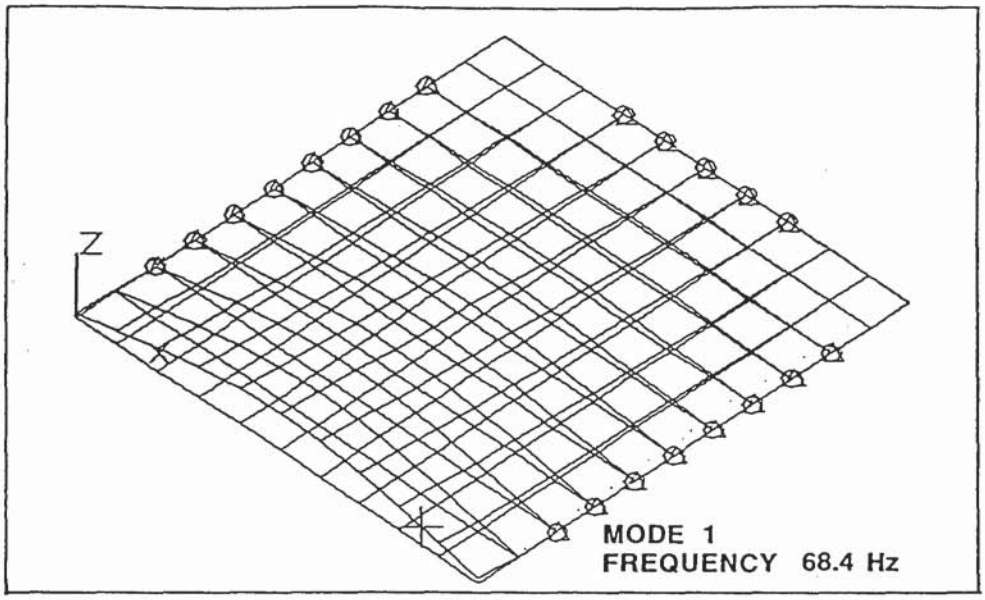

Figure 3.4a Mode shape of the first mode of PCB

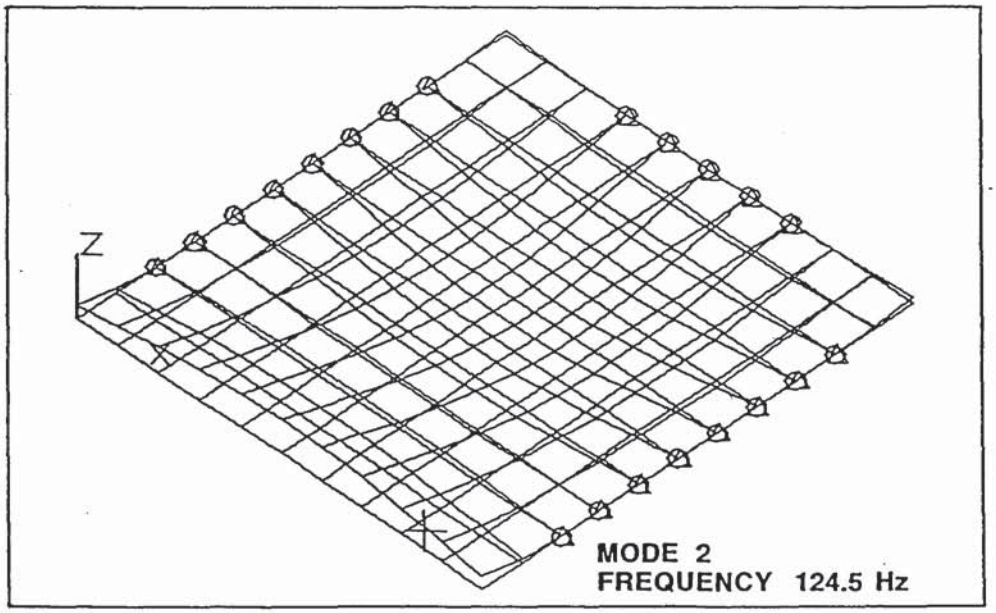

Figure 3.4b Mode shape of the second mode of PCB

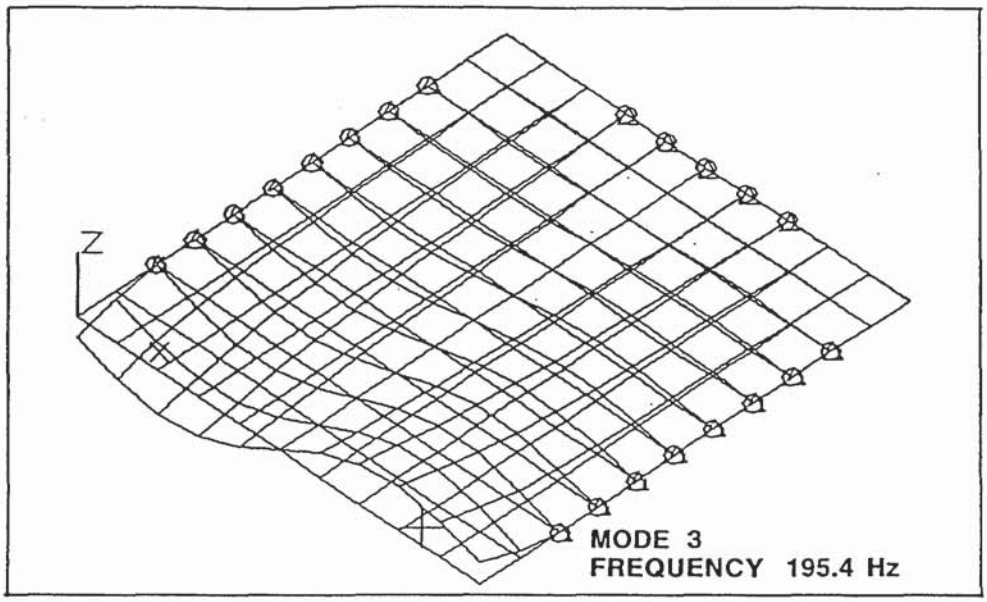

Figure 3.4c Mode shape of the third mode of PCB

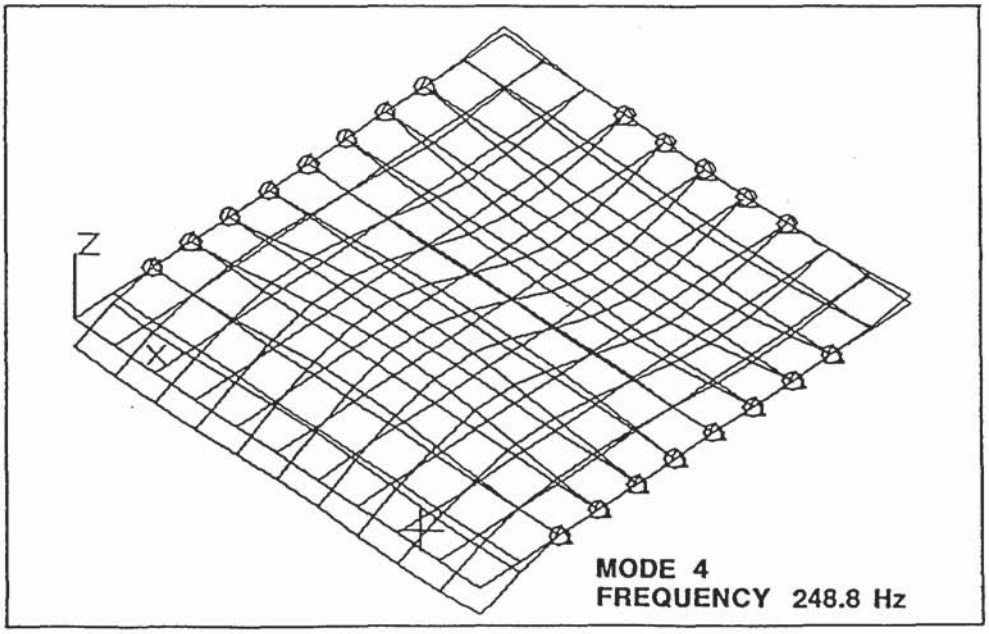

Figure 3.4d Mode shape of the fourth mode of PCB

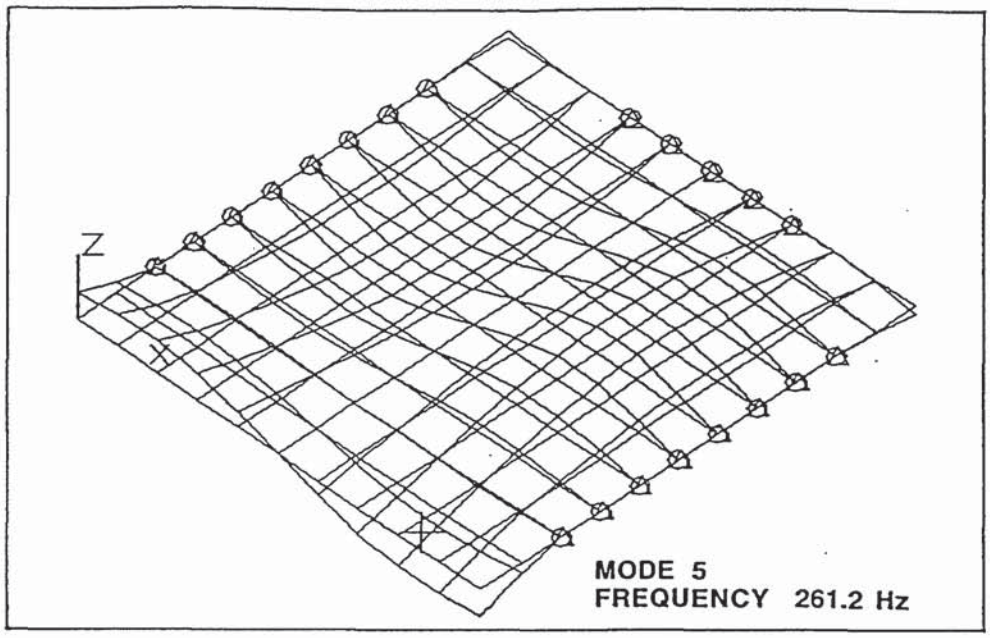

Figure 3.4e Mode shape of the fifth mode of PCB

3.4 EXPERIMENTAL SETUP AND PROCEDURE

In order to mount the PCB structure onto an electromagnetic shaker, a vibration test fixture has to be designed and fabricated. The purpose of the test fixture, which was made of aluminum alloy 6061, was to transfer all the mechanical energy from the shaker head onto the test sample. Apart from ensuring that the test fixture will hold the PCB assembly in a manner as close as possible to its actual in-service environment. Flexibility and ease of assembly were also incorporated in the design so that it could be used to test different sizes of PCBs. In addition, an important factor in the fixture design was to ensure that no untoward fixture resonance will occur over the frequency range of the various tests (Klee et al. 1971). The final design of the test fixture comprises an adapter plate, two retainer brackets and a connector bracket. The adapter plate has countersunk holes drilled in order that it could be bolted to the shaker head. Figure 3.5 shows the test

fixture and PCB, mounted on the shaker head. The assembled test fixture was tested and found to have a resonant frequency of 1,900 Hz, which was well above the frequency range of the vibration tests.

The schematic layout of the vibration test equipment used in the experiment is shown in Figure 3.6. Two accelerometers were used to monitor the vibration test. A control accelerometer was mounted onto the test fixture to sense the reference signal and an auxiliary accelerometer was mounted on the centre of the free edge of the PCB to monitor the response. The PCB, which has dimension of 220mm x 233.4mm and a thickness of 1.58 mm, was made of fiberglass, known as FR-4. One edge of the PCB was soldered onto a 96-pin connector, which was plugged into a 96-pin socket, mounted rigidly in the test fixture. The wedge retainer used was the CALMARK series 225 - "card-lok" retainer, with a full length of 153 mm. The two wedge retainers were

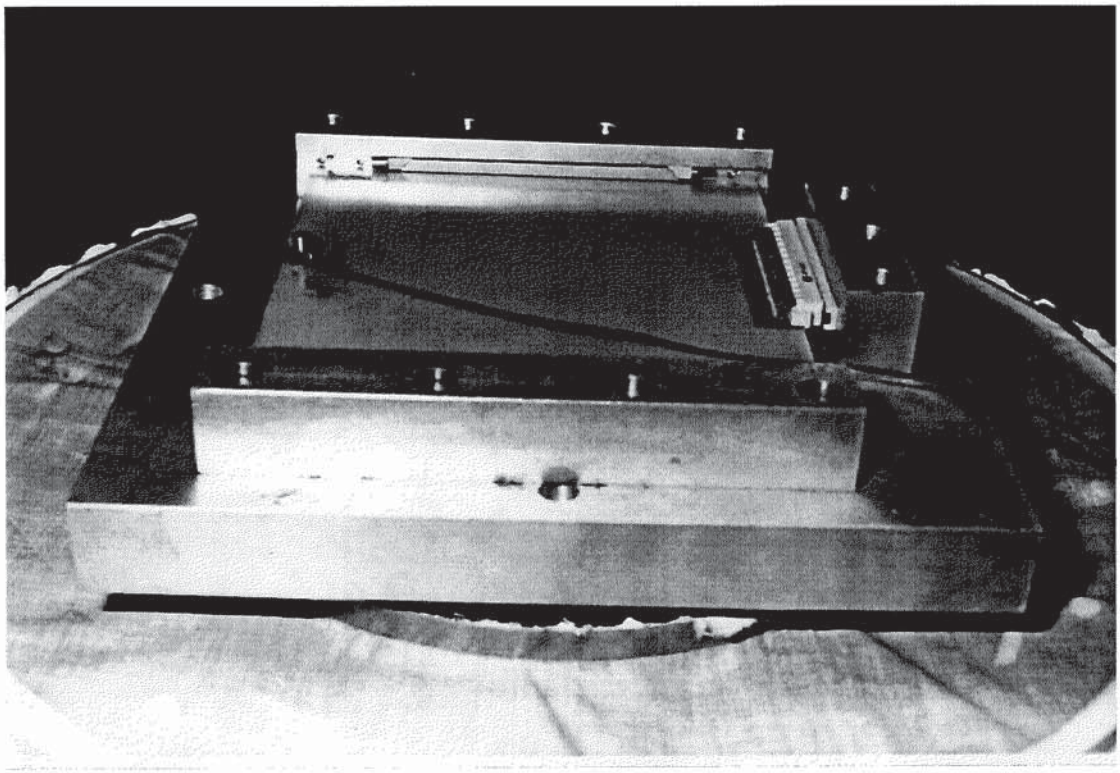

Figure 3.5 Test fixture and PCB mounted onto the shaker

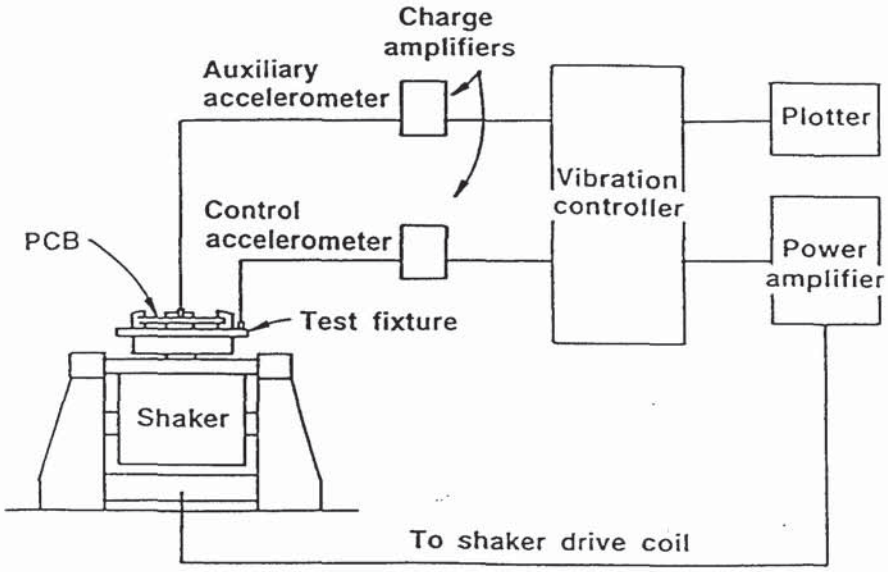

Figure 3.6 Schematic layout of the experimental setup

tightened with a torque wrench to the manufacturer's recommended torque of 0.68 Nm. Figure 3.7 shows some CALMARK series 225 wedge locks, that are available commercially. The vibration test uses a Spectral Dynamics SD1500 controller to control and monitor the Ling A395 electromagnetic shaker, in which the latter was mounted with the test fixture and PCB structure. A random signal with frequency range from 10 to 1,000 Hz was used to excite the shaker.

3.5 RESULTS AND DISCUSSION

The frequencies of the first five modes of the PCB structure obtained under vibration testing were found to be 68, 124, 203, 254, 275 Hz respectively. Figures 3.2 and 3.3 show the effect of varying spring rotational stiffnesses on the system natural frequencies. It is found that the wedge retainer stiffness predominately affect the frequencies of the first, second, third and fifth modes whereas changes in the connector's stiffness

predominantly affect the second, and fourth mode and to a slight extent, the fifth mode frequencies. After various simulation runs, it was found that a spring stiffness (α) of 2.9 x 10^3 Nmm/rad for the wedge retainer and a spring stiffness (β) of 2.9 x 10^3 Nmm/rad for the connector provide very good agreement with experimental frequencies. The experimental results are tabulated together with the FE results in Table 3.3. It may be seen that fine-tuning of the FE model's frequencies resulted in an average % difference of only 2.1% and with the first two modes yielding almost exactly the same frequencies as the experimental frequencies.

Initially, it was thought that the connector, with its rather solid appearance, behaved as a clamped support to the board. However, closer inspection of the connector and socket

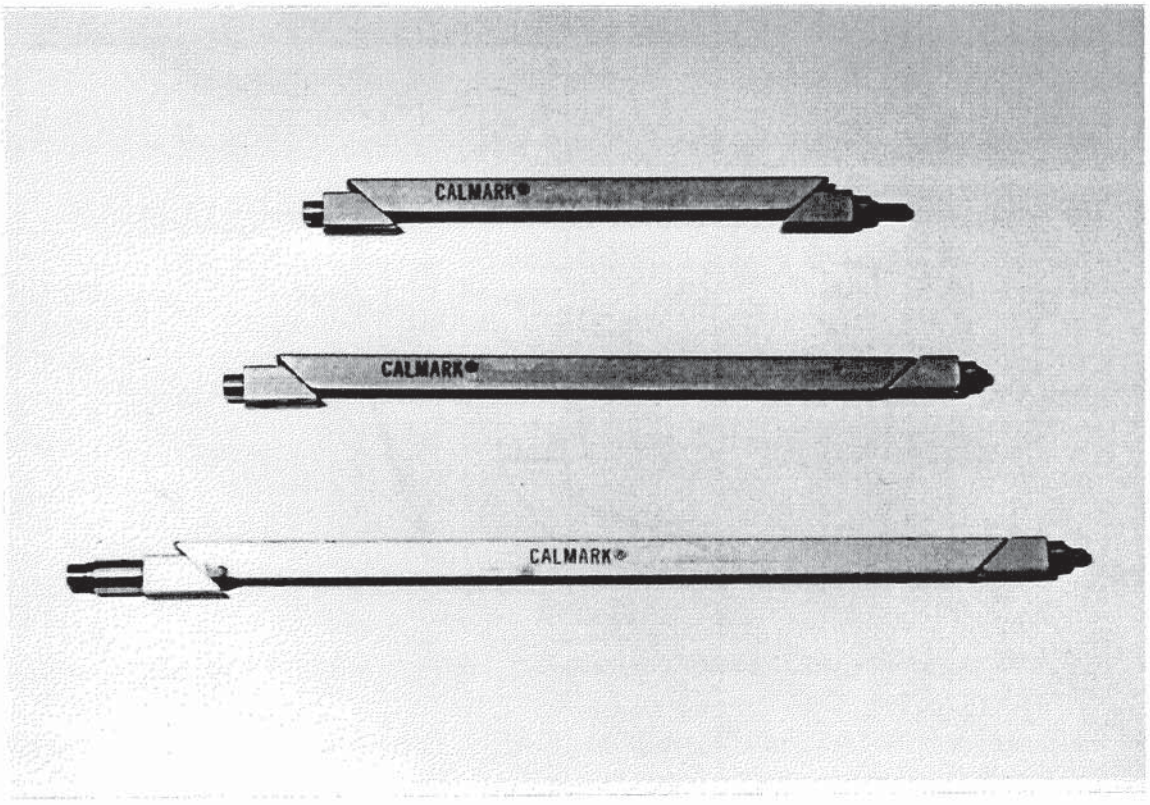

Figure 3.7 Wedge lock retainers - CALMARK series 225

arrangement revealed that the plastic guide slot merely provided rotational restraint to what is a simply supported edge. This is because when the PCB was supported just by the connector and mounted horizontally, the board appeared to deflect by a fairly large inclination angle. In the course of arriving at an accurate FE model for the fundamental frequency, it is found that the fundamental natural frequency of the board is totally dependent on the restraint provided by the two wedge retainers and almost independent of the restraint provided by the connector. This may be more clearly seen from Figures 3.2 and 3.3. Another point to note is that it seems a bit unusual that both the wedge retainer and the connector were found to have the same rotational stiffness value. This is considered to be purely coincidental. Closer examination of the actual contact area of the connector revealed a length of 85 mm and a width of 9 mm, whereas the wedge retainer contact area has a length of 139 mm and width of 5.5 mm. Further, the connector's plastic slot was pushed into a depth of 6.5 mm for the full connection whereas the wedge retainers were tightened by a recommended torque of 0.68 Nm. These conditions show that the physical restraints provide by the wedge retainer and the connector are different.

3.6 SUPPORTS FIXITY

From the experimental results, the restraints provided by the wedge retainer and connector may be expressed in terms of non-dimensional rotational spring factors, R_1 and R_2 respectively. Thus R_1 or R_2 may be calculated by multiplying α or β by the length of plate, a, and divided by the plate flexural rigidity, D, respectively. Further, the frequency may also be expressed in terms of a non-dimensional frequency parameter, λ^2. The non-dimensional rotational spring factor for the wedge retainer (R_1) is found to be 102.3 and R_2 is identical to R_1. R_1 may be compared with the non-dimensional

rotational spring factor for wedge retainer reported by Barker and Chen (1993), which was calculated on a per inch basis. They reported a figure, denoted by K, of about 2 for a three-part wedge lock and a figure of approximately 5 for a five-part wedge lock. On an inch basis, the present work has a K value of about 4. The dimensionless frequency parameter for mode 1 gave a value of 14.9.

The restraints provided by the wedge retainer or connector may be defined as a percentage fixity, using the following equation:

$$P = \frac{f_n - f_s}{f_c - f_s} \tag{3.3}$$

where f is the natural frequency and the subscripts c, s, n, correspond to the clamped support, simple support, and experimentally measured (or actual) wedge retainer or connector support. The percentage fixity indicates the fractional increase over a simple support, and 100% fixity indicates a clamped support. Comparing Tables 3.2 and 3.3, it is seen that the frequencies of all five modes lie between the CCCF and SSSF cases. Further, Table 3.2 shows the first mode frequency of f_c and f_s as 93.7 Hz and 51.3 Hz respectively. The percentage fixity is found to be 39.5%. This compares reasonably well to the result reported in Barker and Chen (1993) and indicates that the fixity of the wedge retainer is approximately constant and independent of the natural frequency. This is also true in this case of the plug-in connector.

Mode No.	Vibration Testing (Hz)	FE Model (Hz)	% Difference
1	68.0	68.4	0.58
2	124.0	124.5	0.40
3	203.0	195.4	- 3.74
4	254.0	248.8	-2.04
5	275.0	261.2	- 5.02

Table 3.3 Comparison of characteristic frequencies

3.7 CONCLUDING REMARKS

An accurate FE model to represent the edge supports provided by the wedge retainers and plug-in connector has been formulated. It is found that these supports are best represented as simply supported with rotational spring stiffnesses along their respective axes. The results show that the wedge retainer stiffness predominately affect the frequencies of the first, second, third and fifth modes whereas changes in the connector's stiffness predominantly affect the second, and fourth mode and to a slight extent, the fifth mode frequencies.

The fundamental natural frequency of the PCB supported by two wedge retainers and a plug-in connector can be found by assuming the supports provide a support fixity of 39.5 percent more than the classical simply supported case.

By comparing the FE results with the vibration test results, it may be seen that fine-tuning of the FE model resulted in an average percent difference of only 2.1% and with the first two modes yielding almost the same frequencies as the experimental frequencies.

CHAPTER 4

SENSITIVITY ANALYSIS OF PCB

4.1 INTRODUCTION

Due to the increasing demand for quality and reliability of PCB assemblies, it becomes essential to be able to predict its dynamic characteristics accurately. In the previous chapter, it is shown that the edge supports provided by plug-in connectors or edge retainers should be modelled as simple supports with rotational stiffnesses along their respective axes and not as clamped or simple supports. Therefore, sensitivity analysis is one of the popular methods in structural dynamics analysis and is applicable to the PCB structure.

4.2 EIGENSENSITIVITY ANALYSIS

The importance of obtaining sensitivities for structures stems from the fact that partial derivatives with respect to the system parameters are extremely important for efficient design modifications under given situations. In the 1960s, gradient-based mathematical programming methods, in which derivatives were used to find search directions toward optimal solutions, were applied in optimal control and automated structural design. Brayton and Spence (1980) discussed the early development of the sensitivity theory. More recently, there has been strong interest in promoting systematic structural optimisation as a useful tool for structural design. Early attempts to use optimisation for large structural systems resulted in excessively long and

expensive computer runs. As a consequence, emerging interest in sensitivity analysis has emphasized on efficient computational procedures. So far, researchers have developed and applied sensitivity analysis for analytical model improvement and assessment of design trends so that structural sensitivity analysis has become more than just an utility for optimisation but a versatile design tool in its own right. More recently, researchers in disciplines such as physical chemistry (Hwang et al. 1978) and aerodynamics (Dwyer & Peterson, 1980), have been using sensitivity analysis to assess the effects of parameter variations in the analytical models and to create designs that are insensitive to parameter variations.

From the above discussion, it is apparent that different sensitivity analysis techniques have been developed and applied to structural dynamics analysis. Among these techniques, eigensensitivity analysis is the most popular method which has been used in a variety of engineering disciplines. Some examples are system identification and automated structural optimisation. Eigensensitivity analysis, which include eigenvalue and eigenvector extractions, is the study of changes in system modal properties with respect to physical design parameter variation for structural modifications. By carefully using the calculated sensitivity data provided by eigensensitivity analysis, designers are able to modify structures efficiently and to predict the eigenvalues and eigenvectors of the modified structures.

Jahn (1948) improved on an approximate set of eigenvalues and eigenvectors by deriving the complete formulae of first-order eigenvalue and eigenvector sensitivities for standard eigenvalue problems. Fox and Kapoor (1968) improved this theory by extending it to the case of generalised symmetric eigenvalue problems by considering

changes to physical parameters in the mass and stiffness matrices. However, the method proposed by Fox and Kapoor requires all the modes of the system to be available in order to calculate the required eigenvalue and eigenvector sensitivities. This is sometimes computationally expensive, especially when systems with large dimensions are considered. In order to avoid such difficulties, Nelson (1976) used the modal properties of the rth mode only to calculate the eigenderivatives of that mode. However, when solving the set of linear algebraic equations, Nelson's method requires a matrix inverse of the system dimension for each mode. An improved modal method was proposed by Lim et al. (1987) which aims to approximately derive the required eigenderivatives by using the calculated lower modes and the known flexibility matrix. Recently, eigenvalue and eigenvector derivatives of a general non-defective matrix and of non-linear eigenvalue problems were discussed by Juang et al. (1989) and Liu et al. (1993) respectively. All these methods can be applied to solve eigenvalue and eigenvector sensitivities associated with distinct modes of a system.

The situation concerning repeated frequencies occurs in many physical systems. Perhaps the most common circumstances under which multiple eigenvalues occur are instances where system symmetry exists, such as bladed disk assembly of turbomachinery. To overcome such difficulty, methods for computing the derivatives of repeated eigenvalues have been developed. In the paper by Huang and Rousselet (1980), the sensitivity coefficients of repeated eigenvalue were computed by solving an associated eigensystem formed by the matrix product of the eigenvectors of the repeated eigenvalues and the derivatives of the stiffness and mass matrices with respect to the specific design variable.

In recent years, a number of methods have been published in the literature to deal with the analytical model improvement by correlating the analytical model with measured modal data. A comprehensive survey is given by Mottershead and Friswell (1993). The philosophy behind this practice is that the analytical model, while containing modelling errors, is assumed to represent the structure with reasonable accuracy so that the limited measured test data available will offer the possibility of updating it. Based initially on the assumption that the mass matrix is correct, Baruch and Itzhack (1978) and Baruch (1978) introduced a type of objective function together with an orthogonality condition so that the analytical modes are optimized in such a way that they are closest to the measured ones in a weighted Euclidean sense. These optimised analytical modes could then be used to derive updated stiffness and flexibility matrices. Berman (1979) later extended the theory to the case of mass updating as well. Having recognized the mathematical difficulty of complete system updating, He and Ewins (1986) used simple eigendynamic equations to locate the major modelling errors first and then employ the limited measured modes to turn the updating problem into an overdetermined one.

In the present study, the major modelling errors are due to the simulation of the spring stiffnesses at the boundary supports. Eigensensitivity analysis is used to improve the finite element model of the PCB structure. The technique involves the correlation of two different sets of data containing resonance frequencies and mode shapes of the same structure. One set of data will result from finite element analysis while the other set will be from vibration test data. The joint stiffnesses are updated in an iterative process until correlation between predicted and measured data sets is optimal.

4.3 MODAL SENSITIVITIES

Modal sensitivities are the derivatives of the modal properties of a dynamic system with respect to chosen structural variables. Methods for calculating eigenderivatives have been well documented (Brandon, 1990) and is briefly discussed here for the first order sensitivities.

The matrix representation of an eigenvalue problem is

$$[K]\{\phi\}_i - \lambda_i [M]\{\phi\}_i = \{0\} \tag{4.1}$$

where [M] is symmetric and positive-definite and can be decomposed as

$$[M] = [L][L]^T \tag{4.2}$$

and [L] is a non-singular lower triangular matrix. Upon substitution equation (4.2) into equation (4.1)

$$[K]\{\phi\}_i - \lambda_i [L][L]^T \{\phi\}_i = \{0\} \tag{4.3}$$

Premultiply both sides of equation (4.3) by $[L]^{-1}$ gives

$$[L]^{-1}[K]\{\phi\}_i - \lambda_i [L]^T \{\phi\}_i = \{0\} \tag{4.4}$$

Let $\{z\}_i = [L]^T \{\phi\}_i$ and substitute into equation (4.4), then

$$[L]^{-1}[K][L]^{-T}\{z\}_i - \lambda_i\{z\}_i = \{0\} \tag{4.5}$$

Since $[L]^{-1}[K][L]^{-T}$ is real and symmetric, the complete set of eigenvectors of $\{z\}_i$ forms a complete orthogonal base, regardless of the existence of repeated modes (Golub and Van Loan, 1983). On the other hand, since [L] is non-singular, $[\phi] = [L]^{-T}[z]$ forms a complete linearly independent base.

Differentiating equation (4.1) with respect to the r^{th} design variable p_r gives

$$([K] - \lambda_i[M])\frac{\partial \phi_i}{\partial p_r} + \left(\frac{\partial [K]}{\partial p_r} - \lambda_i \frac{\partial [M]}{\partial p_r} - \frac{\partial \lambda_i}{\partial p_r}[M]\right)\{\phi\}_i = \{0\} \tag{4.6}$$

Assume that $\{\phi\}_i$ is normalised such that

$$\{\phi\}_i^T [M] \{\phi\}_i = 1 \tag{4.7}$$

Multiply both sides of equation (4.6) by $\{\phi\}_i^T$ and using equation (4.1) and equation (4.7), then

$$\frac{\partial \lambda_i}{\partial p_r} = \{\phi\}_i^T \frac{\partial [K]}{\partial p_r}\{\phi\}_i - \lambda_i \{\phi\}_i^T \frac{\partial [M]}{\partial p_r}\{\phi\}_i \tag{4.8}$$

From equation (4.8) it can be seen that the eigenvalue derivative is determined by the mode itself. Since, the complete set of eigenvectors is linearly independent, the i^{th} eigenvector derivative which is a vector can be expressed as a linear combination of all the eigenvectors of the system:

$$\frac{\partial\{\phi\}_i}{\partial p_r} = \sum_{j=1}^{N} \beta_{ij} \{\phi\}_j \tag{4.9}$$

In order to calculate the coefficients β_{ij}, substitute equation (4.9) into equation (4.6) and pre-multiply equation (4.6) by $\{\phi\}_j^T$, then

$$\{\phi\}_j^T([K]-\lambda_i[M])\sum_{j=1}^{N}\beta_{ij}\{\phi\}_j + \{\phi\}_j^T\left(\frac{\partial[K]}{\partial p_r} - \lambda_i\frac{\partial[M]}{\partial p_r} - \frac{\partial\lambda_i}{\partial p_r}[M]\right)\{\phi\}_i = \{0\} \tag{4.10}$$

For $j \neq i$, equation (4.10) can be simplified to give

$$\beta_{ij} = \frac{\{\phi\}_j^T\left(\frac{\partial[K]}{\partial p_r} - \lambda_i\frac{\partial[M]}{\partial p_r}\right)\{\phi\}_i}{\lambda_i - \lambda_j} \qquad for \quad j \neq i \tag{4.11}$$

For j = i, β_{ii} can be computed from the mass-normalisation condition. Differentiating equation (4.7) gives

$$\{\phi\}_i^T\frac{\partial[M]}{\partial p_r}\{\phi\}_i + 2\{\phi\}_i^T[M]\frac{\partial\{\phi\}_i}{\partial p_r} = 0 \tag{4.12}$$

Substitute equation (4.9) into equation (4.12), then β_{ii} becomes

$$\beta_{ii} = -\frac{1}{2}\{\phi\}_i^T\frac{\partial[M]}{\partial p_r}\{\phi\}_i \tag{4.13}$$

4.4 IMPLEMENTATION OF MODAL SENSITIVITIES TO MODEL TUNING

The strategy uses the modal sensitivities directly to predict the effects of proposed structural changes. Based on the Taylor series expansion limited to the linear term, the relationship between the change of modal parameter $\Delta\xi$ ($\Delta\xi$ can be the change of eigenvalue or any eigenvector element) and the vector, $\{\Delta p\}$, representing the change in structural parameters can be expressed as:

$$\Delta\xi = \sum_{i=1}^{L} s_i \Delta p_i \tag{4.14}$$

where s_i are the first order modal sensitivities and L is the number of structural parameters considered for the updating process. In practice, if n (number of measured degrees of freedom) out of N (the total number degrees of freedom specified in the finite element model) degrees of freedom have been measured (n<N) for the i^{th} mode, then equation (4.14) is written as:

$$\begin{bmatrix} \frac{\partial\{\phi_a\}_i}{\partial p_1} & \frac{\partial\{\phi_a\}_i}{\partial p_2} & \cdots & \frac{\partial\{\phi_a\}_i}{\partial p_L} \\ \frac{\partial(\lambda_a)_i}{\partial p_1} & \frac{\partial(\lambda_a)_i}{\partial p_2} & \cdots & \frac{\partial(\lambda_a)_i}{\partial p_L} \end{bmatrix} \begin{Bmatrix} \Delta p_1 \\ \Delta p_2 \\ \cdot \\ \Delta p_L \end{Bmatrix} = \begin{Bmatrix} \{\phi_e\}_i - \{\phi_a\}_i \\ (\lambda_e)_i - (\lambda_a)_i \end{Bmatrix} \tag{4.15}$$

When m modes are measured, then equation (4.15) is modified to become

$$\begin{bmatrix} \frac{\partial\{\phi_a\}_1}{\partial p_1} & \frac{\partial\{\phi_a\}_1}{\partial p_2} & \cdots & \frac{\partial\{\phi_a\}_1}{\partial p_L} \\ \frac{\partial(\lambda_a)_1}{\partial p_1} & \frac{\partial(\lambda_a)_1}{\partial p_2} & \cdots & \frac{\partial(\lambda_a)_1}{\partial p_L} \\ \cdot & \cdot & \cdots & \cdot \\ \cdot & \cdot & \cdots & \cdot \\ \frac{\partial(\phi_a)_m}{\partial p_1} & \frac{\partial(\phi_a)_m}{\partial p_2} & \cdots & \frac{\partial(\phi_a)_m}{\partial p_L} \\ \frac{\partial(\lambda_a)_m}{\partial p_1} & \frac{\partial(\lambda_a)_m}{\partial p_2} & \cdots & \frac{\partial(\lambda_a)_m}{\partial p_L} \end{bmatrix} \begin{Bmatrix} \Delta p_1 \\ \Delta p_2 \\ \cdot \\ \cdot \\ \cdot \\ \Delta p_L \end{Bmatrix} = \begin{Bmatrix} \{\phi_e\}_1 - \{\phi_a\}_1 \\ (\lambda_e)_1 - (\lambda_a)_1 \\ \cdot \\ \cdot \\ \{\phi_e\}_m - \{\phi_a\}_m \\ (\lambda_e)_m - (\lambda_a)_m \end{Bmatrix} \tag{4.16a}$$

$$[S]\{\Delta p\} = \{\Delta\xi\} \tag{4.16b}$$

When all the m measured modes are used, the total number of linear algebraic equations involved in equation (4.16) becomes mx(n+1) since each mode provides (n+1) equations. If, in equation (4.16), the number of equations equals the number of parameters L, Δp can be directly found by simple inversion of the sensitivity matrix.

$$\{\Delta p\} = [S]^{-1}\{\Delta\xi\} \tag{4.17}$$

In practice, this is usually not the case. The exact solution of Δp cannot be obtained directly and an iterative procedure has to be introduced as shown in Figure 4.1. After Δp has been calculated, the analytical model can be updated and the sensitivity matrix [S] is recalculated. Such process is repeated until the new calculated Δp becomes sufficiently small in its Euclidean norm as shown in Figure 4.1.

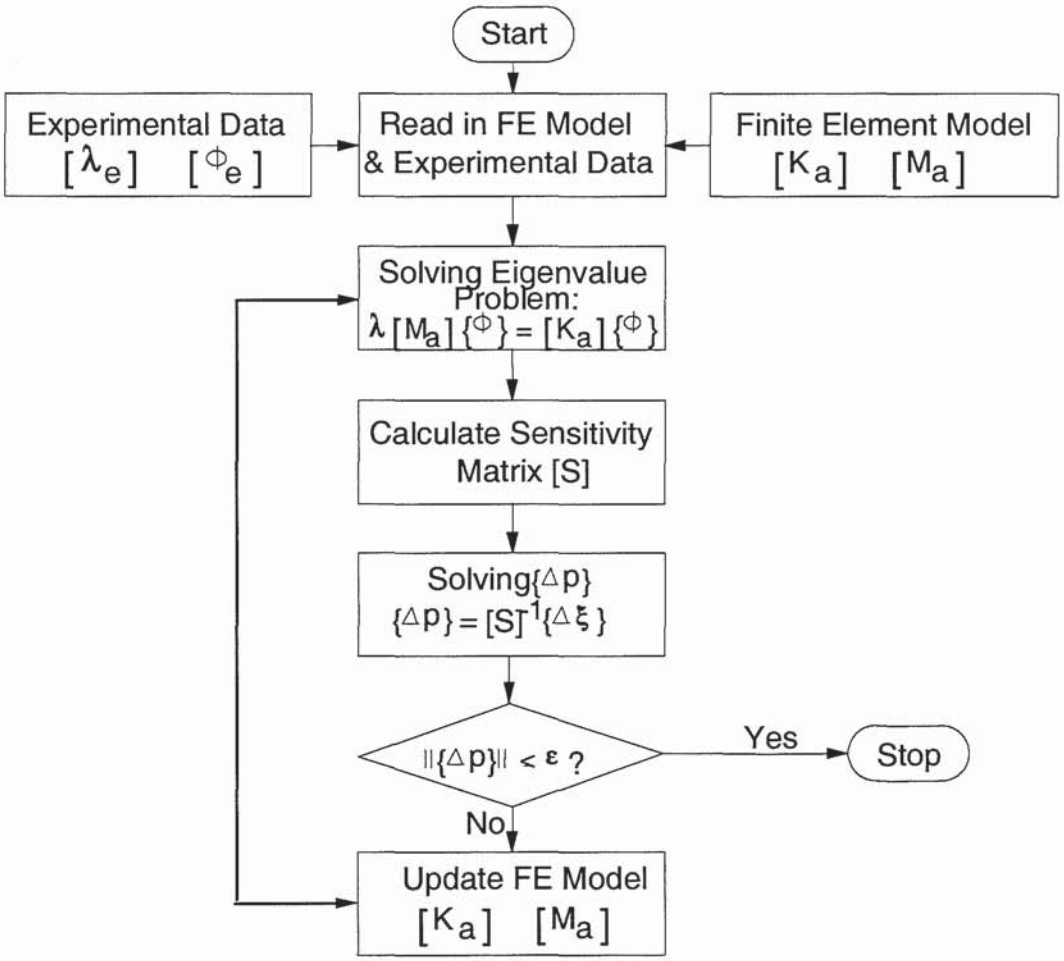

Figure 4.1 Flow Chart for Finite Element Model Tuning

4.5 CASE STUDIES

This section implements the methodologies of the preceding sections. In particular, two case studies are presented. The first is aimed at demonstrating the model tuning method for a PCB with mathematically modelled partially clamped edges on three sides, which in practice is supported by two wedge retainers and a plug-in connector. The second case, applies the technique to develop an accurate representation of the support locations of a PCB.

In both case studies, it is assumed that no mass errors exist in the finite element models. This brings about large simplifications in the equations in the theory. For example, equation (4.8) is simplified and equation (4.13) is reduced to zero.

4.5.1. Case 1: Printed Circuit Board with Assumed Clamped Edges

A rectangular epoxy fibreglass plate is used to demonstrate the effectiveness of the model tuning method in updating the initial boundary conditions from simple supports to clamped supports at all the support locations as indicated by circles and triangles in Figure 3.1. The properties of the plate are elastic bending modulus of 17 GPa, Poisson's ratio of 0.12, density of 1870 kg/m^3, thickness of 1.58mm and sides 220 mm by 233.4 mm.

The first part of this case study is to obtain the first five natural frequencies and mode shapes from the finite element clamped edge boundary condition solution (CCCF) and use them as the reference data for model updating. The fibreglass plate was modelled using four noded quadrilateral flat shell elements (MacNeal, 1978) with 110 elements (10 x 11 mesh). The finite element mesh is shown in Figure 3.1.

As a basis solution for modification, simple support conditions are assumed at the support locations of the initial finite element model (SSSF). In addition, weak rotational springs along the direction of the plate edges were added at the support locations. All the initial rotational spring stiffnesses were set at 100 Nmm/rad for the FEM model. These rotational springs were chosen as the only two parameters for tuning in the automatic model updating process, that is, parameter 1 represents the

rotational spring stiffness along the x direction at the five "Δ" locations and parameter 2 represents the rotational spring stiffness along the y direction at the sixteen circled locations.

4.5.2. Case 1: Results and Discussion

Table 4.1 summarises the natural frequencies between the initial finite element model (SSSF) and the reference data (CCCF). The corresponding superimposed view of the paired mode shapes are shown in Figures 4.2a - 4.2e and the corresponding Modal Assurance Criterion (MAC) matrix (Ewins, 1984) is tabulated and illustrated in Table 4.2. As can be seen from the results, the mode shapes are closely related with high MAC values even before any tuning. The untuned natural frequencies have high order of inaccuracies in the region of 45%. The high errors are due to the difference in the boundary conditions between the SSSF model and the reference model (CCCF).

The updated frequencies from the model tuning process is shown in Table 4.1, and the updated rotational spring stiffnesses at the 7^{th} iteration are given as 0.733×10^8 Nmm/rad and 0.458×10^6 Nmm/rad for parameters 1 and 2 respectively. It may be seen that the fine-tuning of the rotational springs characterisations at the support locations results in a percentage difference in frequencies of less than 0.5% after only seven iterations. The rate of convergence for the five modes is illustrated in Figure 4.3. Note that, after only 4 iterations, the percentage difference in frequencies is less than 1.5%. The convergence for the MAC matrix is even more remarkable with MAC values of more than 99.6% for all the five modes after the first iteration. The MAC matrix before and after one iteration is illustrated in Figures 4.4a and 4.4b respectively.

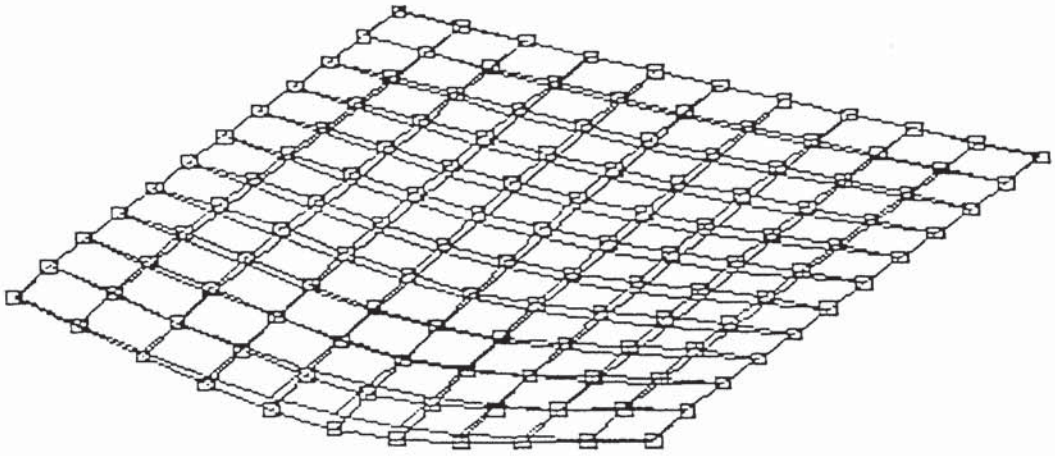

Figure 4.2a Case 1 – superimposed view 1st mode (MAC = 91.5%)
Initial model (SSSF) / Reference data (CCCF)

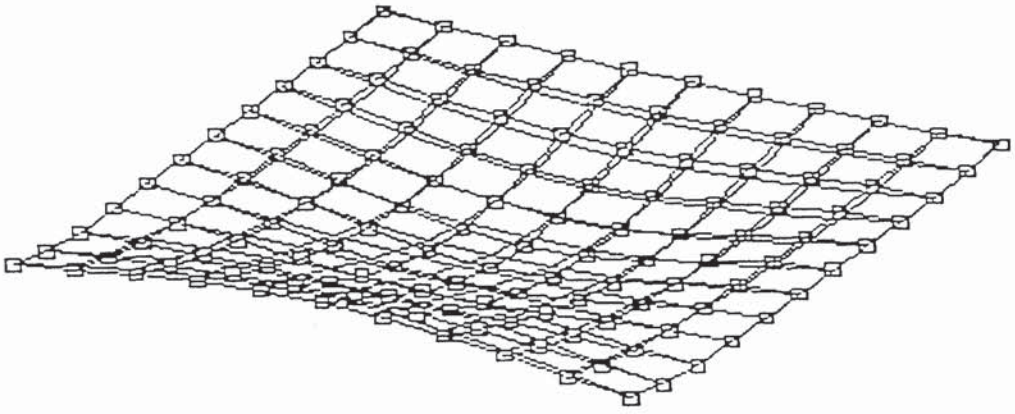

Figure 4.2b Case 1 – superimposed view 2nd mode (MAC = 88.5%)
Initial model (SSSF) / Reference data (CCCF)

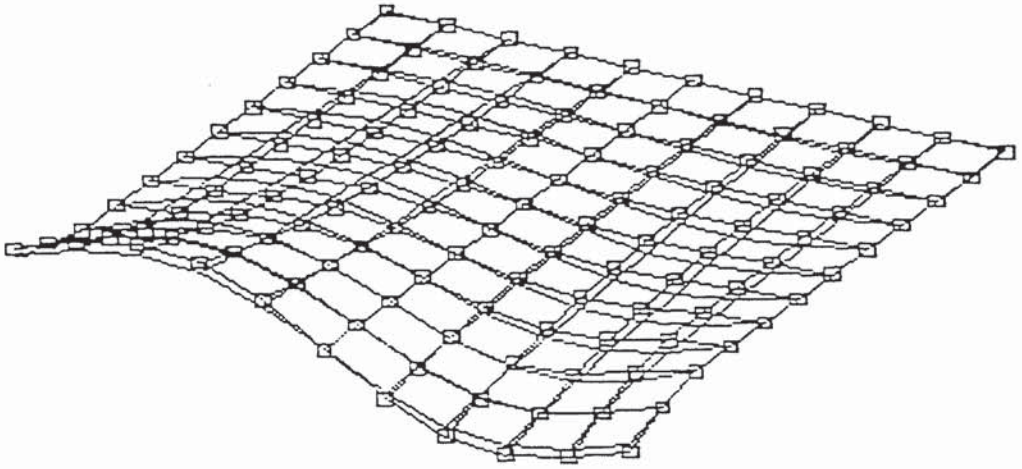

Figure 4.2c Case 1 – superimposed view 3rd mode (MAC = 84.3%)
Initial model (SSSF) / Reference data (CCCF)

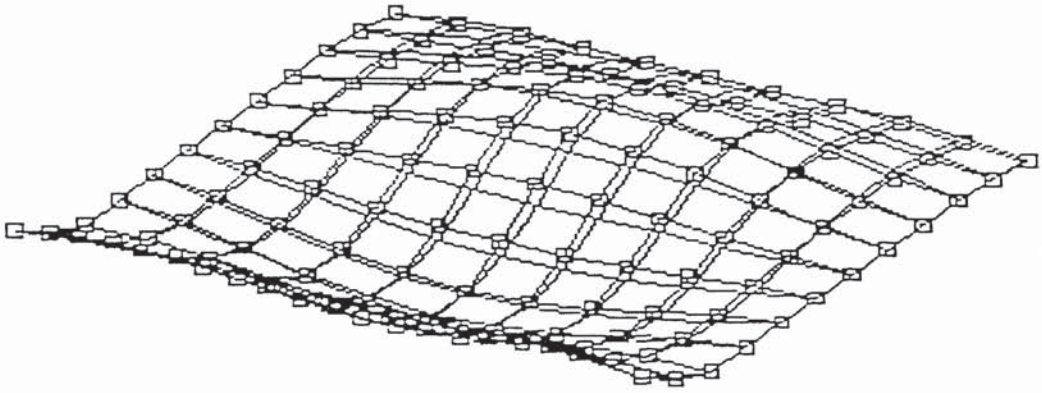

Figure 4.2d Case 1 – superimposed view 4th mode (MAC = 89.4%)
Initial model (SSSF) / Reference data (CCCF)

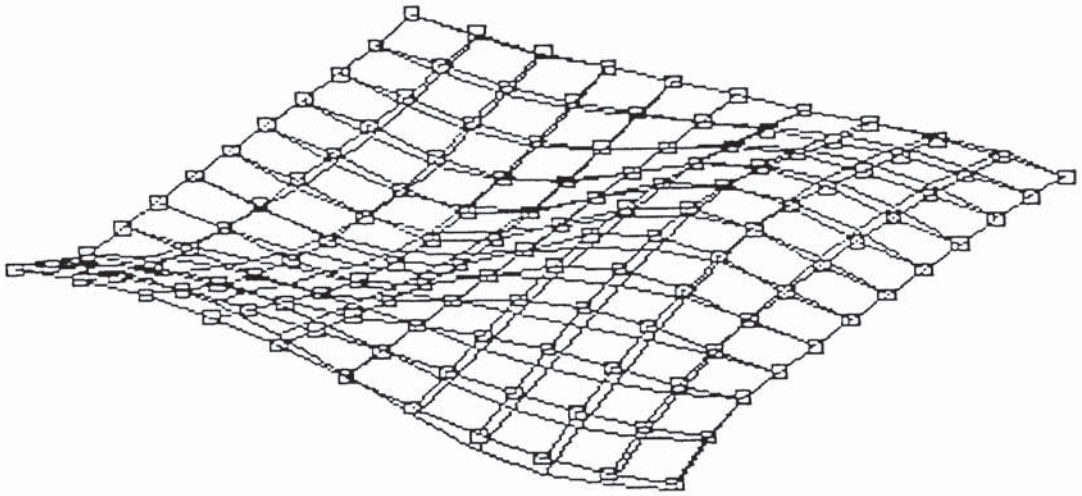

Figure 4.2e Case 1 – superimposed view 5th mode (MAC = 80.7%)
Initial model (SSSF) / Reference data (CCCF)

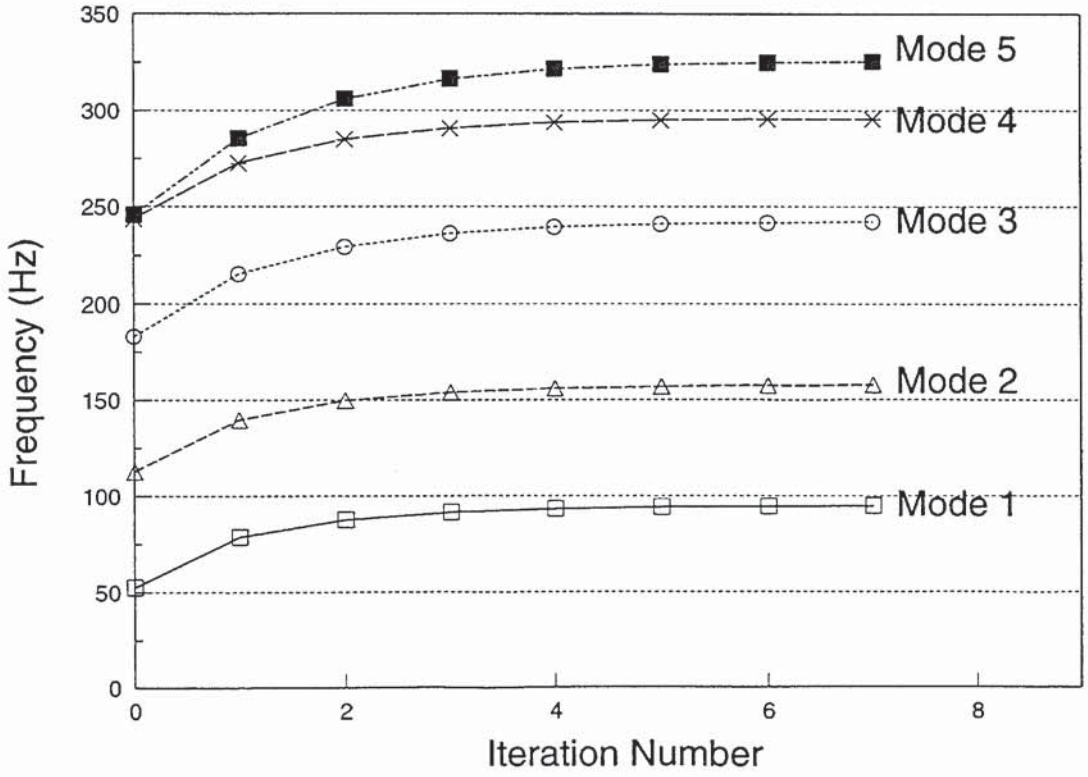

Figure 4.3 Case 1 - variation of frequency against iteration

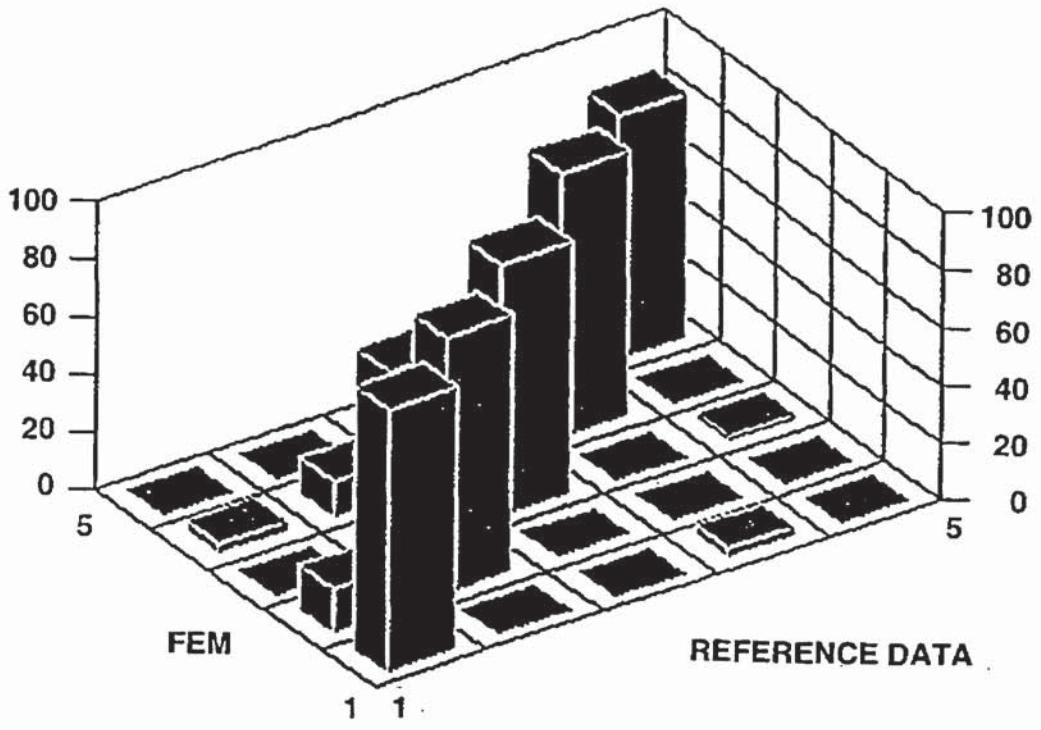

Figure 4.4a Case 1 - MAC matrix before iteration

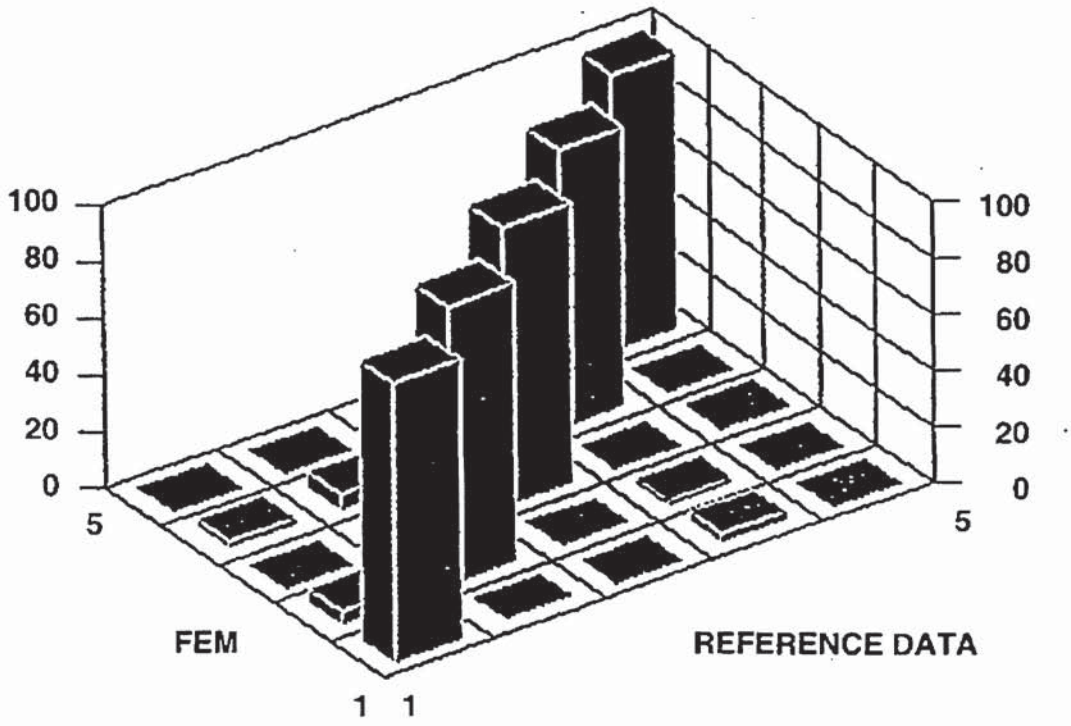

Figure 4.4b Case 1 - MAC matrix after 1 iteration

Mode No:	Reference Data (CCCF) (Hz)	SSSF Model Before Tuning (Hz)	% Diff.	SSSF Model After Tuning (7^{th} Iteration) (Hz)	% Diff.
1	94.53	52.28	-44.69	94.59	0.06
2	158.55	112.53	-29.03	157.83	-0.45
3	242.02	183.20	-24.31	242.20	0.07
4	296.63	243.93	-17.77	295.58	-0.36
5	326.68	245.66	-24.80	325.12	-0.48

Table 4.1. Case 1 - natural frequencies before and after tuning
(model updating process based on CCCF frequencies and mode shapes).

SSSF/CCCF Mode No	1	2	3	4	5
1	91.5	0.8	0.0	3.2	0.0
2	16.1	88.5	0.0	0.1	0.0
3	0.0	0.0	84.3	0.0	3.4
4	4.0	13.3	0.0	89.4	0.0
5	0.0	0.0	25.8	0.0	80.7

Table 4.2. Case 1 - modal assurance criterion matrix (MAC Values):
initial model (SSSF)/reference data (CCCF).

The overall rate of convergence for the above analysis is also illustrated in Figure 4.5 (solid line) by plotting the average absolute percentage error in frequencies for the 5 modes considered in the analysis against iteration where the average absolute percentage error is defined as:

$$\frac{1}{5}\sum_{i=1}^{5} abs\left(\frac{\omega_e - \omega_a}{\omega_e}\right)_i * 100 \tag{4.18}$$

ω_e is the reference data (experimental frequency) and ω_a is the computed frequency from the finite element analysis. The subscript i indicates the mode in question.

As the first five mode shapes for the case 1 plate structure are very similar between the CCCF supports and the SSSF supports, it is worth considering an analysis, where the model updating process is based only on the reference (or experimental) frequencies. This is due to the fact that in an actual test environment, the natural frequencies can be easily obtained with high accuracy but the process of deriving the experimental mode shapes are more complex and will usually contain noise. Even with good experimental technique, it is often the case that each of the individual elements of a mode shape vector will contain relatively high levels of noise but the general shape of the mode will be quite accurate.

The dotted line in Figure 4.5 shows the average absolute percentage error versus the number of iterations for the modal updating procedure which did not include the reference (or experimental) mode shapes in the analysis. All five reference frequencies were used in the analysis. As expected, the rate of convergence is much

slower but will still converge to the reference values. Although, the rate of convergence is slower, the overall time taken for the whole model updating process is reduced substantially. This is due to the fact that the time taken to obtain the experimental data will be substantially reduced as the experimental mode shapes are not required. Furthermore, in terms of computational requirements, the number of equations in equation (4.16) is reduced from mx(n+1) equations to m equations, where m(=5) is the number of modes considered and n(=375) is the total number of degrees of freedom in the CCCF model. The updated frequencies from the model tuning process after the 5^{th}, 10^{th}, 15^{th} and 20^{th} iterations are shown in Table 4.3. The updated rotational spring stiffnesses at the 20^{th} iteration are given as 0.826×10^5 Nmm/rad and 0.397×10^6 Nmm/rad for parameters 1 and 2 respectively.

4.5.3. Case 2: Printed Circuit Board with in-service Support Conditions

Figure 3.5 shows the PCB assembly mounted onto an electromagnetic shaker. The test fixture holding the PCB structure was designed to ensure that the test fixture will hold the PCB assembly in a manner as close as possible to its actual in-service environment. In addition, it was ensured that the fixture design has no untoward fixture resonance over the range of the required experimental frequencies. In this case, the assembled test fixture have a resonant frequency of 1900 Hz, which was well above the frequency range of the vibration tests. The PCB, which has a dimension of 220 mm x 233.4 mm and a thickness of 1.58 mm, was made of fiberglass, known as FR-4. The material properties are the elastic bending modulus of 17 GPa, Poisson's ratio of 0.12 and density of 1870 kg/m^3. One edge of the PCB was soldered onto a 96-pin connector, which was plugged into a 96-pin socket, mounted rigidly in the test

fixture. The wedge retainer used was the CALMARK series 225 - "card-lok" retainer, with a full length of 153 mm. The two wedge retainers were tightened to the manufacturer's recommended torque of 0.68 Nm.

The finite element mesh is the same as Case 1 but using actual in-service boundary conditions for this case. The two wedge retainers were modelled as simply supported with rotational springs along their respective edges in both the x and y axes (α_x, α_y). As may be inferred from Figure 3.1, the dominant rotational stiffness for the wedge retainers is α_y. α_y provides stiffness in bending due to the presence of the wedge retainers and is set to an initial value of 100 Nmm/rad. The other rotational springs α_x are parallel to the line of supports for the wedge retainers and can be inferred to have minimal effect on the simulation of the boundary conditions. This is due to the fact that simple supports are already considered along the nodal positions as indicated in Figure 3.1. α_x was set to a value of 10^9 Nmm/rad during the model tuning exercise. Similarly, the plug-in connector was also modelled as simple supports with rotational springs along its edge in both the x and y axes (β_x, β_y). β_x is the controlling parameter for this joint. The initial value of β_x is also set to 100 Nmm/rad. Similarly, β_y which runs parallel to the connector edge was set to a value of 10^9 Nmm/rad.

4.5.4. Case 2: Results and Discussion

The frequencies of the first five modes of the PCB structure obtained under vibration testing were found to be 68, 124, 203, 254 and 275 Hz, respectively. These

experimental frequencies were used as reference data for model updating. No experimental mode shapes were used in the model updating procedure. When using only modal frequencies in model improvement, equation (4.16) is very much simplified. In this particular application, the number of equations is reduced from mx(n+1) to m equations, where m=5. But, if experimental mode shapes are used in the analysis and if all the normal displacements of the PCB structure except the 21 support locations are measured (see Figure 3.1), that is, n=111, then the number of equations required for equation (4.16) is 560.

The dominant stiffnesses of the rotational springs which characterised the joints due to the wedge retainers α_y and the plug-in connector β_x were selected as the two parameters used for the model updating program. In using only two parameters for updating, this again simplifies the analysis. Hence, the sensitivity matrix [S] of

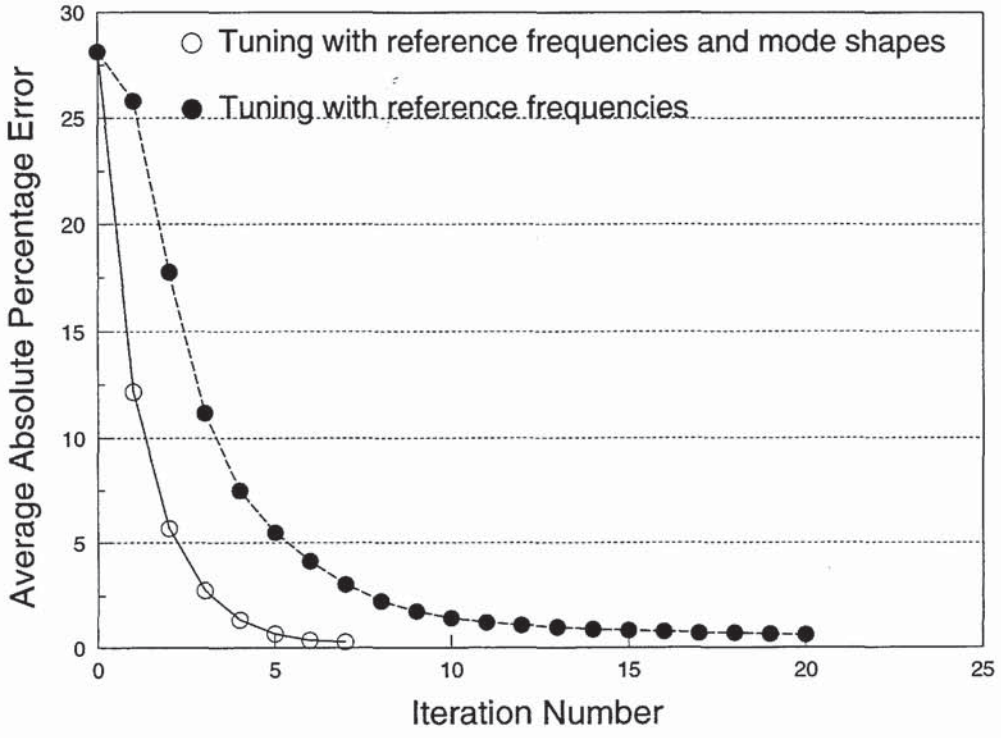

Figure 4.5 Case 1 - rate of convergence

Mode No.	Reference Data (CCCF) (Hz)	FE Model after Tuning (Hz)			
		5^{th} Iteration	10^{th} Iteration	15^{th} Iteration	20^{th} Iteration
1	94.53	92.15	94.14	94.38	94.48
2	158.55	143.97	154.92	156.40	156.84
3	242.02	238.74	241.43	241.91	242.06
4	296.63	265.69	285.96	291.75	292.87
5	326.68	313.71	321.67	323.72	324.21

Table 4.3. Case 1 - natural frequencies at different iterations (model updating process based on reference frequencies).

Mode No	Experimental Freq. (Hz)	Original Freq. (Hz)	% Diff.	Updated Freq. (Hz)	% Diff.
1	68	52.9	-22.3	68.9	1.3
2	124	112.0	-9.7	124.7	0.6
3	203	182.2	-10.3	202.4	-0.3
4	254	242.6	-4.5	253.3	-0.3
5	275	244.2	-11.2	266.4	-3.1

Table 4.4. Case 2 - natural frequencies before and after tuning (PCB structure with in-service support conditions).

equation (4.16) has dimensions of 5 x 2, where 5 is the number of modal frequencies considered and 2 is the number of parameters.

Table 4.4 summarises the resonance frequencies of the FEM before and after the tuning process. It can be seen from Table 4 that significant improvement in the ability of the FEM to represent the joint characteristics has been achieved. The converged rotational spring stiffnesses are shown in Table 4.5. The converged stiffnesses for α_y and β_x are 2950 and 963 Nmm/rad respectively. This is consistent with the fact that both wedge retainers gave firm grips along the two edges of the PCB whereas the connector/socket provided very minute rotational restraint and is considered to be very close to a simply supported edge. In fact, when the PCB was supported just by the connector and mounted horizontally, the board deflected by a large inclination angle to the horizontal. However, when the board is supported by just one wedge retainer, the deflection angle of the board is very small. To test the validity of the original assumption for α_x and β_y which assumes that these rotational stiffnesses have minimal effect on the dynamics of the structure, simulation runs were conducted. The results of the simulation runs as shown in Table 4.6 confirms this assumption.

Wedge Stiffness (Nmm/rad)		Connector Stiffness (Nmm/rad)	
α_x	α_y	β_x	β_y
10^9	2950	963	10^9

Table 4.5. Case 2 - converged rotational springs stiffnesses.

Mode No	$\alpha_x = 0$ $\beta_y = 10^9$ (Hz)	$\alpha_x = 10^9$ $\beta_y = 0$ (Hz)	$\alpha_x = 0$ $\beta_y = 0$ (Hz)
1	68.6	68.9	68.6
2	123.6	124.7	123.3
3	199.9	202.4	199.9
4	250.6	253.2	250.6
5	263.6	266.3	263.6

Table 4.6. Case 2 - effect of α_x and β_y on natural frequencies ($\alpha_y = 2950$, $\beta_x = 963$)

4.6 CONCLUDING REMARKS

Dynamic finite element modelling can be an effective tool in the study of engineering structures. This chapter shows that by using an eigensensitivity method, the rotational stiffnesses representing the boundary supports of a PCB structure can be updated effectively and shown to be capable of representing the dynamics of the PCB structure accurately. The result shows that the percentage error in the fundamental frequency of the PCB finite element model is found to be substantially reduced from 22.3% to 1.3%.

The procedure demonstrated the effectiveness of using only the vibration test frequencies as reference data when the mode shapes of the original untuned model are almost identical to the referenced modes/experimental data. When using only modal frequencies in model improvement, the analysis is very much simplified. That is, in terms of computational requirements, the number of equations in equation (4.16) is m equations, where m is the number of modal frequencies considered for the analysis. Furthermore, the time taken to obtain the experimental data will be substantially reduced as the experimental mode shapes are not required.

CHAPTER 5

POINT CONSTRAINT ON BEAM STRUCTURE

5.1 INTRODUCTION

The vibration analysis of beams and plates have attracted the interest of many researchers. Depending on the boundary condition in which the beam or plate is supported, i.e., free, simply-supported or clamped support, it is possible to determine the natural frequencies and mode shapes through the use of the Rayleigh-Ritz method (Shames & Dym, 1982).

However, point supported beams and plates have non-classical boundary conditions and cannot be solved using the above method. Chi (1972) proposed analytical solutions for the vibration modes of a circular plate having three simple support points on the circumference. Irie and Yamada (1978) presented a theoretical method to analyse free vibrations of circular plates having some elastic supports at some points. They also show the natural frequencies and mode shapes for circular plates having a simple support at a single internal point, and also results for circular plates simply-supported at three equally-spaced interior points. Gorman (1982) applied an analytical method based on the principle of superposition to analyse the free vibration of rectangular plates with various point supports. However, his method is limited to symmetrically distributed point supports. Using the Rayleigh-Ritz method and simple polynomial co-ordinate functions, Cortinez and Laura (1986) calculated the fundamental frequency of a clamped or simply supported circular plate at the centre.

Azimi (1989) used the modal expansion technique and the receptance method to formulate the axisymmetric frequency and mode shape equations for circular plates with free, simply supported or clamped outer boundary and an elastic or rigid point support. According to the results shown by Azimi, this method showed poor convergence similar to that exhibited by a Fourier series approximation of an impulse function. More recently, Pitarresi and Di Edwardo (1993) have described a sequential search approach to successively move from one set of support locations on a rectangular plate to the next. However, their result is dependent on the initial guess and the number of iterations necessary for convergence to an optimal solution. Therefore, the time taken for the analysis can be prohibitive. Cheung and Zhou (1999) analysed the vibrations of symmetrically rectangular composite plates with point supports using static beam functions that satisfy the boundary conditions and point-support conditions. Their method was found to be computationally intensive.

This chapter describes the approach to analyse the free vibration of beams with the objective of determining the location of the point supports that would yield the maximum percentage increase in the fundamental natural frequency of a beam structure.

5.2 METHODOLOGY

5.2.1 Cantilever Beam with a Point Support

The methodology used is illustrated using a simple cantilever beam. A cantilever beam is a beam clamped on one end with the other end free. Equations for determining its natural

frequencies and mode shapes are available from many textbooks on vibration analysis (Blevins, 1979).

The natural frequency, f_i, for a beam may be calculated by the following equation:

$$f_i = \frac{\lambda_i^2}{2\pi L^2}\left(\frac{EI}{m}\right)^{\frac{1}{2}} \tag{5.1}$$

where L is the span;

E is the modulus of elasticity;

I is the moment of inertia about the neutral axis;

λ_i is the eigenvalue obtained from standard table;

m is the mass per unit length.

The dynamic response of a structure under force excitation can be written as a summation of the contributions from its normal modes. For example, the response, $\{x(t)\}$, for an n-degree-of-freedom system can be written as:

$$\{x(t)\} = \{\phi_1\}q_1(t) + \{\phi_2\}q_2(t) + \{\phi_3\}q_3(t) + \ldots\ldots + \{\phi_n\}q_n(t) \tag{5.2}$$

where $\{\phi_i\}$ is the i^{th} mode shape

and $q_i(t)$ represents the contribution from the i^{th} mode.

Consider the case, where additional supports are added on to an existing structure so as to increase the structural stiffness and thereby increase its fundamental frequency to an acceptable level. In this case, the mechanical designer is faced with the task of optimising

the locations of a given number of point supports for the maximum increase in the structure's fundamental frequency.

The method advocated here assumes that the ideal positions for the additional supports should be placed at locations, which will sweep out the maximum number of lower modes as possible from equation (5.2). Furthermore, the supports should be placed along the nodes of the highest possible mode from the original configuration, so that all the other lower modes are eliminated by the introduction of the extra supports to the structure.

To illustrate the proposed methodology, consider the flexural vibration of a uniform cantilever beam as shown in Figure 5.1a. If only one extra simple support is to be added to the uniform cantilever beam structure, mathematically, it is only possible to eliminate the lowest mode shape $\{\phi_1\}$ from equation (5.2). As shown in Figure 5.1a, it is evident that the lowest mode shape of Figure 5.1b will be swept out if the additional simple support is located at the nodal point of the second mode. By placing the additional support at the nodal point of the second mode, the new configuration will converge to the second mode of transverse vibration as shown in Figure 5.1c. The fundamental frequency of the beam after the imposed constraint will be raised from $\frac{3.516}{L^2}\left(\frac{EI}{\rho A}\right)^{1/2}$ to $\frac{22.03}{L^2}\left(\frac{EI}{\rho A}\right)^{1/2}$.

For a simplified justification of the proposed technique, consider the case where the extra point support is located at the end of the cantilever. This choice of support location is reasonable as the end of the cantilever has the highest relative deflection amplitude of the fundamental frequency. But in placing the support at the free end, the fundamental frequency of the altered structure is $\frac{15.42}{L^2}\left(\frac{EI}{\rho A}\right)^{1/2}$.

By introducing a point constraint at the free end of the cantilever beam, the eigenvalue of the beam increases to 15.42 (under clamped-pinned boundary condition). Since the area moment of inertia, the modulus of elasticity and the span of the beam are unchanged, the percentage increase in fundamental frequency can be simply calculated as follows:

$$\% \text{ increase} = \frac{22.03 - 15.42}{15.42} \text{ x } 100\%$$

$$= 86.83\% \qquad (5.2)$$

Clearly, it can be seen that placing the support at the nodal position of mode 2 is far more superior than placing it at the free end. However, the justification for the above procedure will be fully illustrated from the results in section (5.3) on numerical examples.

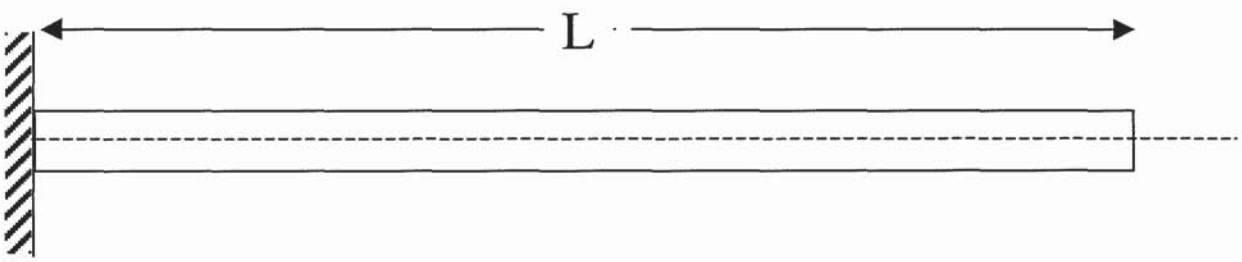

Figure 5.1a A uniform cantilever

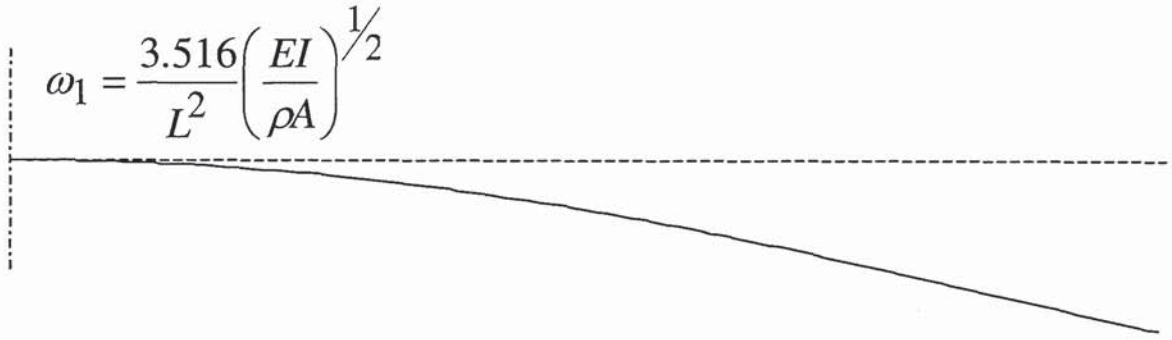

Figure 5.1b First mode of transverse vibration of a uniform cantilever

5.2.2 Beam with Two Supports

Consider the case where two extra simple supports are added on to the original cantilever. In this circumstance, the supports should be placed at the two nodal positions of mode 3 as shown in Figure 5.1d. With the two extra supports at the stated positions, the fundamental frequency will then be raised to $\frac{61.70}{L^2}\left(\frac{EI}{\rho A}\right)^{1/2}$. The first two lower modes of the original structure will be swept out and the fundamental mode shape of the new configuration will then be exactly the same as the third mode of the original cantilever structure. In general, the proposed method advocates that additional supports should be placed at the nodal positions of the next lowest mode of the original structure which is not eliminated by the introduction of the extra supports to the

structure. Hence, the fundamental frequency of the new configuration will be forced to converge to this particular mode.

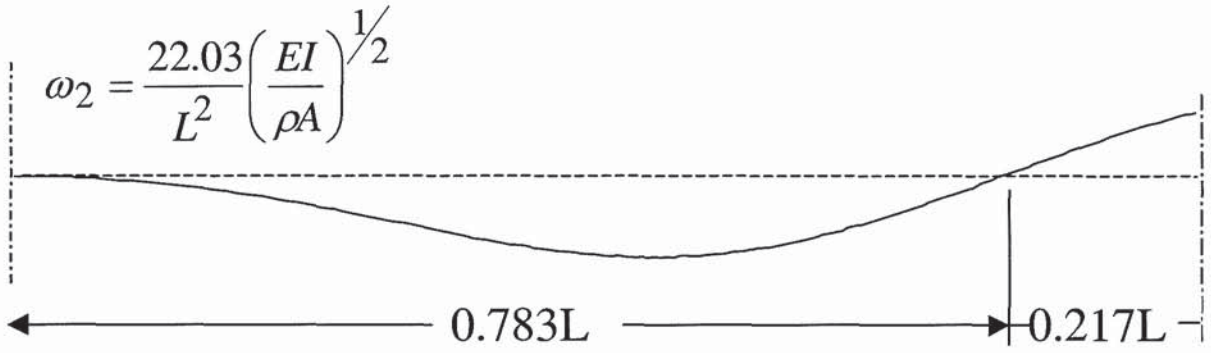

Figure 5.1c Second mode of transverse vibration of a uniform cantilever

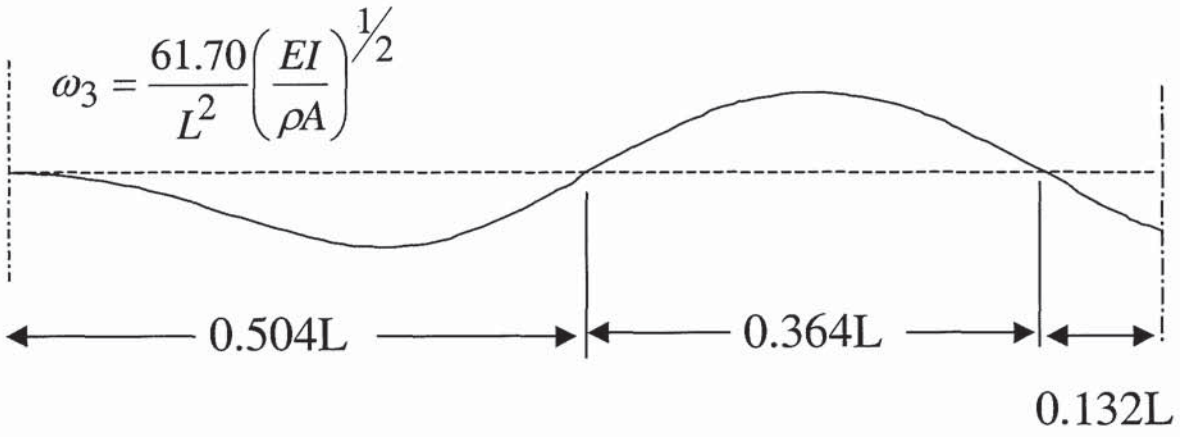

Figure 5.1d Third mode of transverse vibration of a uniform cantilever

The above strategy is for the case, where additional supports are added on to an existing structure. However, it is usually the case that a simple adjustment to the existing support conditions can significantly improve the dynamic characteristic of the structure. For example, consider the case of a simply supported uniform beam as shown in Figure 5.2. It is intended here to relocate the two support locations so as to achieve maximum dynamic stiffening of the structure and hence yield the maximum fundamental frequency.

In this particular condition, where no extra supports are added to the structure, the determination of the ideal support locations should be based on the mode shapes of the structure with completely free-free boundary conditions. The first two modes of a free-free beam are the rigid body translation and the rigid body rotation modes. The third mode is the first elastic mode of the free-free beam. The first three mode shapes for the transverse vibration of a free-free beam are as shown in Figures 5.3a, 5.3b and 5.3c. From Figure 5.3c, it is obvious that the two simple supports should be relocated to the nodal positions of the first elastic mode as shown in Figure 5.3c. With this simple adjustment of the support conditions, the original fundamental frequency of $\frac{\pi^2}{L^2}\left(\frac{EI}{\rho A}\right)^{1/2}$ for a simply supported beam at both ends will be increased to $\frac{(1.506\pi)^2}{L^2}\left(\frac{EI}{\rho A}\right)^{1/2}$.

$$\% \text{ increase} = \frac{1.506^2 - 1^2}{1^2} \text{ x } 100\%$$

$$= 126.80\% \qquad (5.3)$$

Note that there are two equations relating to the two simple supports. Hence, theoretically, it is only possible to eliminate a maximum of two modes from the free edge boundary solution. Thus, as advocated, the supports are relocated to the nodal positions of the first elastic mode.

5.3 NUMERICAL EXAMPLES

The general methodologies of the preceding sections are applied to the free-vibration problems of beams. Three case studies are presented. The examples chosen are aimed at

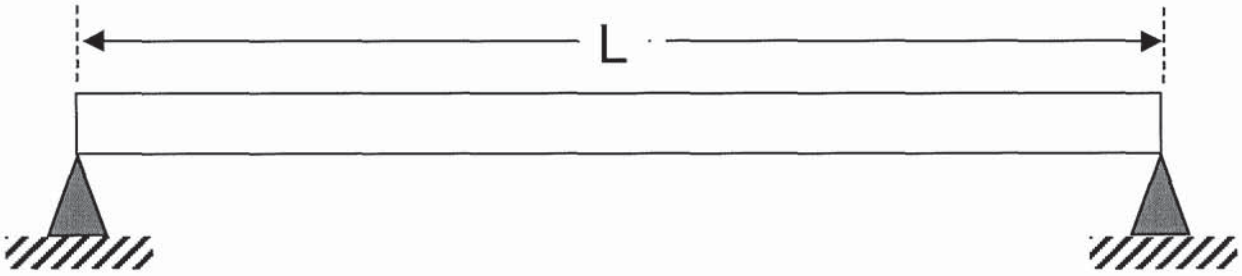

Figure 5.2 A uniform beam with simply supported ends

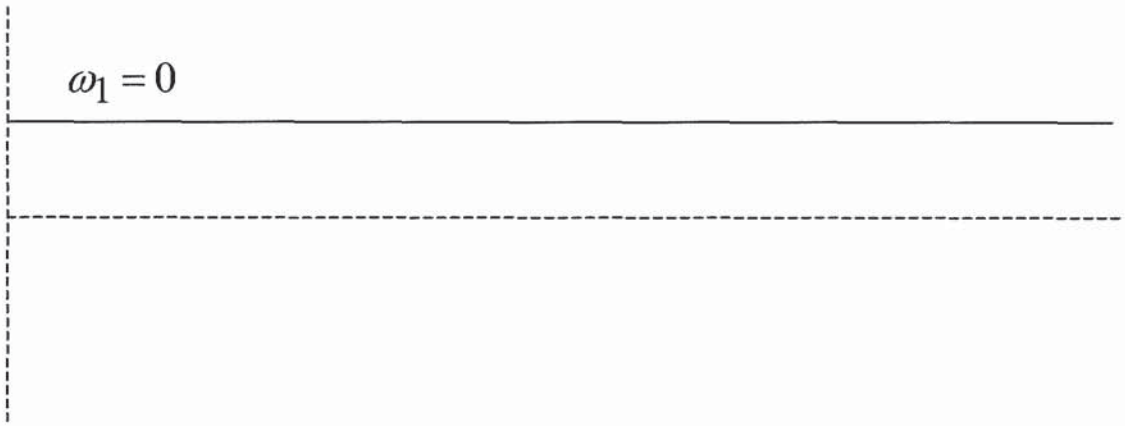

Figure 5.3a Rigid body translation of a free-free beam

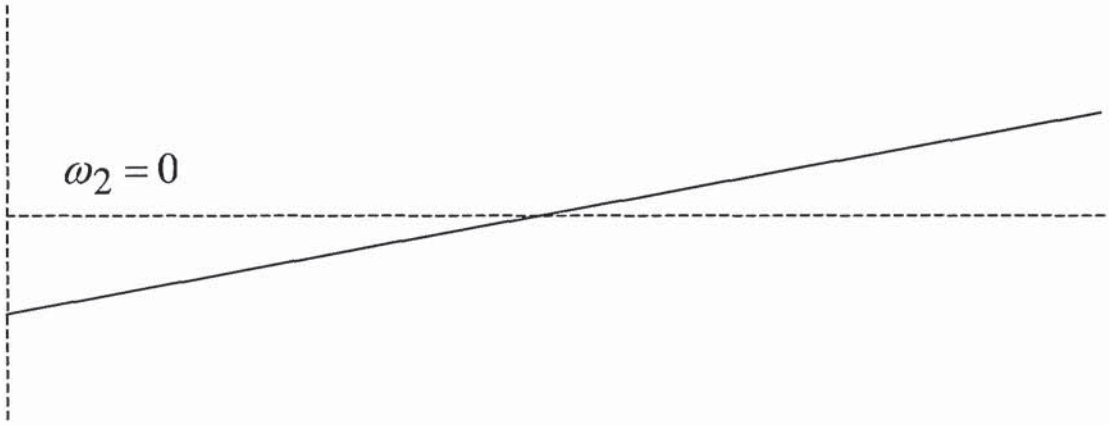

Figure 5.3b Rigid body rotation of a free-free beam

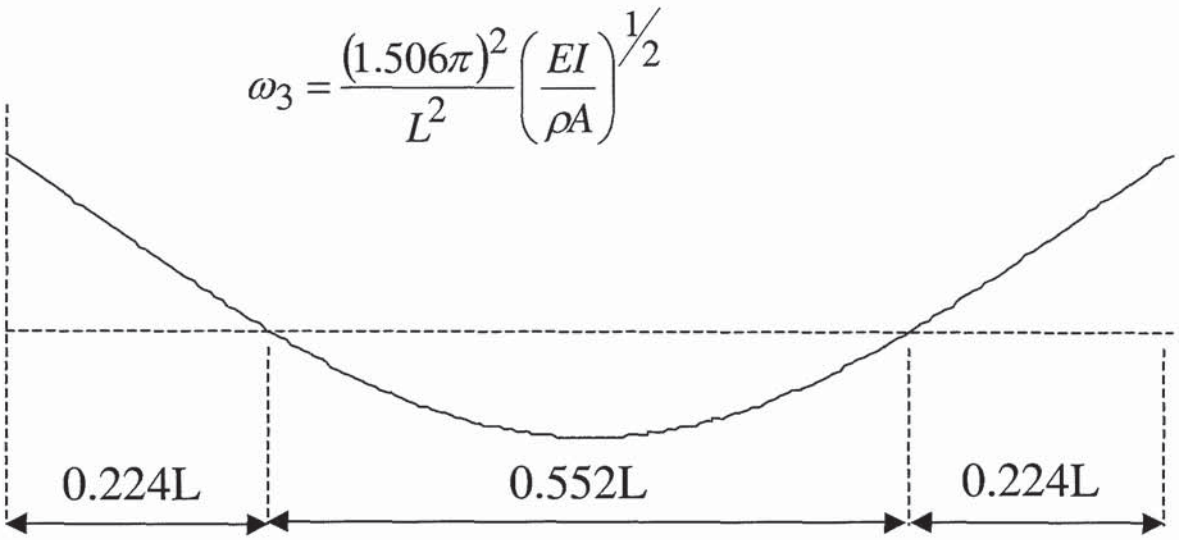

Figure 5.3c First elastic mode of a free-free beam

demonstrating the effectiveness of the proposed support location improvement techniques. A commercially available FE program, ANSYS, was used for computing the natural frequencies and mode shapes of all the examples.

5.3.1 Case 1: Clamped-Simply Supported (CS) Beam

Consider the free-vibration of a uniform cantilever beam as shown in Figure 5.1a. It is intended to introduce a simple point support as shown in Figure 5.4a, somewhere along the length of the beam so as to maximise the increase in the fundamental frequency of the beam. The dimensions are length L = 1000 mm, width w=30 mm and height h = 10 mm and its material properties of Young's modulus, shear modulus and mass density are E = 73 GPa, G =28 GPa and ρ = 2800 kg/m^3, respectively. The structure was modelled

with twenty simple beam elements, equally spaced along the length of the beam. Transverse vibrations in one principal plane only were considered. Consistent mass formulation and the subspace iteration method were chosen for the analysis.

Numerical results for the first five natural frequencies with respect to variation in the support location are shown in Table 5.1. Figure 5.4b shows the variation of the fundamental frequency with respect to the support location, where a is the distance of the support from the fixed end. As can be seen from the results, the optimal support location corresponds to the nodal position of mode 2 as shown in Figure 5.1c. By placing the support point at the nodal position of mode 2 as shown in Figure 5.1c, the fundamental mode of vibration for the clamped-simply supported beam is raised to coincides exactly with the second mode of the base cantilever beam.

Hence, the result as shown in Figure 5.4b is consistent with the method advocated in the previous section. That is, the methodology assumes that the optimal positions for the additional supports should be placed at locations, which will sweep out the maximum number of lower modes as possible from the original structure. It should be noted that with the introduction of a single simple point support on a cantilever, only a single mode could be eliminated from the eigenvalue solution of the base cantilever structure.

5.3.2 Case 2: Clamped-simply-simply supported (CSS) beam

Reconsider the problem of the cantilever beam, as shown in Figure 5.5a, where two simple supports are to be added to the base cantilever structure. Here, it is intended to find the best support locations for the two extra supports, A & B. It should be noted that

with the introduction of two simple point supports on a cantilever, two modes could be eliminated from the eigenvalue solution of the base cantilever structure.

Tables 5.2a & 5.2b summarise the fundamental frequency of the beam obtained with the variation of support locations A and B. The results are plotted in Figure 5.5b. The best combination for the dimensionless support locations are at a/L = 0.5 and b/L = 0.85, giving a fundamental frequency of 142.81 Hz. These two support locations are very close to the two nodal points of the third mode of the base cantilever as shown in Figure 5.1d.

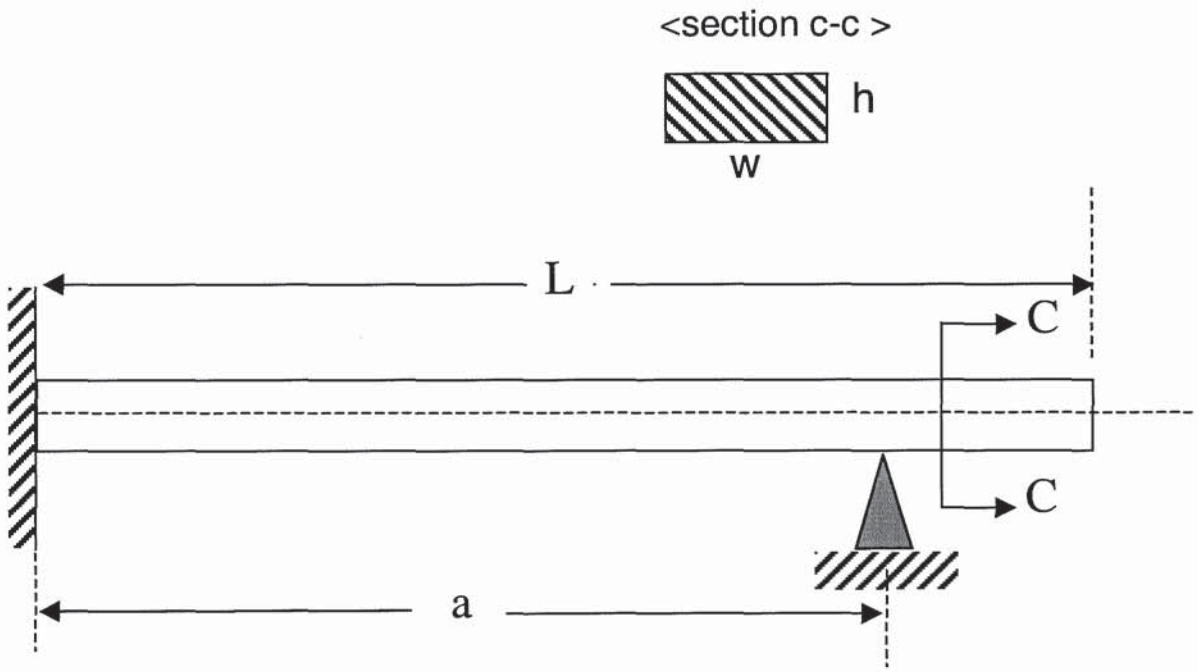

Figure 5.4a Case 1 - Clamped-simply supported beam

When the support locations are moved to exactly the nodal positions, that is at a/L = 0.504 and b/L = 0.868, the fundamental frequency is raised further to a value of 144.69 Hz, which coincides exactly with the third mode of the base cantilever beam. The results reinforce the concept that nodes of the modes of vibrations are ideal locations for choosing support locations.

5.3.3 Case 3: Beam with Two Simple (SS) Supports

The problem considered here is to find the best support locations of a simply supported beam as shown in Figure 5.6a, which gives the maximum fundamental frequency. The dimensions are L = 1000 mm, w=30 mm and h = 10 mm and its material properties

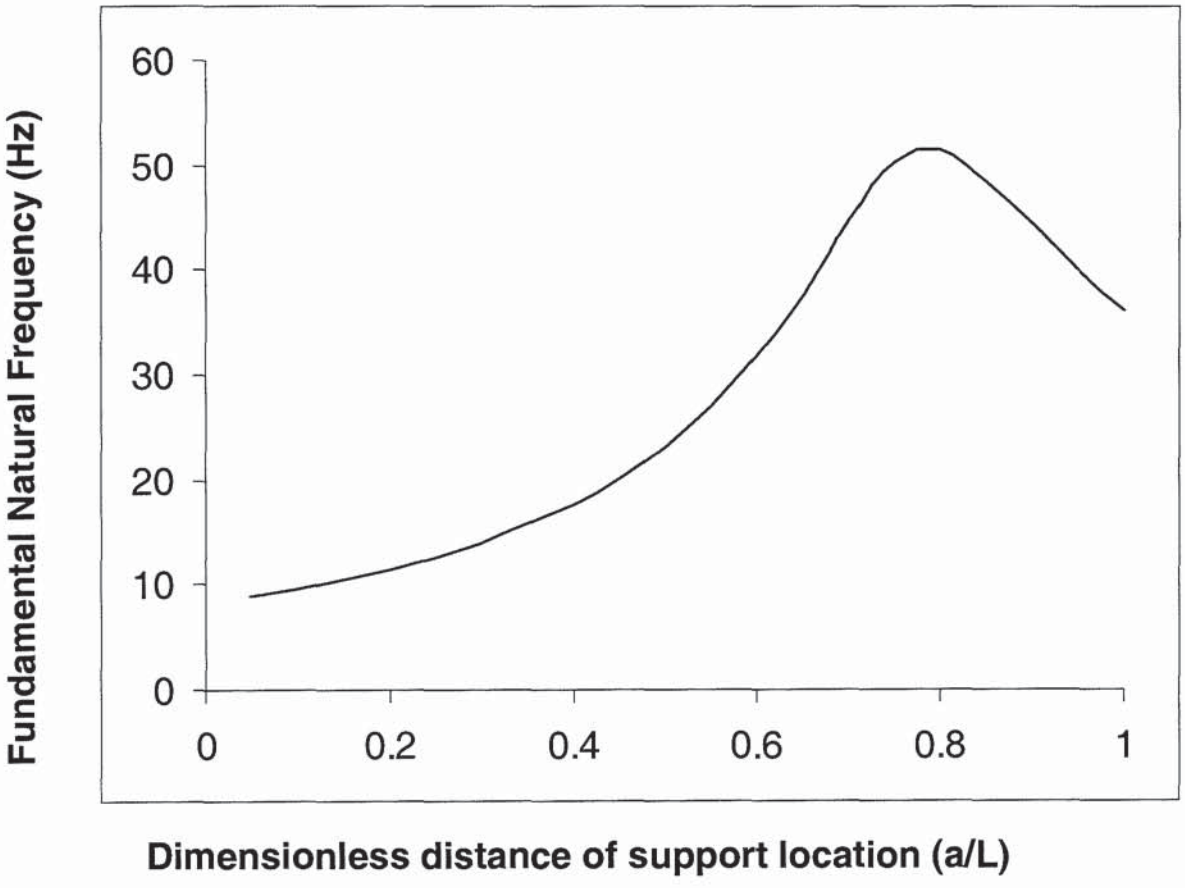

Figure 5.4b Case 1- Fundamental frequency versus support location of beam

of Young's modulus, shear modulus and mass density are E = 73 GPa, G = 28 GPa and ρ = 2800 kg/m^3, respectively. The support points, A and B, are to be varied, whereas the rest of the beam parameters are fixed. A mesh of twenty simple beam elements, equally spaced, has been taken for eigenvalue analysis using the subspace iteration method. Table 5.3 shows the fundamental frequency of the simply supported beam against the variation of support locations A and B. The data of Table 5.3 is plotted and shown in Figure 5.6b. As can be seen from Figure 5.6b and Table 5.3, the highest fundamental frequency of 51.44 Hz is obtained when the dimensionless distance of both support locations, viz., a/L and b/L is 0.20. These two support locations are very close to the two nodal points of the first elastic mode of a free-free beam as shown in Figure 5.3c.

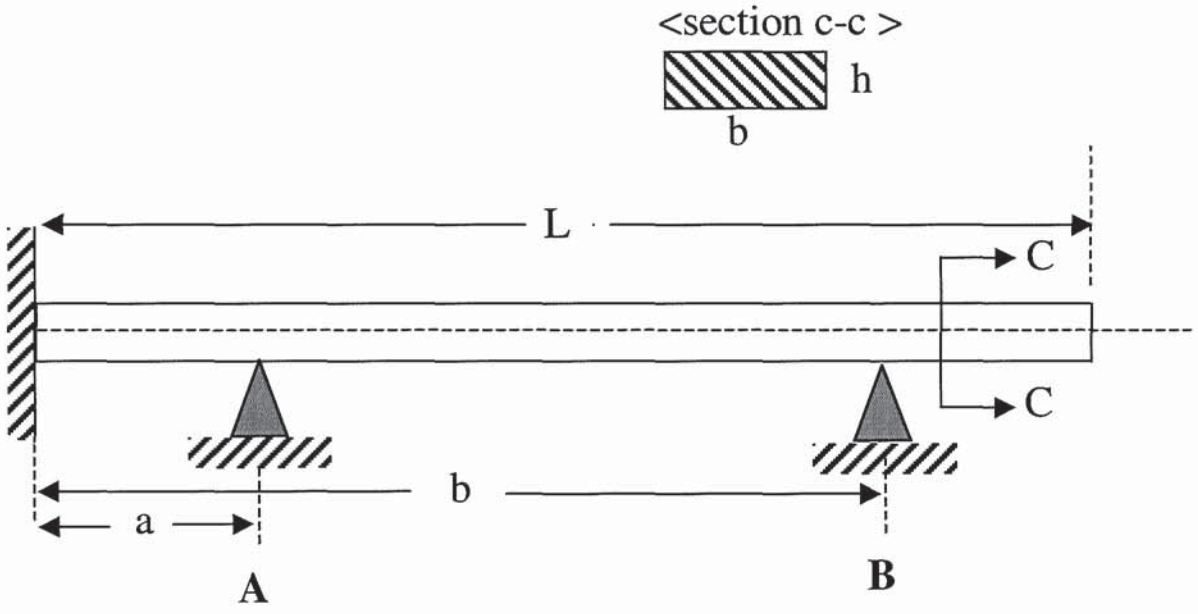

Figure 5.5a Case 2 - Beam with clamped-simple-simple supports

When the support locations are moved to exactly the nodal positions, that is at a/L = 0.224 and b/L = 0.224, the fundamental natural frequency is raised further to a value of

Dimensionless distance of support location (a/L)	Natural frequencies for clamped-simply supported beam (Hz)				
	Mode 1	Mode 2	Mode 3	Mode 4	Mode 5
0.05	8.91	55.88	156.57	307.01	507.81
0.10	9.66	60.79	170.78	335.63	556.13
0.15	10.52	66.60	187.82	370.06	613.90
0.20	11.52	73.53	208.22	410.63	677.42
0.25	12.69	81.83	232.42	454.09	671.95
0.30	14.06	91.87	259.94	455.19	579.71
0.35	15.60	104.01	282.65	384.55	627.13
0.40	17.69	118.50	263.90	380.22	696.01
0.45	20.12	134.44	226.55	427.78	642.27
0.50	23.15	144.63	208.31	468.49	578.39
0.55	26.97	136.92	224.37	427.59	642.16
0.60	31.82	122.37	261.62	379.28	696.06
0.65	37.90	110.03	283.07	380.72	626.99
0.70	44.87	102.9	262.11	452.26	577.06
0.75	50.49	105.38	237.31	455.98	666.93
0.783	**51.68**	115.23	225.49	429.14	696.20
0.80	51.43	122.79	222.32	415.64	679.95
0.85	48.53	143.08	241.06	388.72	622.16
0.90	44.32	141.15	283.05	442.42	614.69
0.95	40.04	129.53	269.46	458.80	695.80
1.00	36.17	117.19	244.47	417.98	637.68

Table 5.1 Case 1 - First five natural frequencies of beam with clamped-simple supports

Dimensionless distance of support location B (b/L)	Dimensionless distance of support location A (a/L)									
	0.05	**0.10**	**0.15**	**0.20**	**0.25**	**0.30**	**0.35**	**0.40**	**0.45**	**0.50**
0.05										
0.10	9.87									
0.15	10.75	11.03								
0.20	11.76	12.05	12.42							
0.25	12.95	13.26	13.63	14.09						
0.30	14.35	14.68	15.08	15.55	16.12					
0.35	16.03	16.39	16.82	17.32	17.91	18.63				
0.40	18.05	18.46	18.93	19.47	20.11	20.86	21.78			
0.45	20.54	21.01	21.53	22.13	22.83	23.64	24.61	25.69		
0.50	23.64	24.18	24.79	25.47	26.25	27.16	28.22	29.49	31.04	
0.55	27.57	28.22	28.94	29.74	30.65	31.68	32.87	34.28	35.98	38.07
0.60	32.60	33.43	34.33	35.31	36.40	37.63	39.02	40.64	42.55	44.88
0.65	39.01	40.17	41.40	42.70	44.11	45.65	47.36	49.31	51.57	54.26
0.70	46.70	48.57	50.49	52.47	54.52	56.67	58.98	61.51	64.35	67.63
0.75	53.70	57.09	60.61	64.20	67.83	71.49	75.20	79.03	83.06	87.44
0.80	55.80	60.79	66.46	72.81	79.77	87.18	94.78	102.33	109.65	116.53
0.85	52.95	58.18	64.39	71.81	80.72	91.38	103.97	118.29	133.00	**142.81**
0.90	48.24	52.97	58.56	65.31	73.53	83.63	96.08	111.27	128.50	140.8
0.95	43.46	47.47	52.23	57.93	64.82	73.24	83.59	96.31	114.41	125.96
1.00	39.09	42.50	46.50	51.24	56.92	63.77	72.11	82.28	94.51	108.03

Table 5.2a Case 2 - Fundamental frequency (Hz) of beam with clamped-simple-simple supports

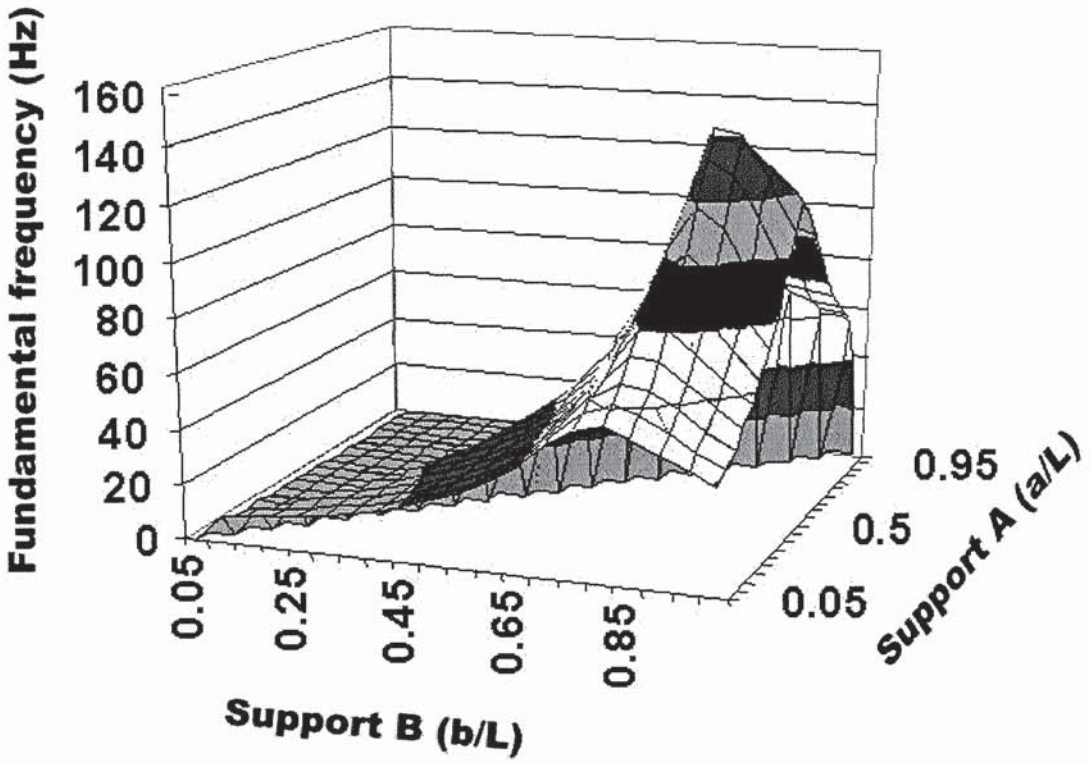

Figure 5.5b Case 2 - Fundamental natural frequency versus support locations A & B

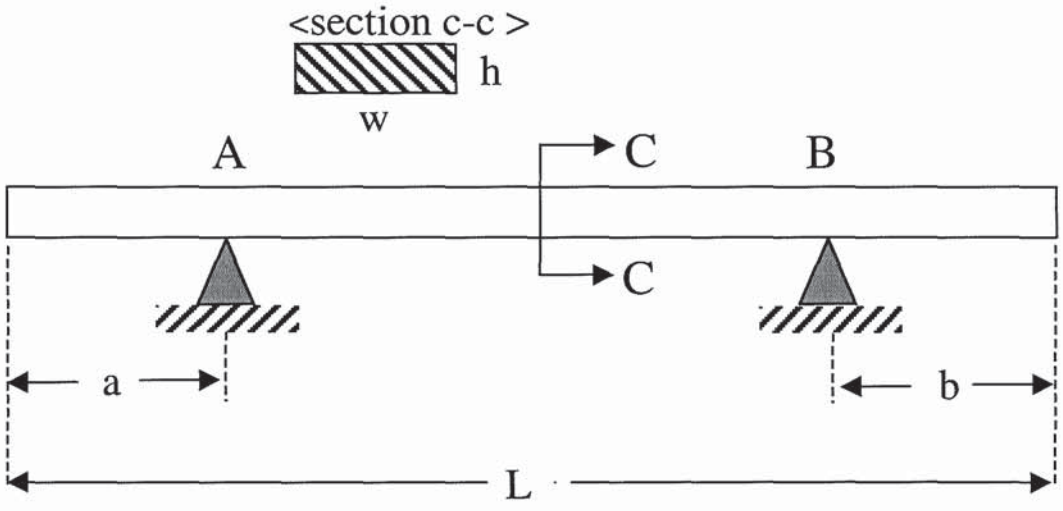

Figure 5.6a Case 3 - Simply supported beam

Dimensionless distance of support location B (b/L)	Dimensionless distance of support location A (a/L)								
	0.55	**0.60**	**0.65**	**0.70**	**0.75**	**0.80**	**0.85**	**0.90**	**0.95**
0.55									
0.60	47.79								
0.65	57.57	61.77							
0.70	71.56	76.46	82.86						
0.75	92.37	98.07	104.24	102.02					
0.80	121.99	120.45	109.83	98.85	89.59				
0.85	136.82	122.04	108.01	96.29	86.73	78.96			
0.90	134.66	119.93	105.92	94.14	84.46	76.56	70.10		
0.95	128.08	116.81	103.72	92.20	82.57	74.62	68.06	62.64	
1.00	117.01	112.33	101.25	90.33	80.89	72.97	66.38	60.89	56.31

Table 5.2b Case 2 - Fundamental natural frequency (Hz) of beam with clamped- simple- simple supports

		Dimensionless distance of support location A (a/L)									
		0.0	**0.05**	**0.10**	**0.15**	**0.20**	**0.25**	**0.30**	**0.35**	**0.40**	**0.45**
Dimensionless distance of support location B (b/L)	**0.0**	23.15	25.64	28.45	31.46	34.29	36.05	35.41	32.24	28.20	24.44
	0.05	25.64	28.55	31.85	35.36	38.52	40.04	38.34	34.08	29.41	25.33
	0.10	28.45	31.85	35.71	39.78	43.23	44.24	41.19	35.85	30.62	26.26
	0.15	31.46	35.36	39.78	44.35	47.95	48.21	43.79	37.53	31.83	27.22
	0.20	34.29	38.52	43.23	47.95	**51.44**	51.16	45.93	39.07	33.04	28.23
	0.25	36.05	40.04	44.24	48.21	51.16	51.41	47.11	40.41	34.26	29.31
	0.30	35.41	38.34	41.19	43.79	45.93	47.11	45.96	41.24	35.46	30.48
	0.35	32.24	34.08	35.85	37.53	39.07	40.41	41.24	40.35	36.46	31.76
	0.40	28.20	29.41	30.62	31.83	33.04	34.26	35.46	36.46	36.28	33.12
	0.45	24.44	25.33	26.26	27.22	28.23	29.31	30.48	31.76	33.12	33.84

Table 5.3 Case 3 - Fundamental natural frequency (Hz) of beam with two simple supports

52.48 Hz, which coincides exactly with the first elastic mode of the beam under free-free boundary conditions. Again, this simple example reinforces the concept of using nodal points as ideal support locations.

5.4 CONCLUDING REMARKS

Vibration analysis of beams has been conducted with a view to maximising its natural frequency by the strategic locations of point constraints. A method has been proposed which assumes that the ideal positions for the additional supports should be placed at locations, which will sweep out the maximum number of lower modes as possible from equation (5.2). Furthermore, the supports should be placed along the nodes of the

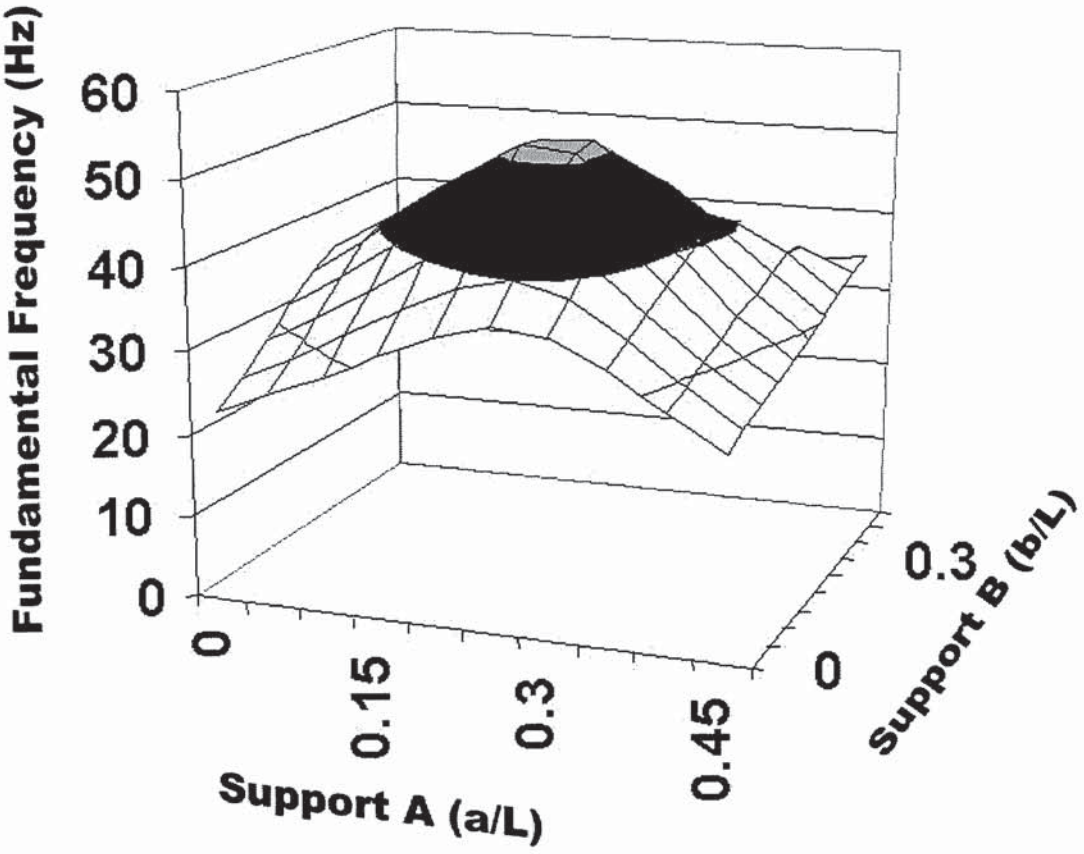

Figure 5.6b Case 3 - Fundamental frequency against dimensionless support locations of A & B

highest possible mode from the original configuration, so that all the other lower modes are eliminated by the introduction of the extra supports to the beam structure.

Three case studies are presented, namely, a clamped-simply supported beam, a clamped-simply-simply supported beam and a beam with two simple supports and the results confirmed the effectiveness of the proposed methodology in choosing support locations to maximise the fundamental natural frequency of vibrating beam structures.

CHAPTER 6

MAXIMISING THE FUNDAMENTAL FREQUENCY OF PCB

6.1 INTRODUCTION

In many engineering structures, one is normally interested in increasing the fundamental frequency of the structure as high as practically possible so as to reduce the effects of the dynamic loads on it. This consideration is especially applicable in the design of PCBs where the shifting of the fundamental natural frequency upward has the desirable effect of reducing dynamic displacements, and thereby increases the fatigue life of the mounted components (Steinberg, 1988).

The natural frequency shift is customarily achieved by structural optimisation algorithm (Brousse, 1988) whereby the focus is primarily on design variables such as thickness, cross-sectional area and stiffening ribs. More recently, for plate problems, Laura et al. (1995) describes experimental results, which show that it is possible to achieve dynamic stiffening effect, when a central circular hole is drilled in the clamped plate. Accordingly, by drilling a central hole, one obtains a lighter structure with a higher fundamental frequency. In addition, Laura and Cortinez (1995) investigated the dynamic stiffening of thin plates of regular polygonal shapes by reducing the thickness over a concentric circular region.

Another class of optimisation, which is gaining popularity, is the determination of optimal support locations for the structure. This is due to the fact that a simple

adjustment of the support conditions can significantly improve the dynamic characteristic of the structure dramatically. Wang and Nomura (1989) proposed a general approach for finding the optimal support location of a free-free rectangular plate to maximise the fundamental frequency. Rayleigh-Ritz formulation using symbolic algebra in conjunction with eigenvalue sensitivity analysis was used to solve the eigenvalue problem. Pitarresi & Di Edwardo (1993), and Pitarresi & Kunz (1992) proposed a simple and rapid method for approximating the optimal support locations of a vibrating plate by using a two-dimensional, nonlinear, least-square fit of the natural frequency against support location data. In general, all the previous works involve an optimisation procedure whereby sequential search algorithm is used to systematically improve the location of the support points. Hence, an optimal result is dependent on the initial guess and the number of iterations required for convergence to the optimal solution. Therefore, the time taken for the optimisation analysis can be prohibitive.

In Chapter 5, it is shown that introducing one or more point supports to a cantilever beam will increase its natural frequency. Furthermore, it is found that by moving the point support along the length of the beam, the beam structure's fundamental natural frequency increased gradually and reached a maximum and declined immediately thereafter. It was shown that the percentage increase in fundamental frequency occurred when the restraint location was located at the nodal position of the second mode shape.

In this chapter, a general approach for finding the optimal support location to maximise the fundamental frequency of a PCB or plate structure is described. The technique is simple and is not iterative and hence does not require any optimisation or sequential

search algorithm for the analysis. The key to the procedure is to position the necessary supports at positions so as to eliminate the lower modes from the original configuration. This is accomplished by looking at two factors. The most important factor is to introduce supports along the nodal lines of the highest possible mode from the original configuration, so that all the other lower modes are eliminated by the introduction of new or extra supports to the structure. The second factor makes use of the average driving point residues (Imamovic & Ewins, 1997) calculated from the higher modes of vibration to decide on the optimal locations of the supports along the nodal lines.

6.2 METHODOLOGY FOR LOCATING SUPPORT LOCATIONS

As mentioned in the previous chapter, a simple adjustment of the support conditions can significantly improve the dynamic characteristic of the structure dramatically. Often, increasing the number of point supports may also be a way to increase the stiffness of the structure and thereby increase its fundamental frequency to an acceptable level. In either case, the mechanical designer is faced with the task of optimising the locations of a given number of point supports for the maximum increase in the structure's fundamental frequency.

In this section, a simple methodology is proposed for the strategic positioning of support locations so as to achieve the maximum increase in the PCB structure's fundamental frequency. The technique is not iterative and hence does not require any optimisation or sequential search algorithm for the analysis. The key to the procedure is to place the necessary supports at positions so as to eliminate the maximum number of lower modes

from the original configuration and hence converge to the next lowest mode. The general concept for the methodology will be illustrated with plates of various boundary conditions.

PCB Structure with a Point Support

The FE model for the PCB shown in Figure 6.1 was used in carrying out this analysis. The following three cases of boundary conditions were studied:

Case (a) One edge of PCB fully clamped;

Case (b) Two opposite edges fully clamped and

Case (c) Three edges fully clamped.

The FE models for the three cases were created. The natural frequencies and mode shapes for the first three modes for each of the cases were computed. Figures 6.1a to 6.1c, 6.2a to 6.2c and 6.3a to 6.3c show the respective mode shapes and natural frequencies computed.

Next, a point constraint was imposed on each of the three models using the SYSTUNE (1994) software. The location of the constrained points for each of the three cases were shown in Figures 6.4a to 6.4c respectively. The constraint was imposed only at one particular location at a time, i.e., after a constraint was imposed at a location, that particular constraint was removed before proceeding to the next location. At each constrained location, the natural frequencies and mode shapes were re-computed. This

step was repeated for every point shown in Figures 6.4a to 6.4c. The bold lines in Figures 6.4a to 6.4c represent the clamped boundary conditions.

After all the new natural frequencies were computed for each constrained location, a frequency contour was plotted. This frequency contour simply showed the percentage increase in frequency at each of the constrained point as compared to the unconstrained model. These contours were shown in Figures 6.5 to 6.7 for cases (a) to (c) respectively.

Case (a)

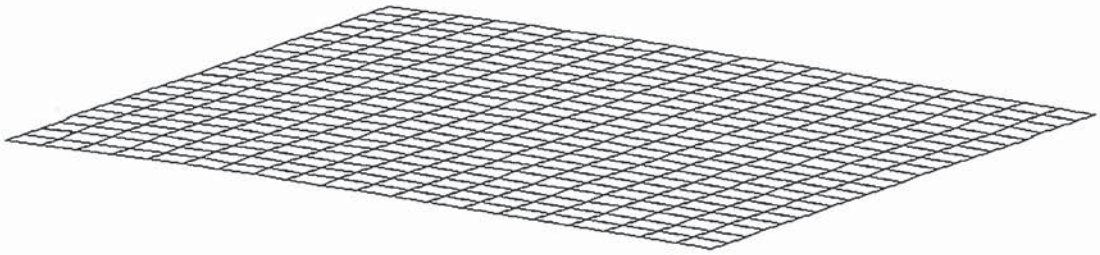

Figure 6.1a First mode shape (Frequency 12.36 Hz)

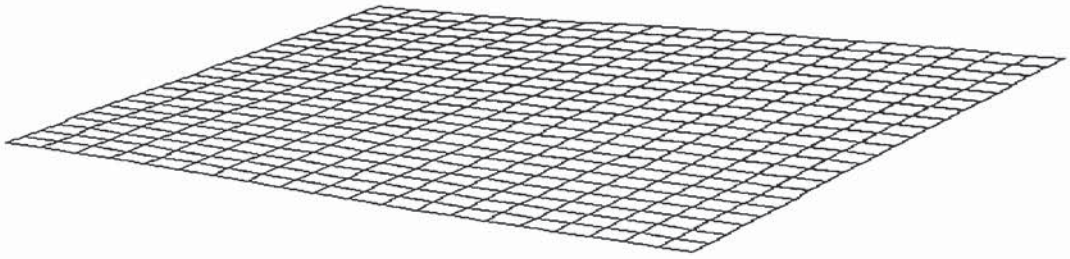

Figure 6.1b Second mode shape (Frequency 36.78 Hz)

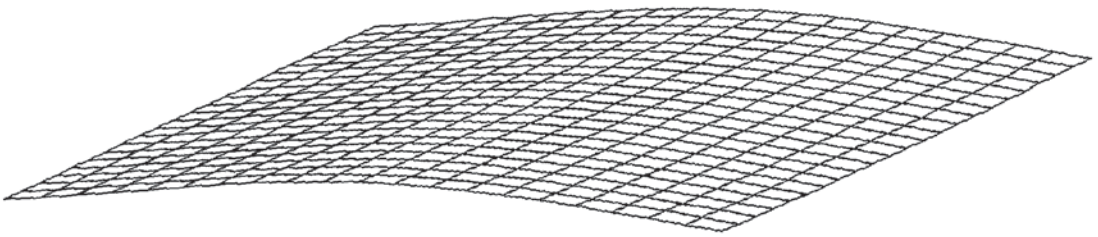

Figure 6.1c Third mode shape (Frequency 79.56 Hz)

Case (b)

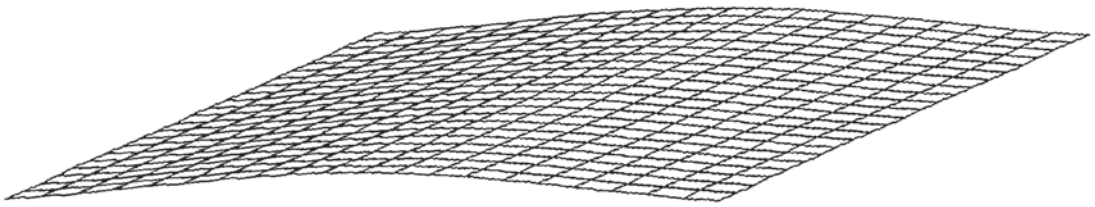

Figure 6.2a First mode shape (Frequency 72.55 Hz)

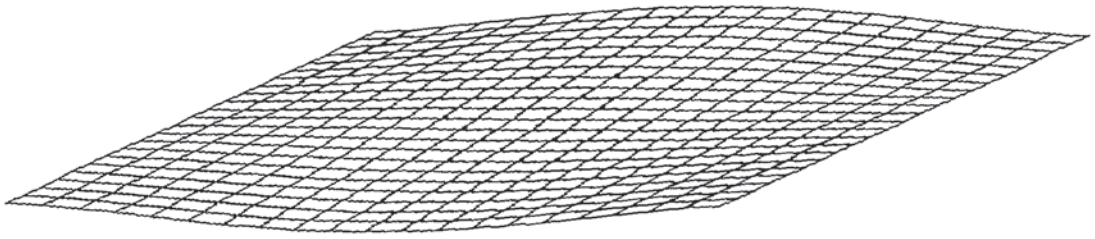

Figure 6.2b Second mode shape (Frequency 96.76 Hz)

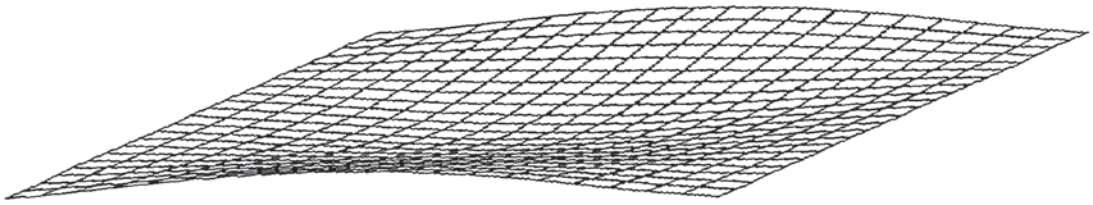

Figure 6.2c Third mode shape (Frequency 180.56 Hz)

Case (c)

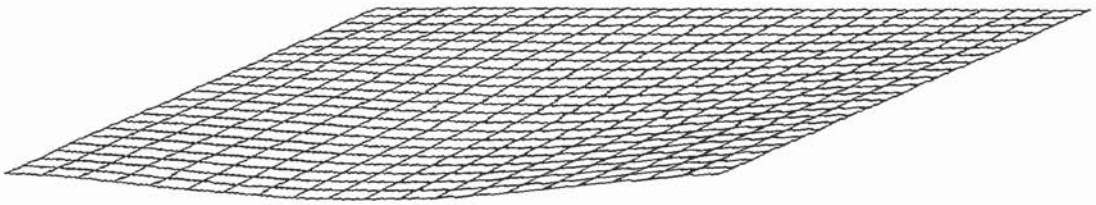

Figure 6.3a First mode shape (Frequency 81.28 Hz)

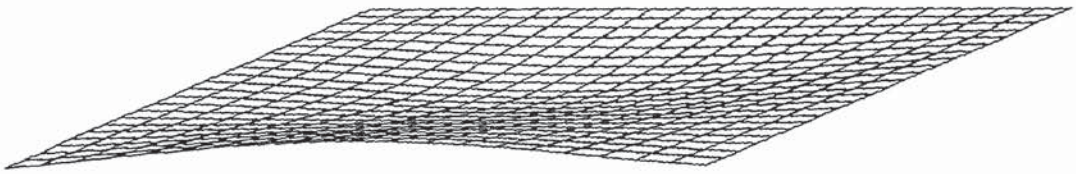

Figure 6.3b Second mode shape (Frequency 151.88 Hz)

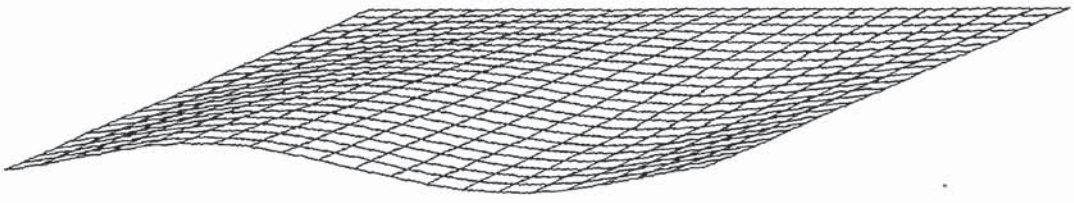

Figure 6.3c Third mode shape (Frequency 217.44 Hz)

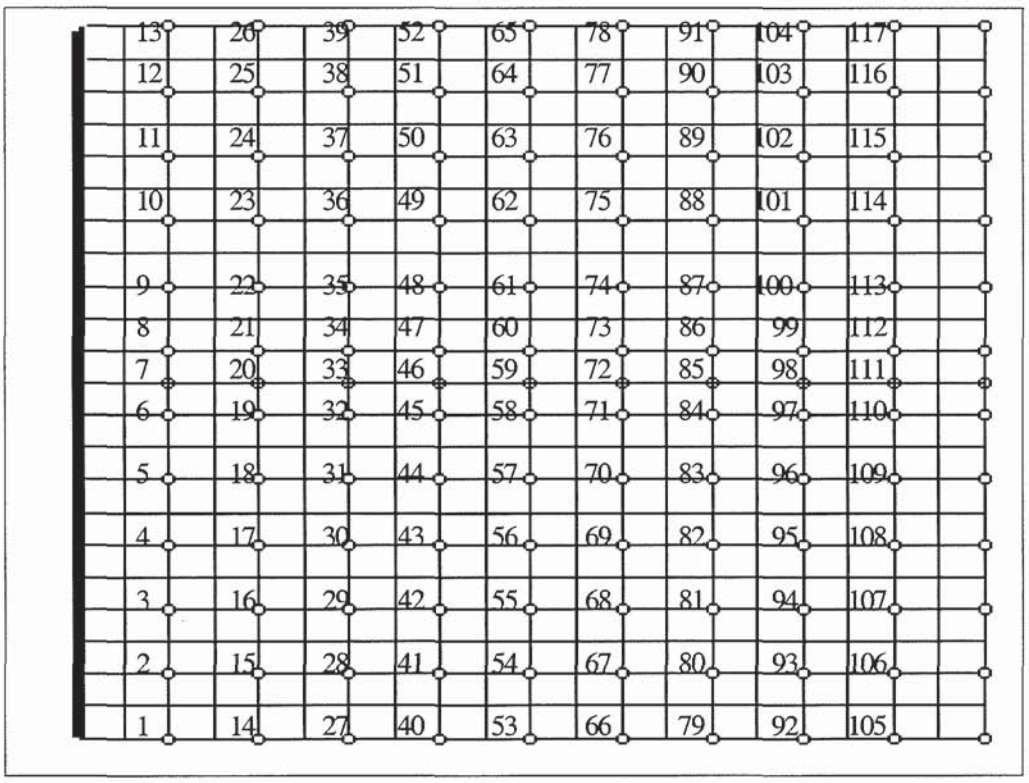

Figure 6.4a Locations of point to be constrained for Case (a)

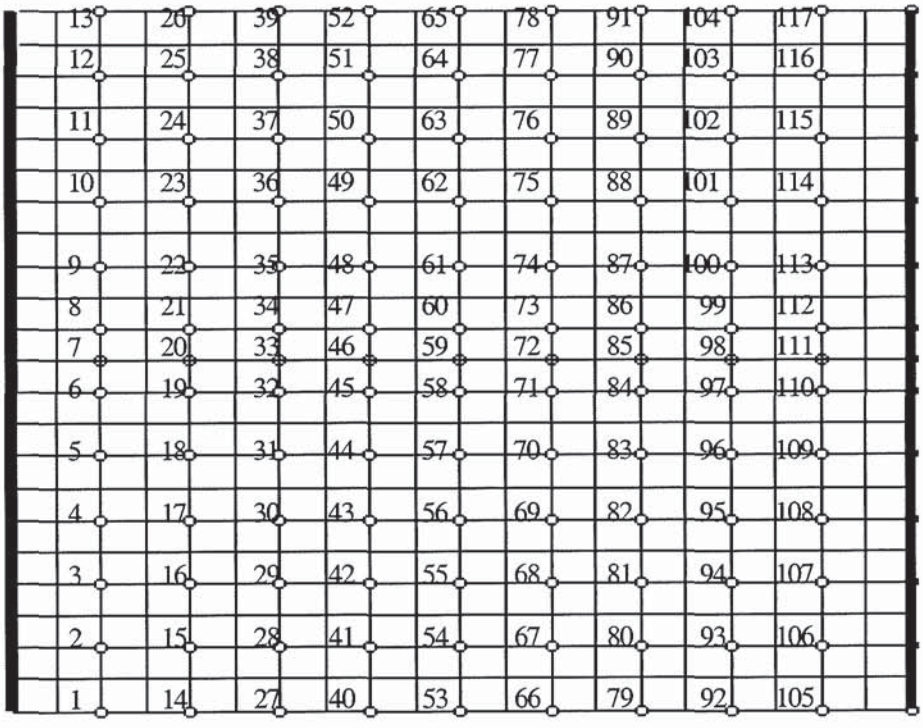

Figure 6.4b Locations of point to be constrained for Case (b)

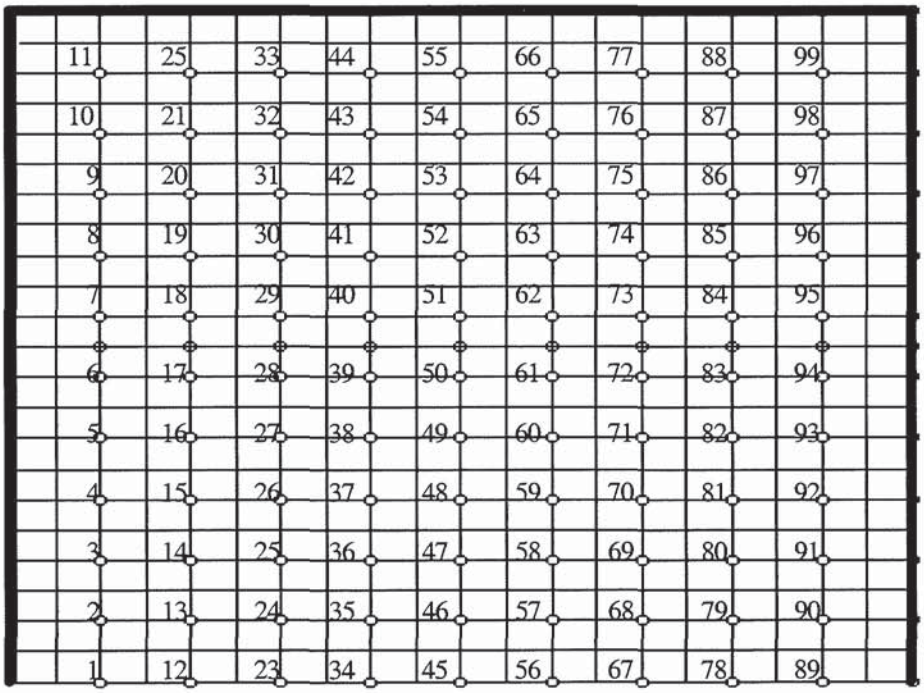

Figure 6.4c Locations of point to be constrained for Case (c)

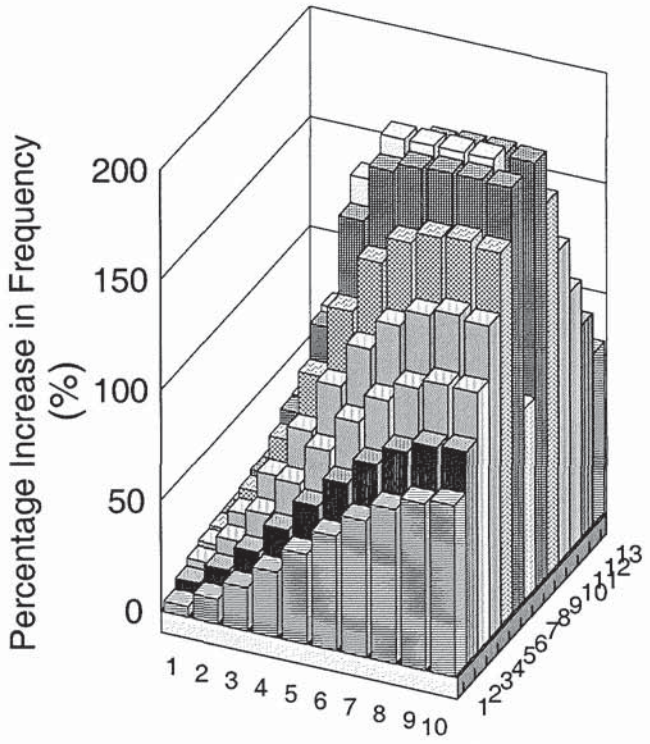

1 Side Fully Clamped

Figure 6.5 First mode frequency contour for Case (a)

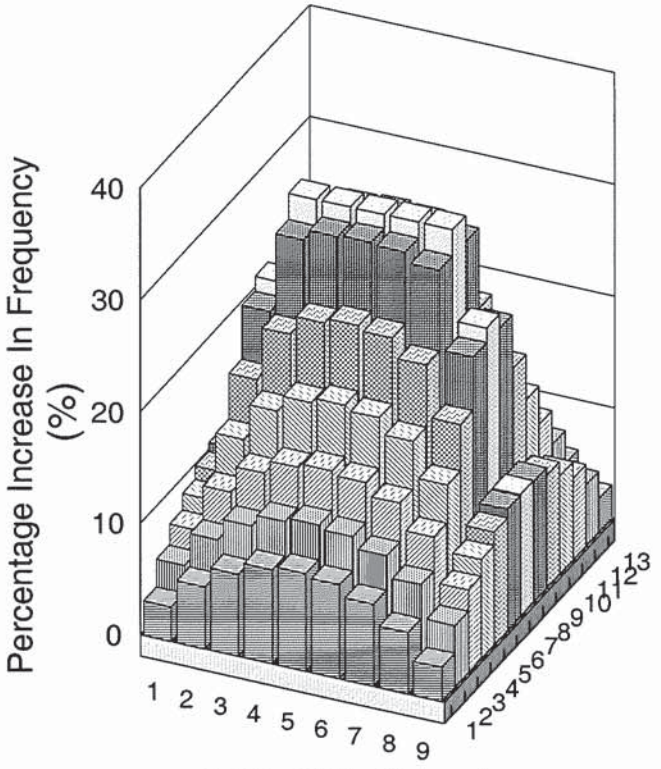

2 Sides Fully Clamped

Figure 6.6 First mode frequency contour for Case (b)

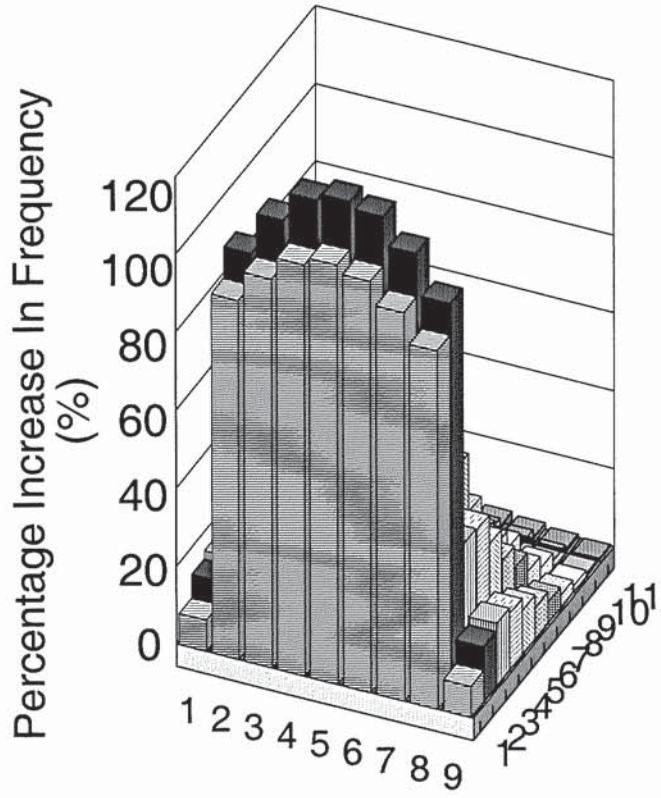

3 Sides Fully Clamped

Figure 6.7 First mode frequency contour for Case (c)

6.3 RESULTS AND DISCUSSION

6.3.1 Eradicating First Vibration Mode

From Figures 6.5 to 6.7, it can be seen that the peaks of the frequency contours actually coincide with the nodal positions of the second mode for the three cases. Figures 6.8 to 6.10 show the superimposed mode shapes for the second mode with the undeformed shape. As indicated by the arrows in these figures, the nodal positions, or nodes with no amplitude relative to the undeformed mode shape, occurred at the regions where the percentage increase in frequency due to a point constraint was the highest. This proved that the methodology proposed using a simple beam was applicable to two dimensional plates as well.

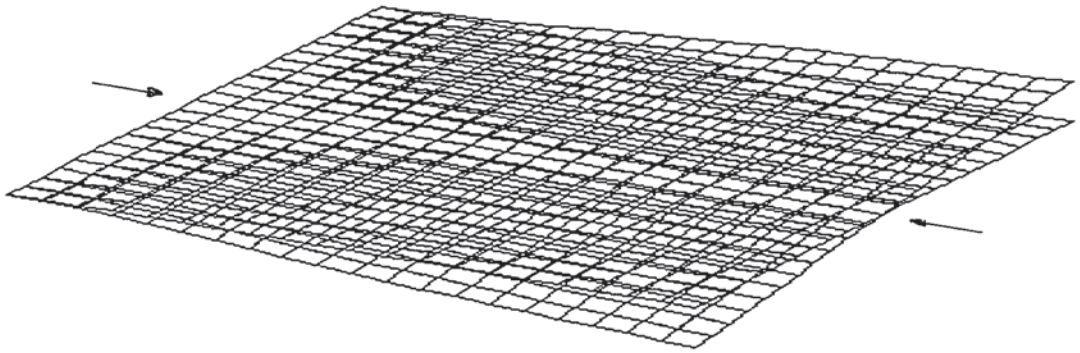

Figure 6.8 Superimposed view of the second mode for Case (a)

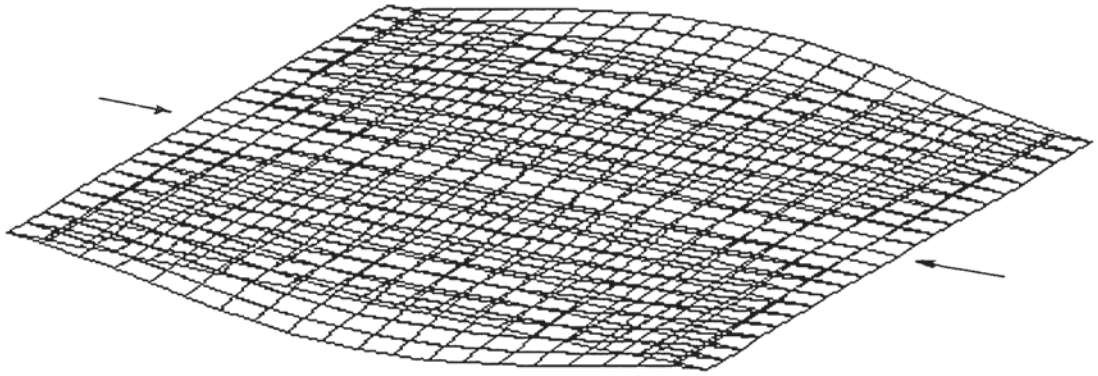

Figure 6.9 Superimposed view of the second mode for Case (b)

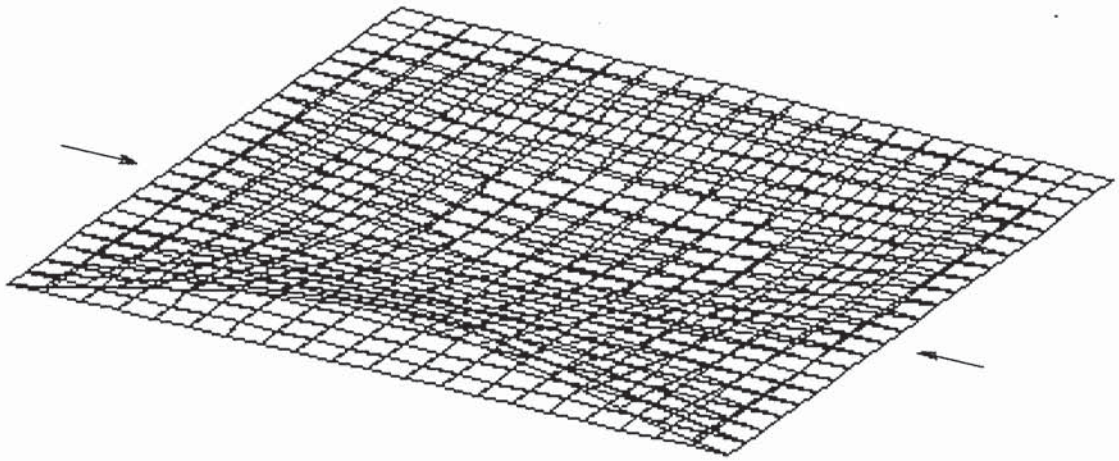

Figure 6.10 Superimposed view of the second mode for Case (c)

However, now that the regions to constraints that could lead to the highest increase in frequency was determined, there is a need to know exactly how many point constraints or, perhaps, a line constraint is required.

In order to do so, referring back to the nodal positions indicated in Figures 6.8 to 6.10, one point constraint is imposed on the point with the highest frequency increase (this is simply the point where the highest peak is in the frequency contours, see Figures 6.5 to 6.7). The percentage increase in frequency was then calculated.

The next step was to increase the number of point constraints and then re-computing the natural frequency for the model. The increase in frequency was then assessed so that the extent of increase for every increase in number of constraints can be analysed. Figures 6.11 to 6.13 plot the number of points constraints against increase in frequency for the three boundary conditions. From these figures, it can be seen clearly that essentially only one point was needed to actually eradicate the first mode of all the three cases of boundary conditions. Excess point constraints were relatively useless in increasing the

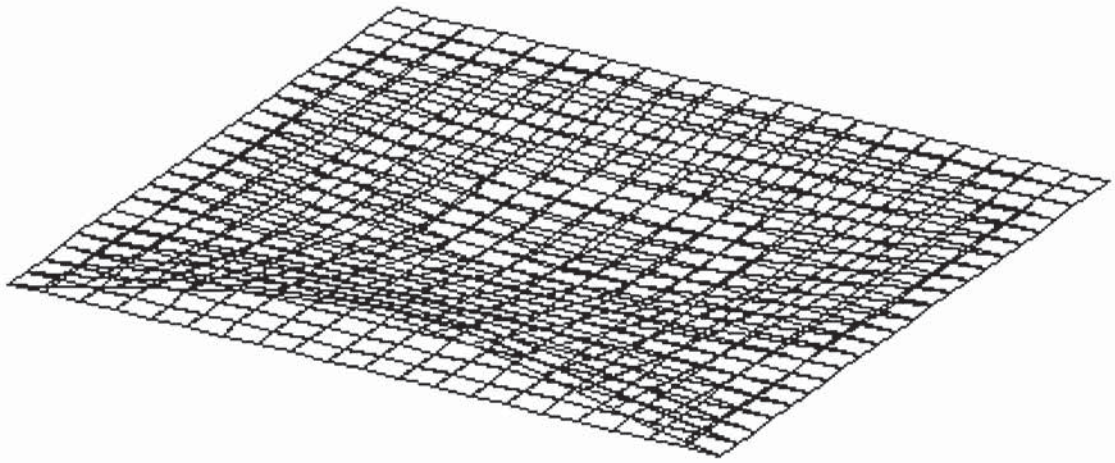

Figure 6.10 Superimposed view of the second mode for Case (c)

However, now that the regions to constraints that could lead to the highest increase in frequency was determined, there is a need to know exactly how many point constraints or, perhaps, a line constraint is required.

In order to do so, referring back to the nodal positions indicated in Figures 6.8 to 6.10, one point constraint is imposed on the point with the highest frequency increase (this is simply the point where the highest peak is in the frequency contours, see Figures 6.5 to 6.7). The percentage increase in frequency was then calculated.

The next step was to increase the number of point constraints and then re-computing the natural frequency for the model. The increase in frequency was then assessed so that the extent of increase for every increase in number of constraints can be analysed. Figures 6.11 to 6.13 plot the number of points constraints against increase in frequency for the three boundary conditions. From these figures, it can be seen clearly that essentially only one point was needed to actually eradicate the first mode of all the three cases of boundary conditions. Excess point constraints were relatively useless in increasing the

natural frequency of the structure as they could not lead to any further increase in frequency.

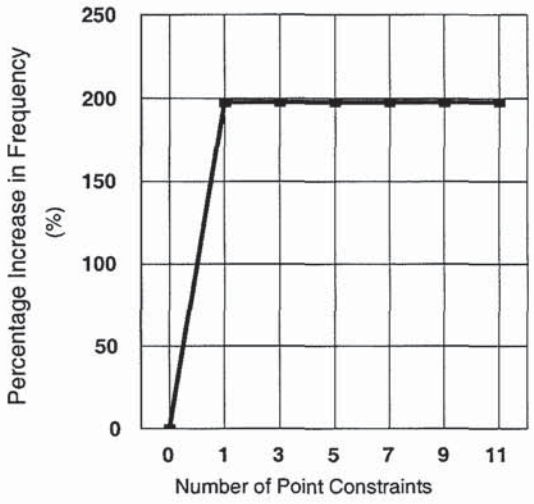

Figure 6.11 Number of constraints against % increase in frequency for Case (a)

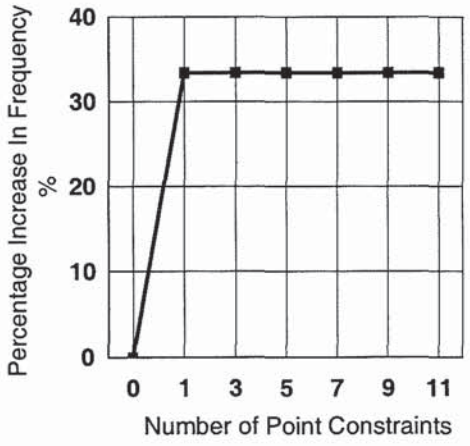

Figure 6.12 Number of constraints against increase in frequency for Case (b)

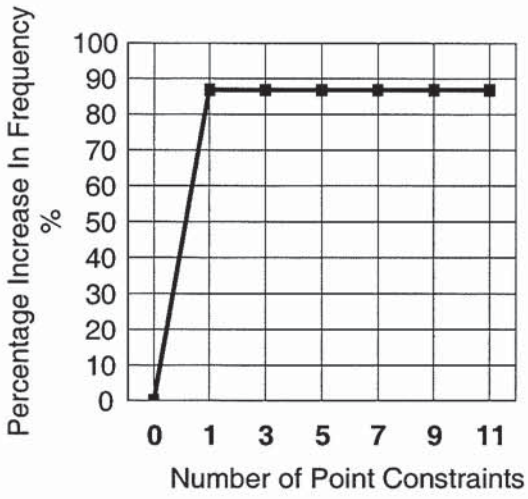

Figure 6.13 Number of constraints against increase in frequency for Case (c)

Therefore, it can be seen clearly that only one point constraint was needed to increase the frequency to that of the second mode. By applying the above results and constraining at one nodal location (points 111, 59 and 48 for the three cases respectively, refer to Figures 6.4a to 6.4c) in each of the three cases, the initial first mode of the model was removed. Now, with the one point constraint, the first mode of the new mode was actually the second mode of the original model. The new mode shapes of the structure for the three cases of boundary conditions were re-computed using the SYSTUNE software. The first modes for the three boundary conditions with one added point constraint were presented in Figures 6.14 to 6.16.

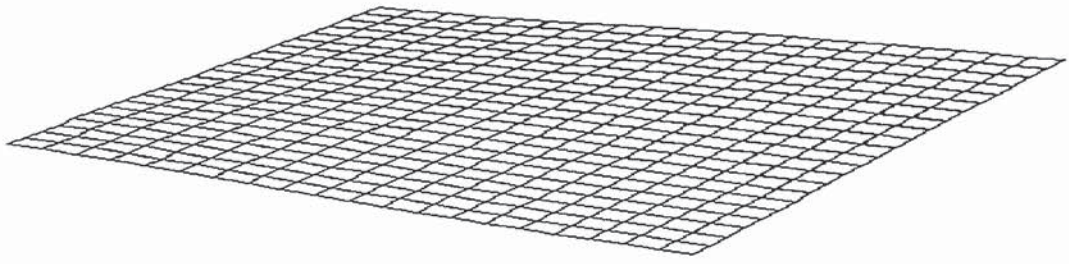

Figure 6.14 First mode shape for Case (a) (Frequency 36.78 Hz)

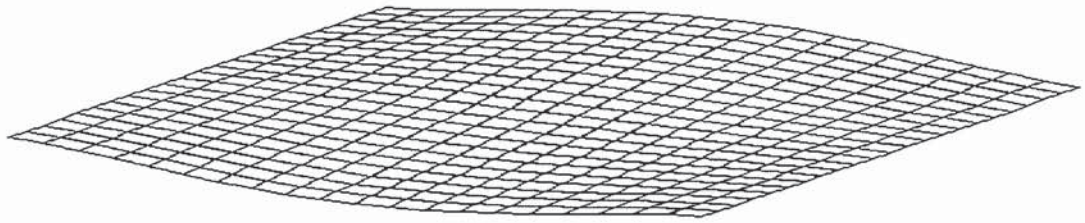

Figure 6.15 First mode shape for Case (b) (Frequency 96.76 Hz)

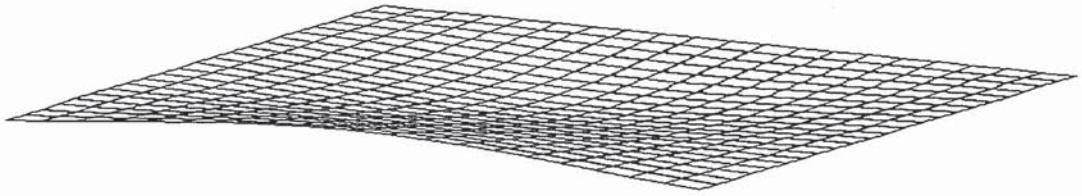

Figure 6.16 First mode shape for Case (c) (Frequency 151.83 Hz)

From the figures above, it can be seen clearly that by placing a constraint in a structure at a nodal position of the next higher mode, the initial first mode could be eliminated. The number of point constraints would depend on the complexity of the structure and which mode of vibration that is to be removed. For the case of a rectangular plate, to remove the first vibration mode, only one point constraint was needed.

6.3.2 Eradicating Second Vibration Mode

To illustrate the process of eradicating the second mode of vibration, there are two approaches:

i) First sweeping off the first mode then based on the new model, sweep off the new first mode; and

ii) Directly sweeping off the second mode based on the original model without attempting to sweep off the first mode.

Approach (i)

First, consider case (c) as an illustration. Based on the model with one point constraint already imposed, the first mode (which was the second mode for the original model) was shown in Figure 6.16. Before attempting to sweep off another mode, the nodal positions of the next mode (second mode) had to be determined. Note that after the point constraint was added, the second mode of this new model may not necessarily be similar to the third mode of the original. Figure 6.17 shows the superimposed second mode with the undeformed structure.

Similarly, now the number of point constraints along the nodal line was plotted against the increase in frequency and shown in Figure 6.18. Again, it can be seen that after two point constraints, addition of more constraints along the nodal line did not lead to any further increase in natural frequency.

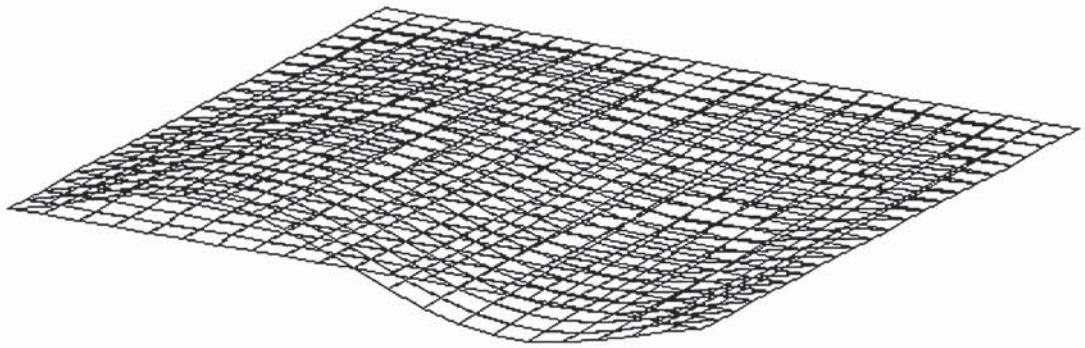

Figure 6.17 Superimposed view of the new second mode shape - Case (c)

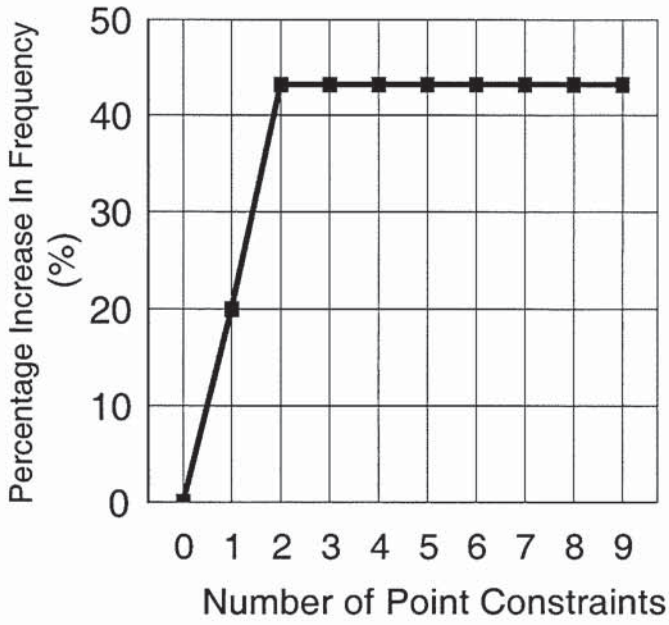

Figure 6.18 Number of constraints against increase in frequency - Case (c)

Therefore, two more point constraints (points 45 and 52, see Figure 6.4c) were imposed on the model. The new first mode was re-computed in SYSTUNE and the new mode shape and frequency were shown in Figure 6.19. Again, it can be seen that the first mode of this new model was actually originally the third mode of the model without any additional point constraints. Therefore, in using this method, three points were needed to skip the first two modes.

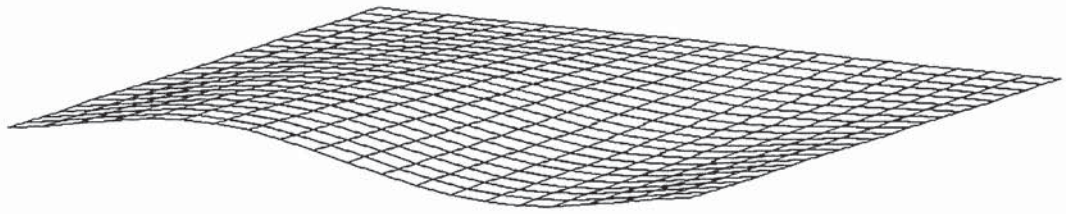

Figure 6.19 Third mode shape for Case (c) (Frequency 217.44 Hz)

Approach (ii)

The second approach stated above requires that there was no need to remove the first mode before attempting to remove the second mode.

In order to sweep off the second mode directly, the frequency contour was analysed. But for this case, how the first mode's frequency changed with point constraints over the plate, as shown in Figure 6.7, was not used. Instead, an attempt was made to directly examine whether the peaks of the second mode frequency contour exhibited any similarity with that the nodal positions as shown in Figure 6.17. From the frequency contour as shown in Figure 6.20, it may be readily seen, the maximum peaks of the frequency contour coincided with the nodal positions indicated in Figure 6.17.

The next step was to determine, among all the points in the nodal line, how many points were required. This step was similar to those done earlier and the result was shown in Figure 6.21. Not surprisingly, the number of points required was two, even without the initial one point constraint to sweep off the first mode first. The two locations were at points 47 and 52 (refer to Figure 6.4c). By implementing the two point constraints, the mode shape and frequency obtained remained exactly the same.

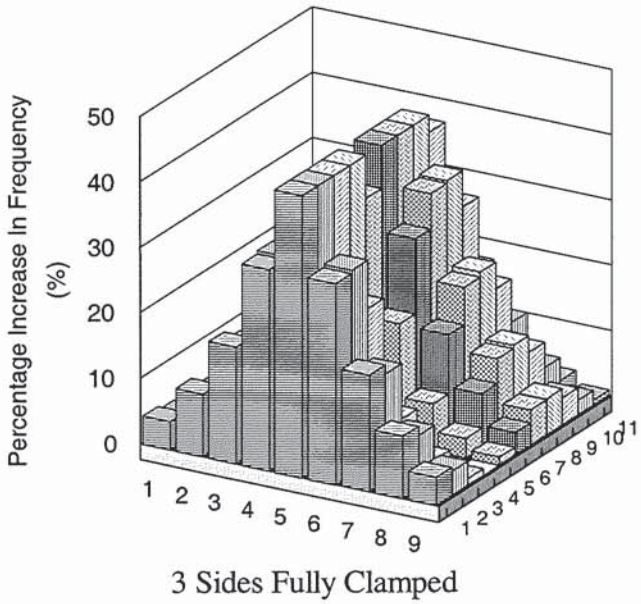

Figure 6.20 Second mode frequency contour for Case (c)

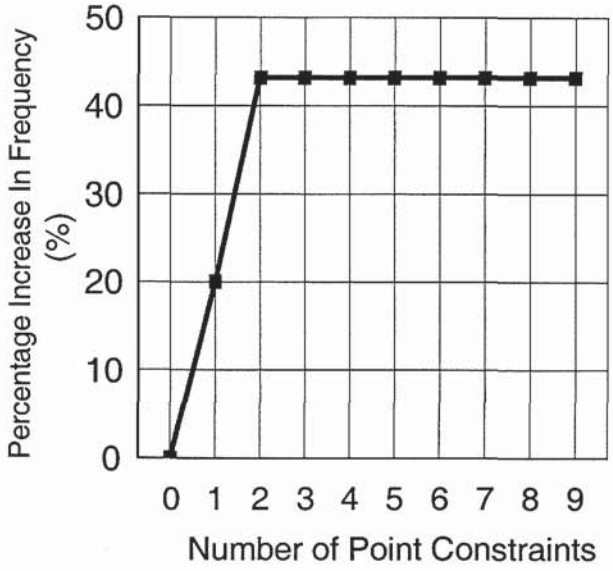

Figure 6.21 Number of constraints against increase in frequency for Case (c)

This latter method had shown that fewer constraints were needed. In this case, only two points were needed. This would mean that the first method was not efficient as the initial one point constraint to remove the first mode was shown to have no effect in sweeping off the second mode at all.

Hence, in the vibration analysis of any structure, the approach to adopt to maximise the natural frequency had to be the latter method. In summary, this approach would require that the nodal positions of the first few modes be known before attempting to determine the number of point constraints needed to sweep off a particular mode. In most cases, frequency contours would be useful as the peaks in the contours enable one to easily determine at a glance, which nodal points to be constrained so that the percent increase in natural frequency is maximised, i.e., if two points were needed, the two highest peaks would normally be the ideal locations to introduce the point constraints.

6.3.3 Methodology for Two-dimensional Analysis – Plate Structures

It is shown from the preceding section that for two-dimensional analysis, the supports should be placed along the nodal lines of the first encountered lower mode, which will not be eliminated by the repositioning of supports or addition of extra supports. But, in two-dimensional analysis, an extra complication arises as the mechanical designer is faced with the extra task of optimising the point support locations along the nodal lines.

It is advocated that to solve the problem, the average driving point residues (Imamovic & Ewins, 1997) along the nodal lines can be inspected to find the best locations of the supports. The average driving point residues (ADPR) for the degree-of-freedom i for the frequency range of interest between mode m to mode n can be computed as:

$$ADPR(i) = \left(\frac{1}{n-m}\right)\sum_{r=m}^{r=n}\frac{\phi_{ir}^2}{\omega_r} \tag{6.2}$$

where ϕ_{ir} = ith component of rth mass normalised mode shape

and ω_r = rth natural frequency.

Driving point residues are equivalent to modal participation factors, and are a measure of how much each mode is excited, or participates in the overall response, at the driving point. Hence, the ADPR of a location is a measure of an overall response of that particular point over the range of frequency of interest. Thus, it appears logical to select locations with the highest relative ADPRs as support locations since the modes of interest at these points will be relatively active and as large as possible. The other

alternative is to choose locations where the ADPRs are the least active and hence will be akin to choosing nodal points. But, in practice, it is found that the mean of all the ADPRs along each nodal line is a better indicator for finding the best support locations. For example, Figure 6.22 shows the ADPRs for 21 candidate support points along a nodal line of a plate structure. The mean of the average driving point residues for the 21 points has a numerical value of 6.5. A minimum of two points is required to define a nodal line. Thus, it can be assumed that the ideal locations for the supports will be somewhere around locations 3 and 19.

6.4 NUMERICAL EXAMPLE ON A SIMPLY SUPPORTED PLATE

A rectangular plate of aspect ratio 2:1 is considered in this example. The properties of the plate are elastic bending modulus of 71.7 GPa, elastic shear modulus of 26.6 GPa, density of 2877 kg/m^3, thickness of 1.58 mm and sides 152.4 mm x 304.8 mm. The plate is modelled using four-node quadrilateral plate finite elements. Only transverse bending is considered in the analysis. Each FE node has three degrees of freedom. These are displacement normal to the plate and two in-plane rotations. Figure 6.23 shows the geometry and FE model of the plate. Initially, the plate is symmetrically supported at the four corner supports (indicated by open circles) as shown in Figure 6.23.

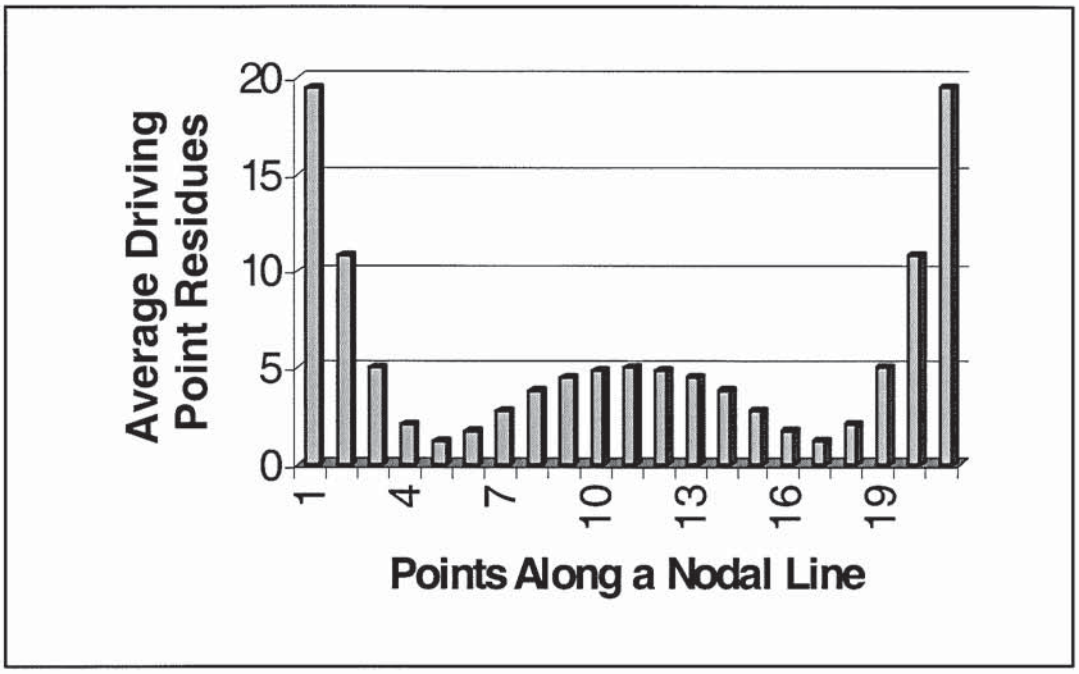

Figure 6.22 Average driving point residues for 21 points along a nodal line

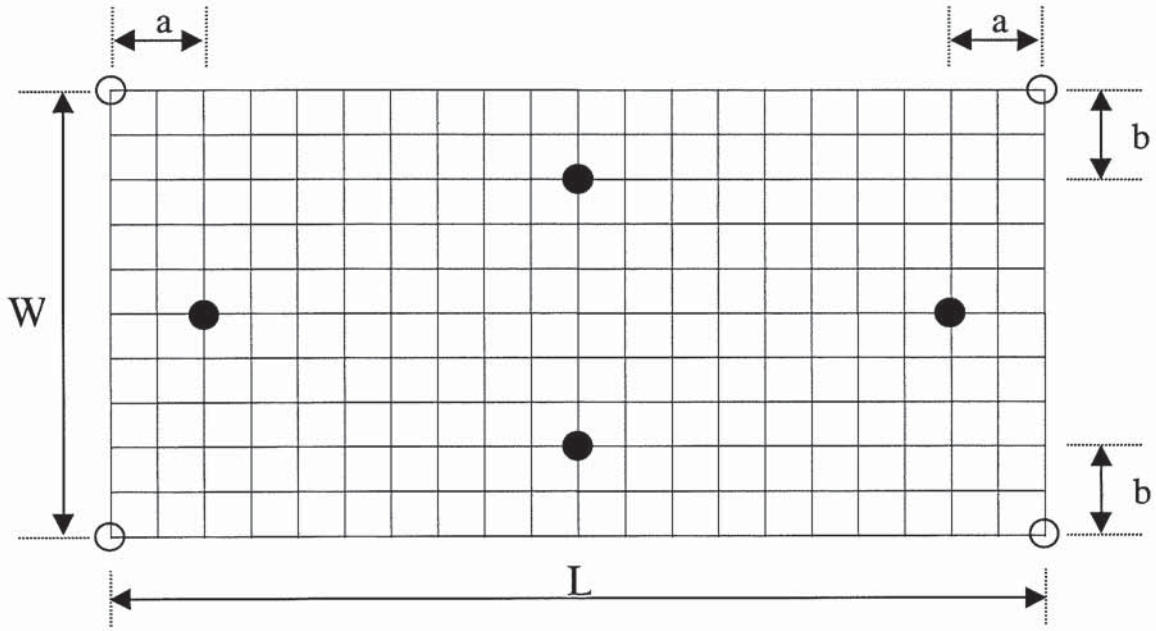

Figure 6.23 Case 4 – Rectangular plate showing corner supports (open circles) and improved supports (solid circles)

The problem considered here is to find the locations of four simply supported points such that the fundamental natural frequency becomes a maximum. The grid lines as shown in Figure 6.23 will be used as a grid of discrete candidate support locations for the four simple supports.

As discussed in the section on methodology, the first part of the optimisation process is to obtain the mode shapes and natural frequencies from the FE free edge boundary condition plate solution. Note that the first three modes of the free edge boundary condition are rigid body modes. The next five mode shapes are the elastic modes. These are displayed in Figures 6.24a to 6.24e and the corresponding natural frequencies are listed in Table 6.1. As there are four equations relating to four simple supports, theoretically, the maximum number of modes that can be eliminated from the free edge boundary solution is equal to four. Hence, as advocated in the procedure, the supports must be placed, somewhere along the nodal lines of the second elastic mode. It is observed that the second elastic mode as shown in Figure 6.24b is a pure torsion, with nodal lines running along the centerlines of the plate structure. Thus, it can be inferred that the four simple supports will be placed along the nodal lines of the second elastic mode and can be considered to be symmetrically located with respect to the center axes of the full plate as shown in Figure 6.23 (indicated by solid circles). Note that, there are ten pairs and five pairs of candidate support locations along the length and breadth of the plate respectively.

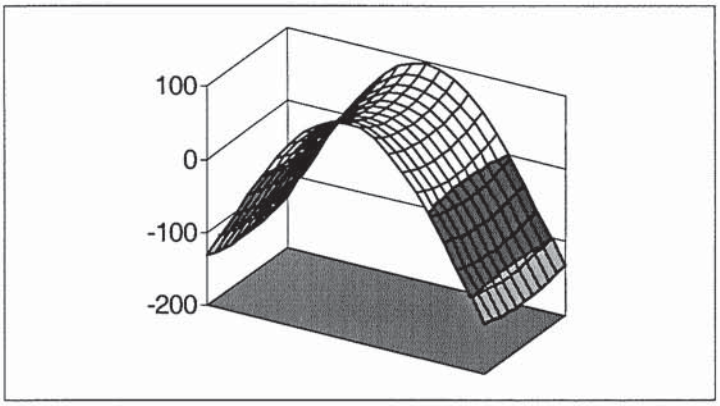

Isometric view of first elastic mode

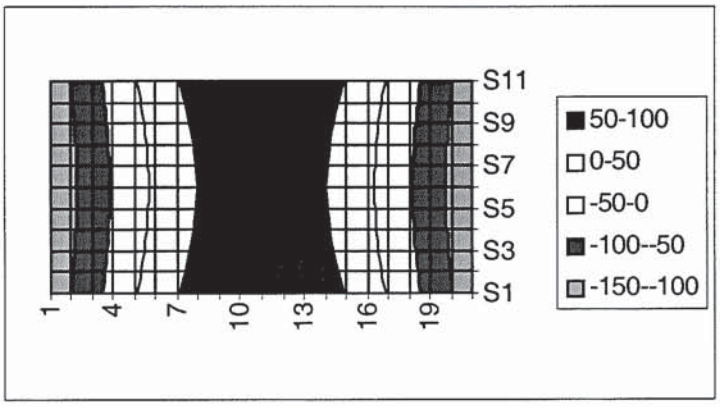

Plan view of first elastic mode

Figure 6.24a Case 4 – First elastic mode under free edge boundary condition

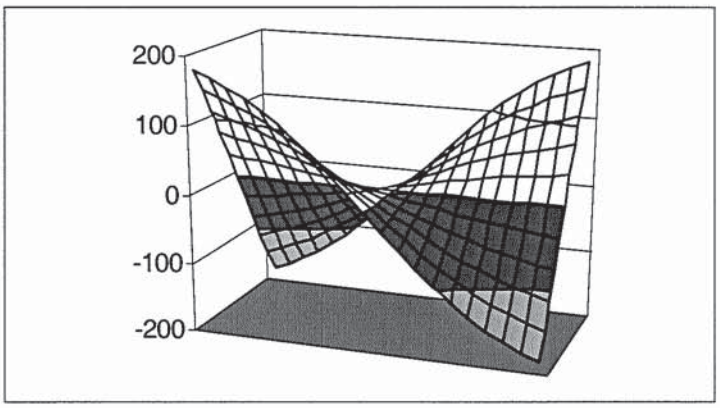

Isometric View of Second Elastic Mode (Torsion)

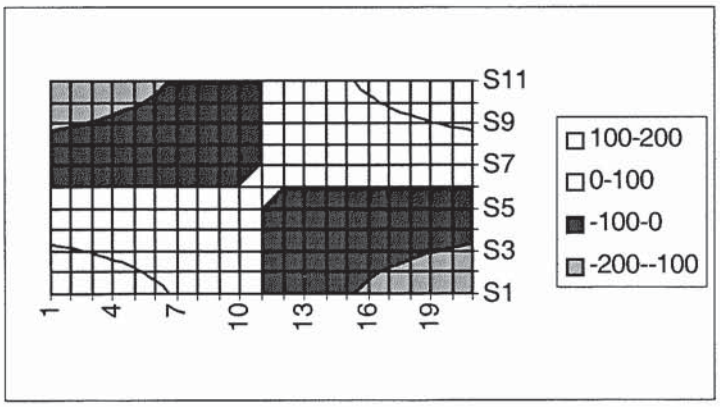

Plan View of Second Elastic Mode (Torsion)

Figure 6.24b Case 4 – Plots of second elastic mode under free edge boundary condition

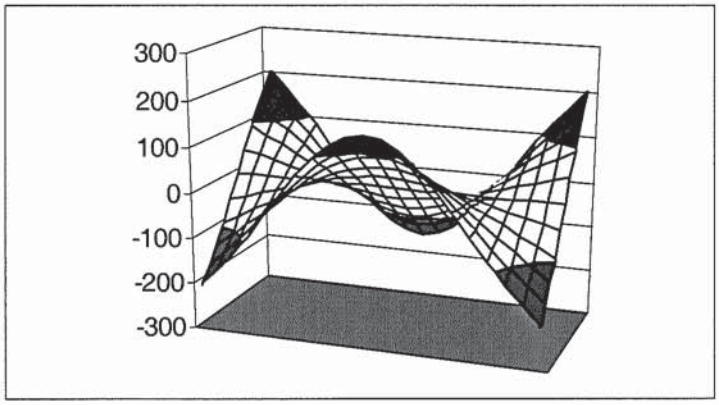

Isometric View of Third Elastic Mode

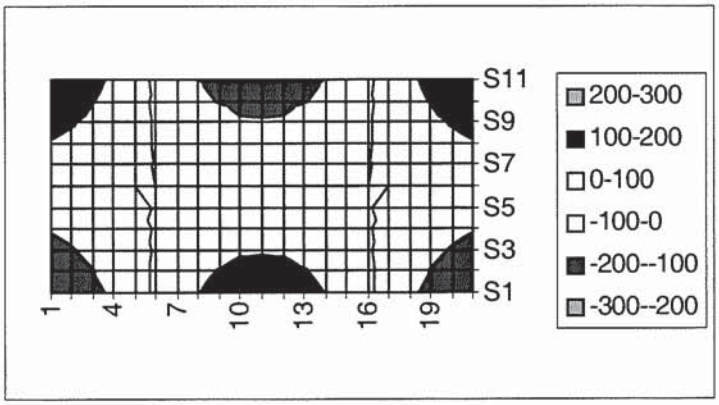

Plan View of Third Elastic Mode

Figure 6.24c Case 4 – Plots of third elastic mode under free edge boundary condition

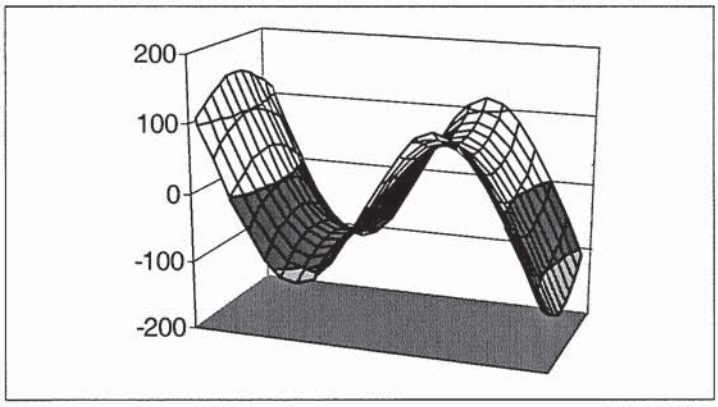

Isometric view of fourth elastic mode

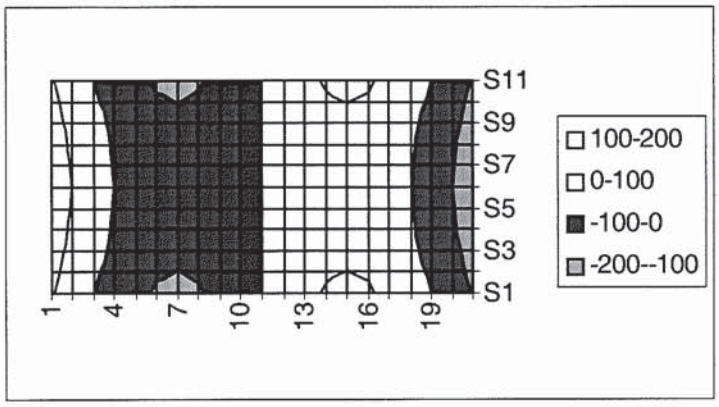

Plan view of fourth elastic mode

Figure 6.24d Case 4 – Plots of fourth elastic mode under free edge boundary condition

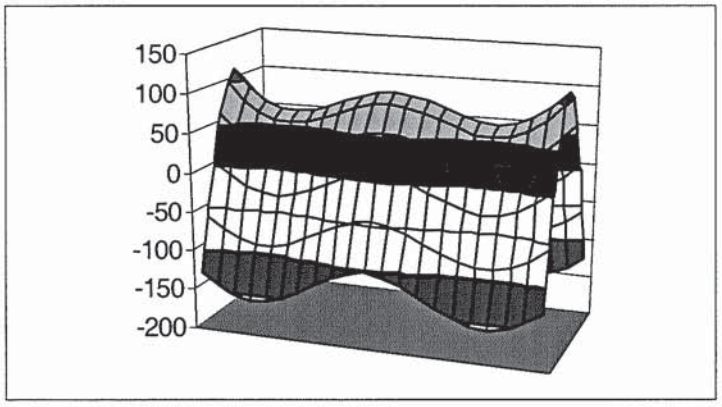

Isometric view of fifth elastic mode

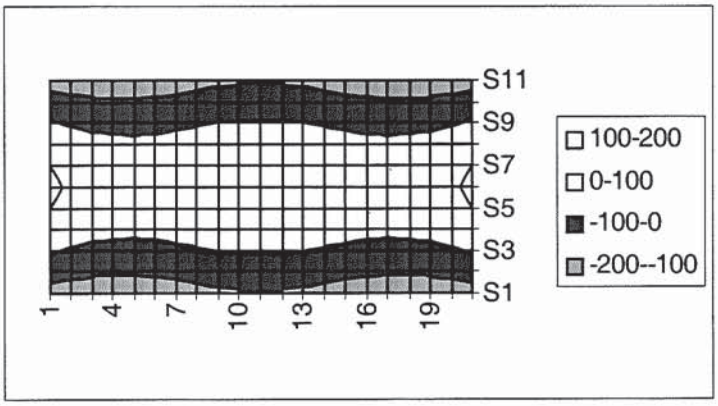

Plan view of fifth elastic mode

Figure 6.24e Case 4 – Plots of fifth elastic mode under free edge boundary condition

Table 6.2 summarises the result of the fundamental frequency of the plate due to the effect of moving the paired support locations along the central axes of the plate. The result is also plotted in Figure 6.10. As can be seen from Figure 6.10 or Table 6.2, there is no unique solution for optimum pairs of support locations. With these improved support locations, the fundamental frequency is 106.94 Hz as compared to the original frequency of 38.29 Hz for the corner-supported plate. The improved fundamental frequency of 106.94 Hz coincides exactly with the second elastic mode for the free edge boundary conditions and does not change with respect to varying support locations within the dimensionless distances of $a/L \leq 0.25$ and $b/W \leq 0.3$. The results are not totally unexpected, as the nodal lines of the second elastic mode for the free edge boundary conditions are straight lines. Furthermore, as expected, each pair of simple supports should be placed as far away from the centre of the nodal lines, so as to forced the fundamental frequency of the modified structure to vibrate at the intended mode of vibration. Hence, when the pair of support points are nearer towards the center of the nodal lines, the results are not optimum and the fundamental mode of vibration of the modified structure differs from the second elastic mode of vibration for the free edge boundary conditions.

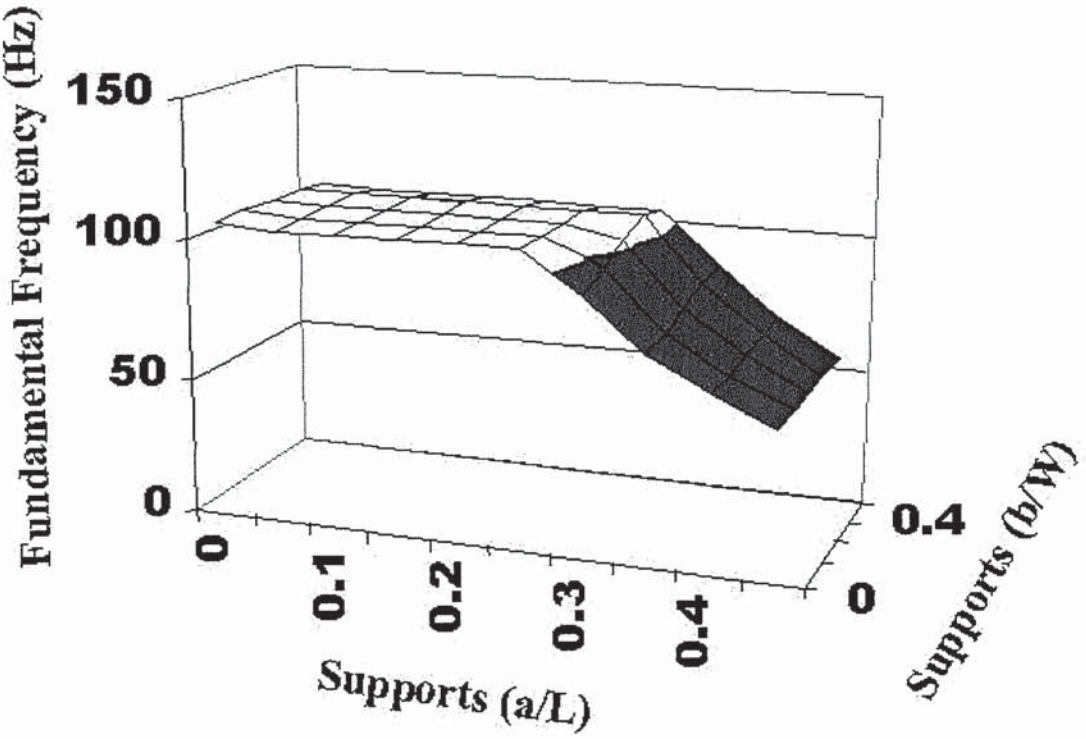

Figure 6.25 Case 4-Fundamental frequency versus plate support locations

Elastic Modes	Natural Frequency (Hz)
1	88
2	106.94
3	236.92
4	245.39
5	364.21

Table 6.1 Case 4 – Natural frequencies of a free rectangular plate

To further scrutinise the results, the overall effect of varying support locations on the changes to the natural frequencies of the plate is tabulated in Table 6.3 and illustrated in Figure 6.11. Figure 6.11 shows a plot of the sum of natural frequencies for the first five modes against support locations. The sum of the plate's natural frequencies (SNF) is defined as

$$SNF = \sum_{i=1}^{5} \omega_i \tag{6.3}$$

where ω_i is the computed frequency from the FE analysis.

The numerical value of SNF provides a relative indication of the maximum overall increase in the lower spectrum natural frequencies of the structure. Hence, as shown

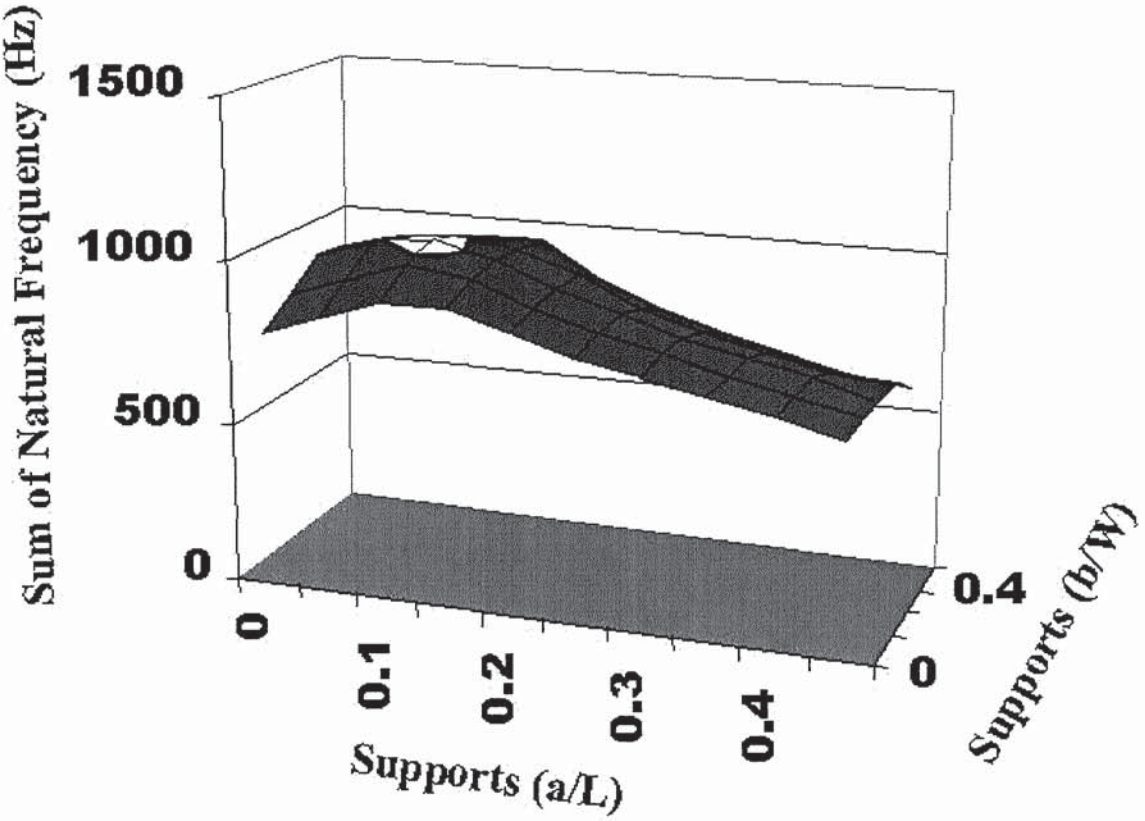

Figure 6.26 Case 4 - Sum of natural frequency (SNF) versus support locations of plate

in Figure 6.26, the best pairs of simple support locations corresponds to the dimensionless support locations of a/L = 0.10 and b/W = 0.2. These paired support locations are shown as solid circles in Figure 6.23.

		Dimensionless distance of support locations (b/W) along vertical nodal line				
		0	**0.1**	**0.2**	**0.3**	**0.4**
Dimensionless distance of support locations (a/L) along horizontal nodal line	**0**	**106.94**	**106.94**	**106.94**	**106.94**	104.72
	0.05	**106.94**	**106.94**	**106.94**	**106.94**	104.72
	0.10	**106.94**	**106.94**	**106.94**	**106.94**	104.72
	0.15	**106.94**	**106.94**	**106.94**	**106.94**	104.72
	0.20	**106.94**	**106.94**	**106.94**	**106.94**	104.72
	0.25	**106.94**	**106.94**	**106.94**	**106.94**	104.72
	0.30	92.51	97.31	102.85	106.62	104.72
	0.35	74.69	76.61	79.97	84.42	84.95
	0.40	63.95	64.22	65.10	67.55	68.24
	0.45	53.37	53.37	53.37	53.37	53.37

Table 6.2 Case 4 – Fundamental frequency (Hz) versus dimensionless support locations of plate

If the ADPR are calculated for the first five modes of vibration, it is noted that the ADPR for each paired support locations are the nearest to the mean of the average driving point residues based on their respective nodal lines in question. As stated in the simple procedure, it is advocated that mean ADPR along each nodal line can be used as an indicator for finding the vicinity of the best support locations.

		Dimensionless distance of support locations (b/W) along vertical nodal line				
		0	**0.1**	**0.2**	**0.3**	**0.4**
Dimensionless distance of support locations (a/L) along horizontal nodal line	**0**	787.5	862.05	934.98	916.02	831.97
	0.05	854.31	929.73	996.53	969.7	887.43
	0.10	912.87	991.68	**1021.85**	991.69	946.08
	0.15	925.49	963.7	972.0	963.41	935.86
	0.20	867.12	885.93	892.5	887.32	826.69
	0.25	815.37	827.84	832.24	803.33	742.08
	0.30	772.91	782.05	784.44	740.44	682.87
	0.35	733.91	740.17	740.4	693.11	637.63
	0.40	693.48	698.09	695.81	657.8	598.72
	0.45	648.81	653.04	649.84	639.43	567.52

Table 6.3 Sum of first five natural frequencies (SNF) versus support locations of plate

6.5 APPLICATION TO PCB WITH IN-SERVICE BOUNDARY CONDITIONS

Based on the preceding discussion, the above methodology is applied to the PCB with two wedge retainers and a plug-in connector, discussed in Chapter 3, where the accurate FE model for the PCB with three supported edges was developed. This PCB configuration is considered to be a typical application case for the study of point support's effect on fundamental frequency. The point support was modelled as a clamped node in the FE model; that is, both the displacement and rotation in the x-direction and y-direction are zero. To determine the location of the single point support

that yields the largest increase in the fundamental frequency, it is obvious that this point should lie along the nodal line of the second mode shape.

The FE mesh generation grid and its node numbers are shown in Figure 3.1 and it may be seen that the first and second natural frequencies and mode shapes of the vibrating PCB under its original boundary conditions are shown in Figures 3.4a and 3.4b respectively. Now, there are altogether 9 candidate points that lie along the nodal line of mode 2, namely, node 35, 36, ..., 43. To introduce an internal point restraint for maximising its fundamental frequency, it is logical to select node 39 as the support location. This is due to the fact that node 39 is located at the mid-point of the nodal line. Furthermore, it can be observed from Figure 3.4b that node 39 lies along a symmetrical plane for the oscillation of the PCB at its second natural frequency.

The effect of the % increase in the fundamental natural frequency at various internal point supports being restrained in turn is shown in the contour plot of Figure 6.27. The maximum increase in fundamental frequencies are due to the point restraints at nodes 35 to node 43, which lie along the nodal line of node 2. It is apparent from the contour plot that the optimal location is at node 39, which is at the mid-point of the nodal line of mode 2. For the designer to identify the physical location of mode 2 nodal line, this occurs at a distance of 72% from the connector edge. Further, the physical location of the nodal line for mode 3 runs along the x-axis and is 50% from one wedge retainer to the other. The increase in fundamental natural frequency is significant, from 68.4 Hz to 146.9 Hz, or 115% higher.

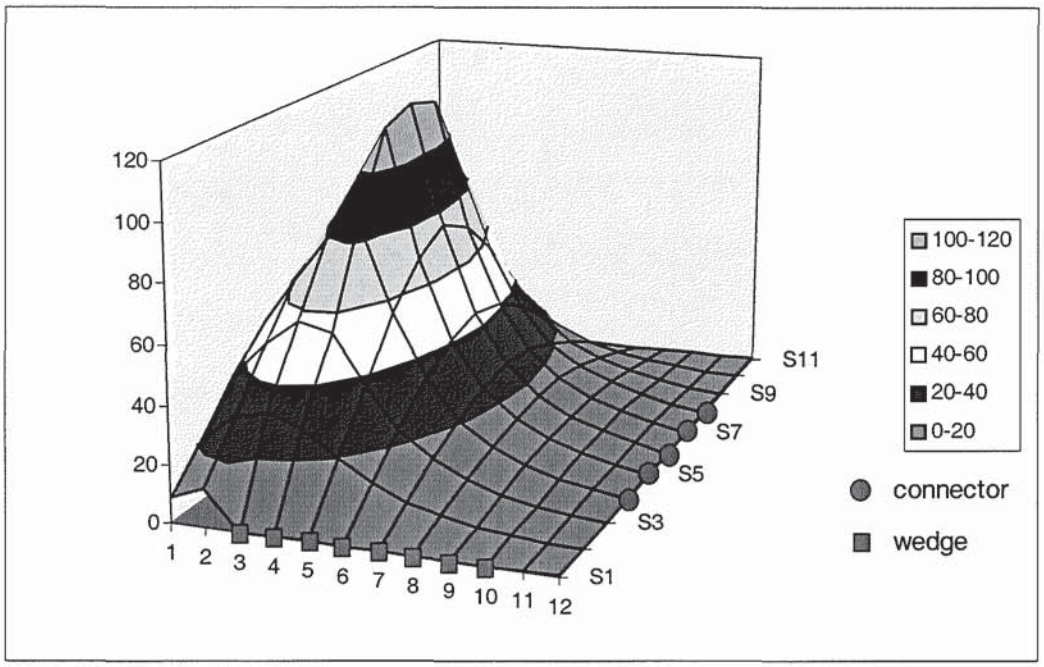

Figure 6.27 Effect of internal point support - % increase of fundamental frequency

Based on a single point restraint at node 39, the mode shapes of the first and second mode are shown in Figure 6.28a and 6.28b respectively. The frequencies of 146.9 Hz and 167.5 Hz corresponded to the mode shapes of modes 1 and 2 respectively. It can be seen that the mode shape for mode 1 is very similar to the mode shape for mode 2 of the case without the point constraint as depicted in Figure 3.4b. However, its frequency is 18% higher, at 146.9 Hz. This is quite reasonable as it is considered that there is still some rotation present at node 39 of the unconstrained case whereas node 39 is a clamped node for internal point constraint. Simulated results also show that the second largest increase of mode 1 frequency of 122.6 Hz, or 79% higher, occurred with a point constraint at node point 17. This internal point restraint also produced the largest increase in second mode frequency of 233 Hz, or 87% higher than the unconstrained

case. The mode shapes of the first and second modes are shown in Figures 6.29a and 6.29b respectively.

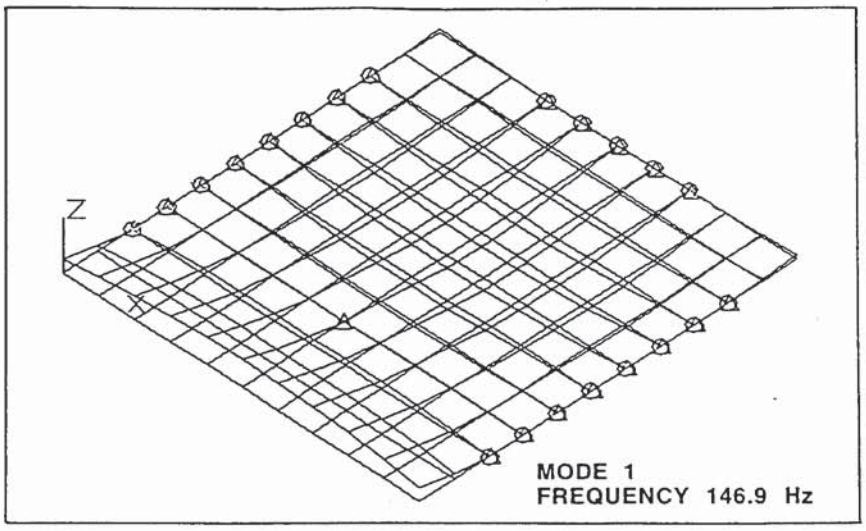

Figure 6.28a Fundamental mode shape with point constraint at node 39

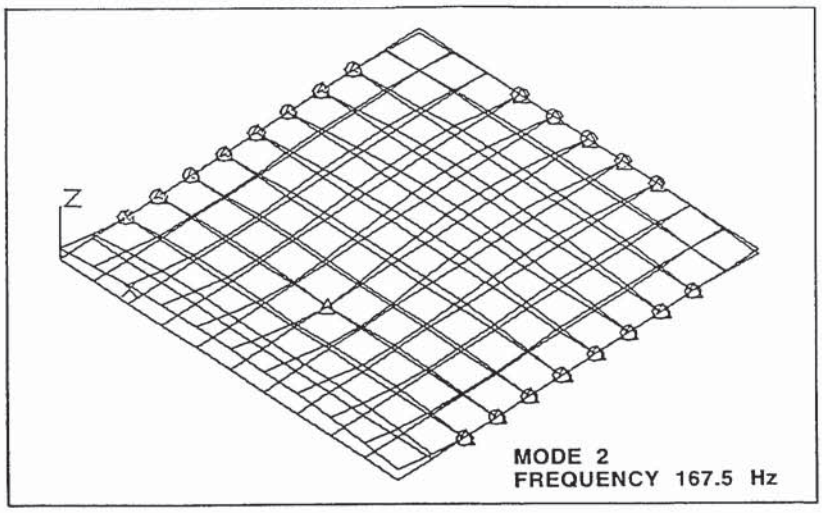

Figure 6.28b Second mode shape with point constraint at node 39

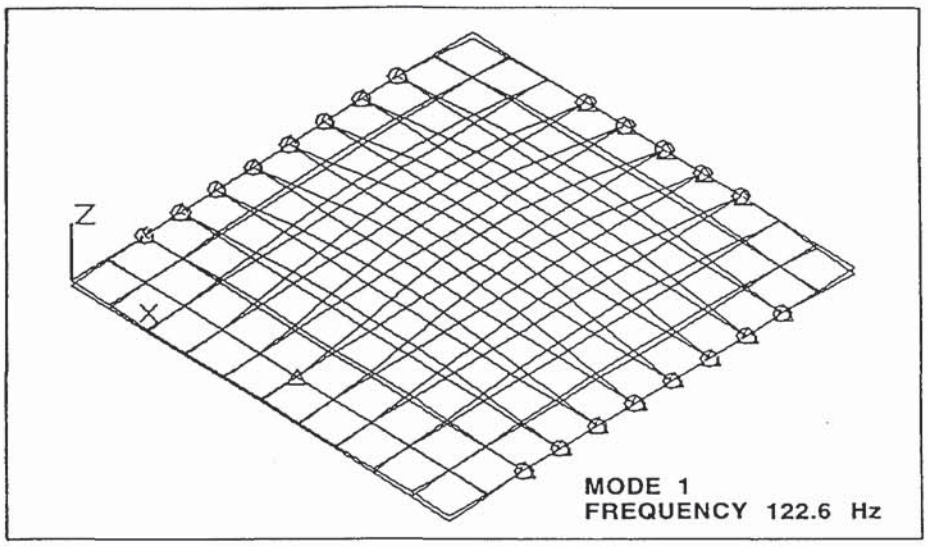

Figure 6.29a Fundamental mode shape with point constraint at node 17

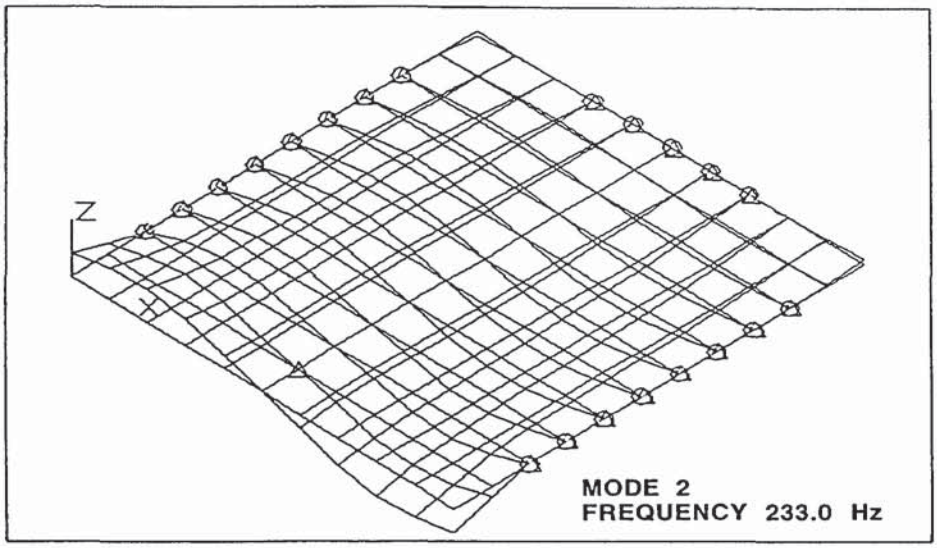

Figure 6.29b Second mode shape with point constraint at node 17

6.6 CONCLUDING REMARKS

This chapter analyses the natural frequencies and mode shapes of simple plate structures, and describes a relatively simple method in determining the support locations for maximising the fundamental natural frequency of vibrating plate structures. The technique is simple and does not require any optimisation or sequential search algorithm in the analysis. The key to the procedure is to position the necessary supports at positions so as to eliminate the lower modes from the original configuration. This is accomplished by introducing point supports along the nodal lines of the highest possible mode from the original configuration, so that all the other lower modes are eliminated by the introduction of the new or extra supports to the structure. It also proposed inspecting the average driving point residues along the nodal lines of vibrating plates to find the optimal locations of the supports.

A numerical example using a plate with four simply supported points is provided and it confirmed the validity of the proposed approach. The validity of the approach is further reinforced by investigating the effect of a point constraint on a PCB, which is supported on its three edges by two wedge retainers and a plug-in connector, as seen in a typical electronic box.

CHAPTER 7

CONCLUSIONS AND RECOMMENDATIONS

7.1 CONCLUSIONS

More PCB assemblies are built for use onboard aircraft, ships and land vehicles. Under dynamic environments, the manner in which the PCB assemblies are supported can considerably affect its reliability and performance. The vibration characteristics of the PCB have been studied by numerical and experimental methods. Based on the results obtained, the following conclusions can be drawn:

1) Wedge retainers and plug-in connectors used on PCBs do not provide the classical boundary support conditions such as simple supports or clamped supports. They should, however, be treated as elastic supports with rotational stiffnesses along its edges.

2) The wedge retainer stiffness predominately affect the frequencies of the first, second, third and fifth modes whereas changes in the plug-in connector's stiffness predominantly affect the second, and fourth mode and to a slight extent, the fifth mode frequencies.

3) Dynamic FE modelling can be an effective tool in the study of engineering structures. It is shown that the in-service support conditions of two wedge retainers and a plug-in connector provide a percent fixity of 39.5% more than the classical simply supported case.

4) By using an eigensensitivity method, the rotational stiffnesses representing the boundary supports of a PCB structure can be updated effectively and shown to be capable of representing the dynamics of the PCB structure accurately. The result shows that the percentage error in the fundamental frequency of the PCB FE model is found to be substantially reduced from 22.3% to 1.3%.

5) The eigensensitivity method demonstrated the effectiveness of using only the vibration test frequencies as reference data when the mode shapes of the original untuned model are almost identical to the referenced modes/experimental data. When using only modal frequencies in model improvement, the analysis is very much simplified. Furthermore, the time taken to obtain the experimental data will be substantially reduced as the experimental mode shapes are not required.

6) A method for determining the support locations for maximizing the fundamental natural frequency of vibrating structures has been developed. The key to the procedure is to position the necessary supports at positions so as to eliminate the lower modes from the original configuration. This is accomplished by introducing point supports along the nodal lines of the highest possible mode from the original

configuration, so that all the other lower modes are eliminated by the introduction of the new or extra supports to the structure. It also proposes inspecting the average driving point residues along the nodal lines of vibrating structures.

7.2 RECOMMENDATIONS

1) The work carried out is based on a bare PCB supported on its three edges and it is assumed that there is negligible mass errors. In the case of a PCB mounted with surface mount components, it is inevitable that there will be mass errors in the FE model developed. It is therefore recommended that future work should investigate the feasibility of the approach presented in this thesis to account for the inclusion of the added mass and stiffness of the components on the PCB.

2) The methodology for maximizing the fundamental frequency was applied to a PCB or simple plate structure. However, most engineering structures are rather complex and irregular in shape. It is recommended that the methodology should be examined further on more complex engineering structures such as a space satellite.

REFERENCES

Abrate, S., 1995, "Vibration of Point-Supported Rectangular Composite Plates", *Composite Science and Technology*, Vol. 53, pp. 325-332.

Algor *Finite Element Analysis Reference Manual*, 1991, Algor Inc., Pittsburgh, PA, USA.

Allemang, R.J. and Brown, D.L., 1986, "Multiple-Input Experimental Modal Analysis – A Survey", *International Journal of Modal Analysis*, January 1986, pp. 37-44.

Allemang, R.J., 1993, "Modal Analysis – Where Do We Go From Here?", *International Journal of Analytical and Experimental Modal Analysis*, Vol. 8, No. 2, pp. 80-91.

Allemang, R.J., Brown, D.L. and Rost, R.W., 1987, "Experimental Modal Analysis and Dynamic Component Synthesis", *AFWAL-TR-87-3069*, Vol. I-IV, Flight Dynamics Laboratory, Wright-Patterson Air Force Base.

Azimi, S., 1989, "Axisymmetric Vibration of Point-supported Circular Plates", *Journal of Sound and Vibration*, Vol. 135, No. 2, pp. 177-195.

Barker, D.B. and Chen, Y.S., 1993, "Modeling the Vibration Restraints of Wedge Lock Card Guides", Transactions of ASME, *Journal of Electronic Packaging*, Vol. 115, No. 2, pp.189-194.

Baruch, M. and Itzhack, I.Y.B., 1978, "Optimal Weighted Orthogonalization of Measured Modes", *AIAA Journal*, Vol. 16, No. 4, 346-351.

Baruch, M., 1978, "Optimization Procedure to Correct Stiffness and Flexibility Matrices Using Vibration Tests", *AIAA Journal*, Vol. 16, No. 11, 1208-1210.

Bathe, K.J. and Wilson, E.L., 1972, "Solution Methods for Eigenvalue Problems in Structural Mechanics", *International Journal of Numerical Methods in Engineering*, Vol. 6, pp. 213-226.

Belvins, R.D., 1979, *Formulas for Natural Frequency and Mode Shape*. Malabar, Florida: Robert E. Krieger Publishing Co.

Berman, A., 1979, "Mass Matrix Correction Using an Incomplete Set of Measured Modes", *AIAA Journal*, Vol. 17, No. 10, pp. 1147-1148.

Bhat, R.B., 1985, "Natural Frequencies of Rectangular Plates Using Characteristics Orthogonal Polynomials in the Rayleigh-Ritz Method", *Journal of Sound and Vibration*, Vol. 114, pp. 493-499.

Brandon, J.A., 1990, *Strategies for Structural Dynamic Modification*, Research Studies Press Ltd., England.

Brayton, R.K. and Spence, R., 1980, *Sensitivity and Optimization*, Elsevier, New York.

Brousse, P., 1988, *Optimization in Mechanics: Problems and Methods*, Elsevier Science Publishers, The Netherlands.

Burgess, J.F., Carlson, R.O., Glascock, H.H., Neugebauer, C.A. and Webster, H.F., 1984, "Solder Fatigue Problems in Power Packages", IEEE *Transactions on Components, Hybrids and Manufacturing Technology*, Vol. 7, No. 4, pp. 405-410.

Caruso, H., 1990, "Tailoring a Temperature-Altitude-Humidity Test Based on Aircraft Mission Profiles", *Proceedings of the Institute of Environmental Sciences*, pp. 558-561.

Chang, T.S. and Magrab, E.B., 1993, "Component Rearrangement on Printed Wiring Boards to Maximize the Fundamental Natural Frequency", *Journal of Electronic Packaging,* Transactions of ASME, Vol. 115, pp. 312-321.

Cheung, Y.K. and Zhou, D., 1999, "Free Vibrations of Rectangular Composite Plates with Point Supports Using Static Beam Functions", *Composite Structures*, Vol. 44, No. 2, pp. 145-154.

Chi, C., 1972, "Modes of Vibration in a Circular Plate with Three Simple Support Points", *AIAA Journal*, Vol. 10, No. 2, pp. 142-147.

Collins, G., 1986, "Vibration Protection, Avoiding the Shakes", *Machine Design*, December, pp. 113-116.

Cortinez, V.H. and Laura, P.A.A., 1986, "A Note of Vibrating Membranes and Plates with an Internal Support", *Journal of Sound and Vibration*, Vol. 104, No. 3, pp. 533-535.

DiTaranto, R.A. and McGraw, J.R. Jr., 1969, "Vibration Bending of Damped Laminated Plates", *Journal of Engineering for Industry*, Vol. 91, pp.1081-1090.

Dwyer, H.A. and Peterson, T., 1980, "A Study of Turbulent Flow with Sensitivity Analysis", *AIAA Journal*, Vol. 18, No. 4, pp. 1377-1397.

Engel, P.A., Lin, C.K., Toda, M.D. and Gjone, R., 1984, "Thermal Stress Analysis of Soldered Pin Connectors for Complex Electronics Modules", *Computers in Mechanical Engineering*, May, pp. 59-69.

Engelmaier, W. and Attawala, A.I., 1989, "Surface Mount Attachment Reliability of Clip-Leaded Ceramic Chip Carriers on FR-4 Circuit Boards", *IEEE Transactions on Reliability*, Vol. 12, No.2, pp. 284-296.

Engelmaier, W., 1984, "Functional Cycles and Surface Mounting Attachment Reliability", *Surface Mount Technology*, pp. 87-114.

Ewins, D.J., 1984, *Modal Testing: Theory and Practice*, Research Studies Press Ltd., England.

Frear, D.R., 1989, "Thermomechanical Fatigue of Solder Joints: A New Comprehensive Test Method", IEEE *Transactions on Reliability*, Vol. 12, No.4, pp. 492-501.

Friswell, M.I. and Mottershead, J.E., 1995, *Finite Element Model Updating in Structural Dynamics*, Kluwer Academic Publishers, London.

Fox, R.L. and Kapoor, M.P., 1968, "Rates of Change of Eigenvalues and Eigenvectors", *AIAA Journal*, Vol. 6, No. 12, 246-249.

Golub, G.H. and Van Loan, C.V., 1983, *Matrix Computations*, North Oxford Academic Publishing Co. Ltd.

Gorman, D.J., 1982, *The Free Vibration Analysis of Rectangular Plates*, Elsevier North Holland Inc., New York, NY.

Ham, S.J. and Lee, S.B., 1996, "Experimental Study for Reliability of Electronic Packaging Under Vibration", *Journal of Experimental Mechanics*, Vol. 36, No. 4, pp. 339-344.

He, J. and Ewins, D.J., 1986, "Analytical Stiffness Matrix Correction Using Measured Vibration Modes", *The International Journal of Analytical and Experimental Modal Analysis*, Vol. 1, No. 3, pp. 9-14.

Huang, E.J. and Rousselet, B., 1980, Design Sensitivity Analysis in Structural Mechanics II: Eigenvalue Variation, *Journal of Structural Mechanics*, Vol. 8, No. 2, pp. 161-186.

Hwang, J.T., Dougherty, E.P., Rabitz, S. and Rabitz, H., 1978, The Green's Function Method of Sensitivity Analysis in Chemical Kinetics, *Journal of Chemical Physics*, Vol. 69, December, pp. 5180-5191.

Imamovic, N. and Ewins, D.J., 1997, "Optimization of Excitation DOF Selection for Modal Tests", *Proceedings of the International Modal Analysis Conference* - IMAC. Vol. 2, SEM, Bethel, CT, USA, pp. 1945-1951.

Irie, T. and Yamada, G., 1978, "Free Vibration of Circular Plate Elastically Supported at Some Points", *Bulletin of Japan Society of Mechanical Engineers*, Vol. 21, No. 161, pp. 1602-1609.

Jahn, H.A., 1948, "Improvement of an Approximate Set of Latent Roots and Modal Columns of a Matrix by Methods Akin to Those of Classical Perturbation Theory", *Quarterly Journal Mechanical Applications in Mathematics*, Vol. 1, pp. 132-144.

Juang, J.N., Ghaemmaghami, P. and Lim, K.B., 1989, "Eigenvalue and Eigenvector Derivatives in a Nondefective Matrix", *Journal of Guidance, Control and Dynamics*, Vol. 12, pp. 480-486.

Klee, B.J., Kimball, D.V. and Tustin, W., 1971, *Vibration and Shock Test Fixture Design*, Tustin Institute of Technology, Santa Barbara, CA, USA.

Koffman, E.B., and Friedman, F.L., 1993, *FORTRAN with Engineering Applications*, 5th Edition, Addison-Wesley.

Lau, J.H. and Harkins, C.G., 1988, "Stiffness of Gull-Wing Leads and Solder Joints for a Plastic Quad Flat Pack", IEEE *Transactions on Components, Hybrids and Manufacturing Technology*, Vol. 13, No. 1, pp. 124-130.

Lau, J.H., Harkins, C.G., Rice, D.W., Kral, J. and Wells, B., 1988, "Experimental and Statistical Analyses of Surface-Mount Technology PLCC Solder-Joint Reliability", IEEE *Transactions on Reliability*, Vol. 37, No. 5, pp. 524-530.

Lau, J.H. and Rice, D.W., 1985, "Solder Joint Fatigue in Surface Mount Technology: State of the Art", *Solid State Technology*, pp.91-104.

Lau, J.H., Powers-Maloney, L.M., Baker, J.R, Rice, D. and Shaw, B., 1990, "Solder Joint Reliability of Fine Pitch Surface Mount Technology Assemblies", IEEE *Transactions on Components, Hybrids and Manufacturing Technology*, Vol. 13, No. 3, pp.534-544.

Laura, P.A.A, Ercoli, L. and La Malfa, S., 1995, "Dynamic Stiffening of a Printed Circuit Board", *Acustica*, Vol. 81, pp. 196-197.

Laura, P.A.A. and Cortinez, V.H., 1995, "Dynamic Stiffening of Thin Plates of Regular Polygonal Shape", *Journal of Sound and Vibration*, Vol. 183, No. 4, pp. 607-614.

Laura, P.A.A. and Grossi, R., 1978, "Transverse Vibrations of a Rectangular Plate Elastically Restrained Against Rotation Along Three Edges and Free on the Fourth Edge", *Journal of Sound and Vibration*, Vol. 59, No. 3, pp. 355-368.

Leissa, A.W., 1973, "The Free Vibration of Rectangular Plates", *Journal of Sound and Vibration*, Vol. 31, pp. 257-293.

Lim, G.H. and Ong, Y.K., 1990, "Effects of Card Guide Types and Lengths on Dynamic Response of Printed Circuit Board", *Proceedings of the MINDEF-NTI Joint R & D Seminar*, Singapore, pp. 12-17.

Lim, K.B., Junkins, J.L. and Wang, B.P., 1987, Re-examination of Eigenvector Derivatives, *AIAA Journal*, Vol. 25, pp. 581-587.

MacNeal, R.H., 1978, "A Simple Quadrilateral Shell Element", *Computers & Structures*, Vol. 8, pp. 175-183.

Markstein, H.W., 1987, "Designing Electronics for High Vibration and Shock", *Electronic Packaging and Production*, April, pp. 40-43.

Markstein, H.W., 1989, "Dealing With Vibration in Electronics", *Electronic Packaging and Production*, June, pp. 30-34.

McConnell, K.G., 1995, *Vibration Testing: Theory and Practice*, Wiley, New York.

Mitchell, L.D., 1988, "A Perspective View of Modal Analysis", *Proceedings of the 6th International Modal Analysis Conference*, Vol. 1, pp. xvii-xxi.

Mottershead, J.E. and Friswell, M.I., 1993, "Model Updating in Structural Dynamics: A Survey", *Journal of Sound and Vibration*, Vol. 167, No. 2, pp. 346-375.

Nelson, R.B., 1976, "Simplified Calculation of Eigenvector Derivatives", *AIAA Journal*, Vol. 14, pp. 1201-1205.

Pitarresi, J.M. and Di Edwardo, A.V., 1993, "A Design Approach for the Systematic Improvement of Support Locations for Vibrating Circuit Cards", *Journal of Electronic Packaging,* Transactions of ASME, Vol. 115, January, pp. 118-123.

Pitarresi, J.M. and Kunz, R.J., 1992, "A Simple Technique for the Rapid Estimation of the Optimal Locations for a Vibrating Plate," *Journal of Vibration and Acoustics*, Vol. 114, No. 1, pp. 112-118.

Rao, S.S., 1995, *Mechanical Vibrations*, 3rd Edition, Addison-Wesley, Mass.

Rayleigh, J.W.S., 1877, *The Theory of Sound,* Vol. 1, MacMillan Co; Dover Publications, Inc., 1945.

Rikards, R., 1993, "Finite Element Analysis of Vibration and Damping of Laminated Composites", *Composite Structures*, Vol. 24, pp. 193-204.

Roberts, J.C. and Stillo, D.M., 1991, "Random Vibration Analysis of a Printed Circuit Board with Electronic Components", *Journal of Institute of Environmental Sciences*, pp. 25-31.

SD-390 *Operator's Manual*, 1991, Spectral Dynamics Inc., U.S.A.

Shames , I.H. and Dym, C., 1985, *Energy and Finite Element Methods in Structural Mechanics*, Hemisphere Publishing Corporation.

Sloan, J.L., 1985, *Design and Packaging of Electronic Equipment*, Van Nostrand, New York.

Solomon, H.D., 1989, "Influence on Temperature on the Low Cycle Fatigue of the Surface Mounted Chip Carrier/Printed Circuit Board Joints", *Proceedings of the Institute of Environmental Sciences*, pp. 177-185.

Soong, T.T. and Grigoriu, M., 1993, *Random Vibration of Mechanical and Structural Systems*, Prentice Hall , Englewood Cliffs, New Jersey.

Steinberg, D.S., 1988, *Vibration Analysis for Electronic Equipment*, Wiley, New York.

Subrahmanyan, R., Wilcox, J.R. and Li, C., 1989, "A Damage Integral Approach to Thermal Fatigue of Solder Joints", IEEE *Transactions on Reliability*, Vol. 12, No. 4, pp. 480-491.

Swanson Analysis Systems, Inc., 1989, *ANSYS Users' Manual*, 7th Edition, New York.

SYSTUNE *Test and Analysis Integration System User's Manual*, 1994, Dynamic Design Solutions, N.V., Ver. 3.2 Documentation, Leuven, Belgium.

Szymkowiak, E., Lesser, H.S. and Kaminski, E.F., 1981, "Stress Level Evaluation of a Printed Circuit Wiring Assembly Containing Large Hybrid Packages", *Proceedings of the Institute of Environmental Sciences*, pp. 77-81.

Thomson, W.T., 1993, *Theory of Vibration with Applications*, 4th Edition, Prentice Hall, Englewood Cliffs, New Jersey.

Tustin, W., and Mercado, R., 1984, *Random Vibration in Perspective,* Tustin Instutute of Technology, Santa Barbara, California.

Wang, B.P, and Nomura, S., 1989, "Optimal Support Location for Maximizing Fundamental Natural Frequency of a Free-Free Rectangular Plate," *Computer Aided Optimum Design of Structures: Recent Advances*, edited by Brebbia, C.A. and Hernandez, S., Springer-Verlag, Berlin, pp. 277-286.

Warburton, G.B., 1954, "The Vibration of Rectangular Plates", *Proceedings of Institution of Mechanical Engineers*, ser. A, Vol. 168, No. 12, pp. 371-384.

Warburton, G.B. and Edney, S.L., 1984, "Vibrations of Rectangular Plates with Elastically Restrained Edges", *Journal of Sound and Vibration*, Vol. 95, No. 4, pp.537-552.

Wong, T-L., Stevens, K.K. and Wang, G., 1991, "Experimental Modal Analysis and Dynamic Response Prediction of PC Boards with Surface Mount Electronic Components", *Journal of Electronic Packaging*, Transactions of ASME, Vol. 113, pp. 244-249.

Yamada, S. E., 1987, "Elastic/Plastic Fracture Analysis for Bonded Joints", *Engineering Fracture Mechanics,* Vol. 27, No. 3, pp. 315-328.

Yamada, S.E., 1989, "A Fracture Mechanics Approach to Solder Joint Cracking", IEEE *Transactions on Components, Hybrids and Manufacturing Technology*, Vol. 12, No. 1, pp. 99-104.

Zienkiewicz, O.C., 1977, *The Finite Element Method*, 3rd Edition, McGraw Hill, London.

Zienkiewicz, O.C. and Taylor, R.L., 1989, *The Finite Element Method, Vol. 1, Basic Formulation and Linear Problems*, 4th Edition, McGraw Hill, London.

APPENDIX A - FEM DATA FILE

FEM Data File

The FEM Data File consists of the following parts :

- Titles
- General Control Parameter
- Data Sets

The data sets are identified by a number. Below is the list of numbers that are actually used:

Set ID	Description
-1	Nodal Coordinates
-2	Element Data
-3	Material Properties
-4	Geometrical Properties
-5	Boundary Conditions
-6	Lumped Masses

The first record of each data set is preceded by an identification line which includes the data set identifier.

Fields that are currently not used are identified with IDUMM or RDUMM which can be any integer or real value (usually zero).

Titles

Three records are used

Record 1: FILE_CODE, MESSAGE (A5,A75)

Field 1:	FILE_CODE	=	'02.01' (5 characters)
Field 2:	MESSAGE	=	Text string (maximum 75 characters)

Record 2: TIFEA (A80)

Field 1:	TIFEA	=	Title referring to the FE mesh (maximum 80 characters)

Record 3: CDATE (A23)

Field 1:	CDATE	=	File creation date and time, stored in a 23 character string (e.g. '02-JAN-1990 15:20:16:78'.

General Control Parameters

Ten records are used, each consisting of 5 fields. The general control parameters define the dimension and characteristics of the FE model. All values are integers.

Record 1:	NPOIN, NELEM, NDIME, NMATS, NGEOP (5IIO)		
Field 1:	NPOIN	=	Total number of nodes in the mesh
Field 2:	NELEM	=	Total number of elements in the mesh
Field 3:	NDIME	=	Dimension of the structure (1, 2 or 3)
Field 4:	NMATS	=	Total number of material types in the mesh
Field 5:	NGEOP	=	Total number of geometry types in the mesh
Record 2:	NNBCI, NNWLM,		NDOFC, IDUMM, IDUMM (5I10)
Field 1:	NNBCI	=	Total number of nodes where boundary conditions are defined
Field 2:	NNWLM	=	Total number of nodes where lumped masses are defined
Field 3:	NDOFC	=	Code referring to the DOF/node
Fields 4 and 5:		=	Dummy variables (not used)
Records 3 to 10	IDUMM, IDUMM,		IDUMM, IDUMM, IDUMM (5I 1 0)
Fields 1 to 5:		=	Dummy variables (not used)

Note All nodes in the mesh need to have the same number of Degrees Of Freedom (DOF). These DOFs are defined by the parameter NDOFC.

Data Set -1 : Nodal Coordinates

This data set is included only if NPOFN is different from zero. The first record contains the data set identifier. Record 2 is repeated for each nodal point (NPOIN records).

Record 1:	ICODE, IDUMM(1=1,9) (10I5)		
Field 1:	ICODE	=	Data set identifier (= -1)

Fields 2 to I0:		=	Dummy variables (not used)
Record 2:	IPOIN, IDUMM, IDUMM, IDUMM, IDUMM, XCOORD,YCOORD,ZCOORD (I10,4I5,3G13.6)		
Field 1:	IPOIN	=	External node number
Fields 2 to 5:		=	Dummy variables (not used)
Field 6:	XCOORD	=	Global X coordinate of the node
Field 7:	YCOORD	=	Global Y coordinate of the node
Field 8:	ZCOORD	=	Global Z coordinate of the node

Note All coordinates are always assumed to be GLOBAL CARTESIAN coordinates.

Data Set -2: Element Data

This data set is included only if NELEM is different from zero. The first record contains the data set identifier. Records 2 and 3 are repeated for each element (NELEM pairs of records).

Record 1:	ICODE, IDUMM(I=1,9) (10I5)		
Field 1:	ICODE	=	Data set identifier (= -2)
Fields 2 to 10:		=	Dummy variables (not used)
Record 2:	IELEM, LTYPE, LMATS, LGEOP, IDUMM, XORNT, YORNT,ZORNT (IIO,4I5,3GI3.6)		
Field 1:	IELEM	=	External element number
Field 2:	LTYPE	=	Element type
Field 3:	LMATS	=	Material identification number. This number refers to an entry in the material properties data set.
Field 4:	LGEOP	=	Geometrical identification number. This number refers to an entry in the geometrical properties data set.
Field 5:	IDUMM	=	Dummy variable (not used)
Field 6:	XORNT	=	X coordinate of a point defining the local XY plane (1D elements only)
Field 7:	YORNT	=	Y coordinate of a point defining the local XY plane (ID elements only)
Field 8:	ZORNT	=	Z coordinate of a point defining the local XY plane (ID elements only)

Record 3: LNODS (8I10)

Fields 1 to 8: LNODS = Element connectivity list. If the number of nodes/element exceeds 8, the connectivity list is continued on additional records. The node numbers in the connectivity list are external numbers.

Data Set -3: Material Properties

This data set is included only if NMATS is different from zero. The first record contains the data set identifier. The number of records per material type that follow is depending on the material type.

Record 1: ICODE, IDUMM(I=1,9) (10I5)

Field 1: ICODE = Data set identifier (= -3)

Fields 2 to I0: = Dummy variables (not used)

Record 2: LMATS, LTMAT, MMPAR, ICODE IDUMM (5I10)

Field 1: LMATS = Material number. This number corresponds with a material number in the element data set.

Field 2: LTMAT = Material type

Field 3 MMPAR = Number of specified material properties

Field 4: ICODE = 1 if the properties corresponding with material 5 are defined in global axis. Not used for other material types.

Field 5: IDUMM = Dummy variable (not used)

If LTMAT 0 no other records are written.

Record 3: PROPS (6GI3.6)

Fields 1 to 5: PROPS = MMPAR material properties listed in the sequence.
If MMPAR exceeds 6, the list is continued on additional records.
If MMPAR is zero, the record is not written.

If LTMAT = 6, an additional record is written:

Record 4: NLAYER, (LMATS,LGEOP),ILAYER =I, NLAYER)

(I5, 200I5)

Field 1:	NLAYER	=	Number of layers (<= I 00)
Fields 2 - (2*NLAYER+1):			(LMATS,LGEOP) For each layer, a material and geometry number is written. These materials and geometries must be defined in the same SNF file.

Data Set -4 : Geometrical Properties

This data set is included only if NGEOP is different from zero. The **first** record contains the data set identifier. The number of records per geometry that follow is depending on the geometry type.

Record 1:	ICODE, IDUMM(I= 1,9) (10I5)		
Field 1:	ICODE	=	Data set identifier (= -4)
Fields 2 to 10:		=	Dummy variables (not used)
Record 2:	LGEOP, LTGEO, MGPAR, IDUMM, IDUMM (51 *1* 0)		
Field 1:	LGEOP	=	Geometry number. This number corresponds with a geometry number in the element data set.
Field 2:	LTGEO	=	Geometry type (see table 2.6.)
Field 3:	MGPAR	=	Number of geometrical properties
Fields 4 and 5:		=	dummy variables (not used)

If LTGEO = 0 no other record is written.

Record 3:	PROPS (6G13.6)		
Fields 1 to 6:	PROPS	=	MGPAR geometrical properties If MGPAR exceeds 6, the list is continued on additional records. If MGPAR is zero, the record is not written. Geometrical properties of 1-D elements are defined in the LOCAL element axis as defined in data set -2 ("Element data"). This must be the principal axis (hence $I_{xy} = 0$).

Data Set -5 : Boundary Conditions

This data set is included only if NNBCI is different from zero. The first record contains the data set identifier. The number of records per geometry that follow is depending on the boundary condition type.

Record 1: ICODE, IDUMM(I=1,9) (10I5)

Field 1:	ICODE	=	Data set identifier (= *-5)*
Fields 2 to 10:		=	Dummy variables (not used)

Record 2: NODBC, NELCN, NBCOD I, NBCOD2, NBCOD3, NBCOD4, NBCOD5, NBCOD6 (II 0,I5,6I2)

Field 1:	NODBC	=	External node number where boundary conditions are defined
Field 2:	NELCN	=	Number of DOFs where elastic constraints or imposed displacements are defined
Fields 3 to 8:	NBCODX	=	Code identifying for all DOFs the type of constraint. All six codes are required. Zeros can be added for unused DOFS. 0 : free 1 : fixed 2 : elastic 3 : imposed displacement

If NELCN is different from zero, an additional record (= record 3) has to be added. Otherwise record 2 is repeated for the next value of NODBC.

Record 3: BCOIN I, BCOfN2,... (6G13.6)

Fields 1 to NELCN:	$BCOIN_X$	=	Elastic constraint values for all DOFs corresponding with $NBCOD_X$ = 2 and imposed displacements for all DOFs corresponding with $NBCOD_X$ = 3.

Remarks

DOF appear in the following order:

1 . displacement X (UX)
2. displacement Y (UY)
3. displacement Z (UZ)
4. rotation X (RX)
5. rotation Y (RY)
6. rotation Z (RZ)

All values are defined in GLOBAL axis.
Elastic constraints and imposed displacements cannot be used together at the same node. Combinations with other types of boundary conditions are allowed.

Data Set -6 : Lumped Masses

This data set is included only if NNWLM is different from zero. The first record contains the data set identifier. Records 2 and 3 are repeated for each node where lumped masses are defined (NNWLM pairs of records).

Record 1:	ICODE, IDUMM(1=1,9) (10I5)		
Field 1:	ICODE	=	Data set identifier (= -6)
Fields 2 to I0:		=	Dummy variables (not used)
Record 2:	NODCM (I10)		
Field 1:	NODCM	=	Node number where lumped mass values are defined
Record 3:	CMASS (6G13.6)		
Fields 1 to 21:	CMASS	=	The upper triangle of a 6 x 6 matrix, describing the lumped mass properties and written line after line. The properties are defined in the GLOBAL axis. The number of values is 21.

EMA Data File

The file consists of the following parts:

- Titles
- General Control Parameters
- Data Sets

The data sets are identified by a number. Below is the list of numbers that are actually used:

Set ID Description

-30 Measurement point coordinates
-31 Measurement point connectivities
-32 Experimental resonance frequencies
-33 Experimental normal or complex modes

The first record of each data set is preceded by a CONTROL LINE. Fields that are currently not used are identified with IDUMM or RDUMM which can be any integer or real value (usually zero).

Titles

Three records are used:

Record 1: FILE_CODE, MESSAGE (5A1,75A1)

- Field 1: FILE_CODE = '11.01' (5 characters)
- Field 2: MESSAGE = Text string (max. 75 characters)

Record 2: TIEMA (80A1)

- Field 1: TIEMA = Title referring to the EMA data (max. 80 characters)

Record 3: CDATE (23A1)

- Field 1: CDATE = File creation date and time, stored in a 23 character string

Control Parameters

Ten records are used, each consisting of 5 fields. The control parameters define the dimension of the problem. All values are integers.

Record 1: NMFRE, NMPPM, NCOPM, NDIMM, NDOFC (5110)

- Field 1: NMFRE = Number of resonance frequencies in the file.
- Field 2: NMPPM = Number of measurement points per mode. If ICODI = 1 (see record 2) then NMPPM is also the number of mode shapes in the file.
- Field 3: NCOPM = Number of connected measurement points per mode.
- Field 4: NDIMM Dimension of the structure (1, 2 or3).
- Field 5: NDOFC Code referring to the DOF/point

Record 2: NMCOE, ICOD I, 1COD2, IDUMM, IDUMM (5I10)

- Field 1: NMCOE = Maximum number of connected points
- Field 2: ICOD1 = Key indicating the presence of modal displacement information:
  0 = no modal displacements
  1 = modal displacements

If ICOD I = 1, then modal displacements must be defined in all NMPPM points for NDOFN degrees of freedom per point for NMFRE modes.

Field 3: ICOD2 = Key indicating if the ENM model has been merged with a FEM model or not:
0 = not merged
1= merged

Fields 4 and 5: = Dummy variables (not used)

Record 3: ICPX2 IDUMM, IDUMM, IDUMM, IDUMM (5I10)

Field 1: ICPX2 = 0 : normal modes
1 : complex modes

Fields 2 to 5: = Dummy variables (not used)

Records 4 to I0: IDUMM, IDUMM, IDUMM, IDUMM, IDUMM (5110)

Fields 1 to 5: = Dummy variables (not used)

Data Set -30: Measurement Point Coordinates

The first record contains a data set identifier followed by NMPPM records.

Record 1: ICODE, IDUMM(I=1,9) (IOI5)

Field 1: ICODE = Data set identifier (= -30)

Fields 2 to 10: = Dummy variables (not used)

Record 2: IPOIN, IDUMM, IDUMM, IDUMM, IDUMM, XCOORD, YCOORD, ZCOORD (IIO,4I5,3GI3.6)

Field 1: IPOIN = External point number

Fields 2 to 5: = Dummy variable (not used)

Field 6: XCOORD = Global x coordinate of the point

Field 7: YCOORD = Global y coordinate of the point

Field 8: ZCOORD = Global z coordinate of the point

Record 2 is repeated for each measurement point.

Note: All coordinates are always assumed to be GLOBAL CARTESIAN coordinates.

Data Set -31: Measurement Point Connectivities

The first record contains a data set identifier followed by NCOPM records.

Record 1: ICODE, IDUMM(I=1,9) (10I5)

Field 1: ICODE = Data set identifier (= -31)

Fields 2 to 10: = Dummy variables (not used)

Record 2: MEUSR,NNODE,MNODS (8I10)

Field 1: MEUSR = Connection number

Field 2: NNODE If ICOD2 = 0 then NNODE is the number of connected points. This value must be 2.
If 1COD2 = I then NNODE is the number of connected points according to the element type code as used in the corresponding FE model.

Field 3: MNODS. If 1COD2 = 0 : list of connected points (2 values).
If 1COD2 = I : list of connected points (the number of values depends on the element type). If the number of connected points exceeds 6, additional records are added.

Record 2 is repeated for each measurement point connection.

Data Set -32: Experimental Resonance Frequencies

The first record contains a data set identifier followed by NMFRE records.

Record 1: ICODE, IDUMM(1=1,9) (1015)

Field 1: ICODE = Data set identifier (= -32)

Fields 2 to 10: = Dummy variables (not used)

Record 2: IEIGV, IDUMM,EEIVA, RDUMM, RDUMM, RDUMM (215,4G 1 3.6)

Field 1: IEIGV = Mode number

Field 2: IDUMM = Dummy variable (not used)

Field 3 EEIVA = Resonance frequency (Hertz)

Fields 4 to 6: = Dummy variables (not used)

Record 2 is repeated for each resonance frequency.

Data Set -33: Experimental Normal or Complex Modes

Record 1: ICODE, IDUMM(1=1,9) (10I5)

Field 1: ICODE = Data set identifier (= -33)

Fields 2 to I0: = Dummy variables (not used)

Record 2: IMPPM,IEEIV (2I10)

Field 1:	IMPPM	=	External point number
Field 2:	IEEIV	=	Mode shape number
Record 3:	EEIVE (6G13.6)		
Field 1 - NDOFN:	EEIVE	=	Components of normal modes or real part of complex modes at point IMPPM, corresponding with frequency IEEIV, for NDOFN DOF (NDOFN is depending on the value of NDOFC).
Record 4:	EEIVE (6G13.6)		
Field 1 - NDOFN:	EEIVE	=	Imaginary part of mode components at point IMPPM, corresponding with frequency IEEIV, for NDOFN DOF (NDOFN is depending on the value of NDOFC). This record is only used if ICPX2 = 1.

If ICOD1 = 1, records 2 and 3 are repeated NMPPM*NMFRE times. If ICOD1 = 0, this data set will not be included.

APPENDIX B – Data File

```
02.01- SYSTUNE FEM DATA FILE - VERSION WIN 3.2P
Test Vibration Analysis for Fibre-glass Printed Circuit Board (PCB)
29-JAN-1997
   483   440     3     1     1
   483     0     3     0     0
     0     0     0     0     0
     0     0     0     0     0
     0     0     0     0     0
     0     0     0     0     0
     0     0     0     0     0
     0     0     0     0     0
     0     0     0     0     0
     0     0     0     0     0
-1   0   0   0   0   0   0   0   0   0
     1   0   0   0   0 0.000000E+00 220.000    0.000000E+00
     2   0   0   0   0 233.400     220.000    0.000000E+00
     3   0   0   0   0 23.3400     220.000    0.000000E+00
     4   0   0   0   0 46.4800     220.000    0.000000E+00
     5   0   0   0   0 70.0200     220.000    0.000000E+00
     6   0   0   0   0 93.3600     220.000    0.000000E+00
     7   0   0   0   0 116.700     220.000    0.000000E+00
     8   0   0   0   0 140.040     220.000    0.000000E+00
     9   0   0   0   0 163.380     220.000    0.000000E+00
    10   0   0   0   0 186.720     220.000    0.000000E+00
    11   0   0   0   0 210.060     220.000    0.000000E+00
    12   0   0   0   0 233.400     0.000000E+00 0.000000E+00
    13   0   0   0   0 233.400     200.000    0.000000E+00
    14   0   0   0   0 233.400     180.000    0.000000E+00
    15   0   0   0   0 233.400     160.000    0.000000E+00
    16   0   0   0   0 233.400     140.000    0.000000E+00
    17   0   0   0   0 233.400     120.000    0.000000E+00
    18   0   0   0   0 233.400     100.000    0.000000E+00
    19   0   0   0   0 233.400     80.0000    0.000000E+00
    20   0   0   0   0 233.400     60.0000    0.000000E+00
    21   0   0   0   0 233.400     40.0000    0.000000E+00
    22   0   0   0   0 233.400     20.0000    0.000000E+00
    23   0   0   0   0 0.000000E+00 0.000000E+00 0.000000E+00
    24   0   0   0   0 210.060     0.000000E+00 0.000000E+00
    25   0   0   0   0 186.720     0.000000E+00 0.000000E+00
    26   0   0   0   0 163.380     0.000000E+00 0.000000E+00
    27   0   0   0   0 140.040     0.000000E+00 0.000000E+00
    28   0   0   0   0 116.700     0.000000E+00 0.000000E+00
    29   0   0   0   0 93.3600     0.000000E+00 0.000000E+00
    30   0   0   0   0 70.0200     0.000000E+00 0.000000E+00
    31   0   0   0   0 46.6800     0.000000E+00 0.000000E+00
    32   0   0   0   0 23.3400     0.000000E+00 0.000000E+00
    33   0   0   0   0 0.000000E+00 20.0000    0.000000E+00
    34   0   0   0   0 0.000000E+00 40.0000    0.000000E+00
    35   0   0   0   0 0.000000E+00 60.0000    0.000000E+00
    36   0   0   0   0 0.000000E+00 80.0000    0.000000E+00
    37   0   0   0   0 0.000000E+00 100.000    0.000000E+00
    38   0   0   0   0 0.000000E+00 120.000    0.000000E+00
    39   0   0   0   0 0.000000E+00 140.000    0.000000E+00
    40   0   0   0   0 0.000000E+00 160.000    0.000000E+00
    41   0   0   0   0 0.000000E+00 180.000    0.000000E+00
    42   0   0   0   0 0.000000E+00 200.000    0.000000E+00
    43   0   0   0   0 23.3400     200.000    0.000000E+00
```

44	0	0	0	0	23.3400	180.000	0.000000E+00
45	0	0	0	0	23.3400	160.000	0.000000E+00
46	0	0	0	0	23.3400	140.000	0.000000E+00
47	0	0	0	0	23.3400	120.000	0.000000E+00
48	0	0	0	0	23.3400	100.000	0.000000E+00
49	0	0	0	0	23.3400	80.0000	0.000000E+00
50	0	0	0	0	23.3400	60.0000	0.000000E+00
51	0	0	0	0	23.3400	40.0000	0.000000E+00
52	0	0	0	0	23.3400	20.0000	0.000000E+00
53	0	0	0	0	46.6800	200.000	0.000000E+00
54	0	0	0	0	46.6800	180.000	0.000000E+00
55	0	0	0	0	46.6800	160.000	0.000000E+00
56	0	0	0	0	46.6800	140.000	0.000000E+00
57	0	0	0	0	46.6800	120.000	0.000000E+00
58	0	0	0	0	46.6800	100.000	0.000000E+00
59	0	0	0	0	46.6800	80.0000	0.000000E+00
60	0	0	0	0	46.6800	60.0000	0.000000E+00
61	0	0	0	0	46.6800	40.0000	0.000000E+00
62	0	0	0	0	46.6800	20.0000	0.000000E+00
63	0	0	0	0	70.0200	200.000	0.000000E+00
64	0	0	0	0	70.0200	180.000	0.000000E+00
65	0	0	0	0	70.0200	160.000	0.000000E+00
66	0	0	0	0	70.0200	140.000	0.000000E+00
67	0	0	0	0	70.0200	120.000	0.000000E+00
68	0	0	0	0	70.0200	100.000	0.000000E+00
69	0	0	0	0	70.0200	80.0000	0.000000E+00
70	0	0	0	0	70.0200	60.0000	0.000000E+00
71	0	0	0	0	70.0200	40.0000	0.000000E+00
72	0	0	0	0	70.0200	20.0000	0.000000E+00
73	0	0	0	0	93.3600	200.000	0.000000E+00
74	0	0	0	0	93.3600	180.000	0.000000E+00
75	0	0	0	0	93.3600	160.000	0.000000E+00
76	0	0	0	0	93.3600	140.000	0.000000E+00
77	0	0	0	0	93.3600	120.000	0.000000E+00
78	0	0	0	0	93.3600	100.000	0.000000E+00
79	0	0	0	0	93.3600	80.0000	0.000000E+00
80	0	0	0	0	93.3600	60.0000	0.000000E+00
81	0	0	0	0	93.3600	40.0000	0.000000E+00
82	0	0	0	0	93.3600	20.0000	0.000000E+00
83	0	0	0	0	116.700	200.000	0.000000E+00
84	0	0	0	0	116.700	180.000	0.000000E+00
85	0	0	0	0	116.700	160.000	0.000000E+00
86	0	0	0	0	116.700	140.000	0.000000E+00
87	0	0	0	0	116.700	120.000	0.000000E+00
88	0	0	0	0	116.700	100.000	0.000000E+00
89	0	0	0	0	116.700	80.0000	0.000000E+00
90	0	0	0	0	116.700	60.0000	0.000000E+00
91	0	0	0	0	116.700	40.0000	0.000000E+00
92	0	0	0	0	116.700	20.0000	0.000000E+00
93	0	0	0	0	140.040	200.000	0.000000E+00
94	0	0	0	0	140.040	180.000	0.000000E+00
95	0	0	0	0	140.040	160.000	0.000000E+00
96	0	0	0	0	140.040	140.000	0.000000E+00
97	0	0	0	0	140.040	120.000	0.000000E+00
98	0	0	0	0	140.040	100.000	0.000000E+00
99	0	0	0	0	140.040	80.0000	0.000000E+00
100	0	0	0	0	140.040	60.0000	0.000000E+00
101	0	0	0	0	140.040	40.0000	0.000000E+00
102	0	0	0	0	140.040	20.0000	0.000000E+00

103	0	0	0	0	163.380	200.000	0.000000E+00
104	0	0	0	0	163.380	180.000	0.000000E+00
105	0	0	0	0	163.380	160.000	0.000000E+00
106	0	0	0	0	163.380	140.000	0.000000E+00
107	0	0	0	0	163.380	120.000	0.000000E+00
108	0	0	0	0	163.380	100.000	0.000000E+00
109	0	0	0	0	163.380	80.0000	0.000000E+00
110	0	0	0	0	163.380	60.0000	0.000000E+00
111	0	0	0	0	163.380	40.0000	0.000000E+00
112	0	0	0	0	163.380	20.0000	0.000000E+00
113	0	0	0	0	186.720	200.000	0.000000E+00
114	0	0	0	0	186.720	180.000	0.000000E+00
115	0	0	0	0	186.720	160.000	0.000000E+00
116	0	0	0	0	186.720	140.000	0.000000E+00
117	0	0	0	0	186.720	120.000	0.000000E+00
118	0	0	0	0	186.720	100.000	0.000000E+00
119	0	0	0	0	186.720	80.0000	0.000000E+00
120	0	0	0	0	186.720	60.0000	0.000000E+00
121	0	0	0	0	186.720	40.0000	0.000000E+00
122	0	0	0	0	186.720	20.0000	0.000000E+00
123	0	0	0	0	210.060	200.000	0.000000E+00
124	0	0	0	0	210.060	180.000	0.000000E+00
125	0	0	0	0	210.060	160.000	0.000000E+00
126	0	0	0	0	210.060	140.000	0.000000E+00
127	0	0	0	0	210.060	120.000	0.000000E+00
128	0	0	0	0	210.060	100.000	0.000000E+00
129	0	0	0	0	210.060	80.0000	0.000000E+00
130	0	0	0	0	210.060	60.0000	0.000000E+00
131	0	0	0	0	210.060	40.0000	0.000000E+00
132	0	0	0	0	210.060	20.0000	0.000000E+00
133	0	0	0	0	0.000000E+00	210.000	0.000000E+00
134	0	0	0	0	0.000000E+00	190.000	0.000000E+00
135	0	0	0	0	0.000000E+00	170.000	0.000000E+00
136	0	0	0	0	0.000000E+00	150.000	0.000000E+00
137	0	0	0	0	0.000000E+00	130.000	0.000000E+00
138	0	0	0	0	0.000000E+00	110.000	0.000000E+00
139	0	0	0	0	0.000000E+00	90.0000	0.000000E+00
140	0	0	0	0	0.000000E+00	70.0000	0.000000E+00
141	0	0	0	0	0.000000E+00	50.0000	0.000000E+00
142	0	0	0	0	0.000000E+00	30.0000	0.000000E+00
143	0	0	0	0	0.000000E+00	10.0000	0.000000E+00
144	0	0	0	0	233.400	210.000	0.000000E+00
145	0	0	0	0	233.400	190.000	0.000000E+00
146	0	0	0	0	233.400	170.000	0.000000E+00
147	0	0	0	0	233.400	150.000	0.000000E+00
148	0	0	0	0	233.400	130.000	0.000000E+00
149	0	0	0	0	233.400	110.000	0.000000E+00
150	0	0	0	0	233.400	90.0000	0.000000E+00
151	0	0	0	0	233.400	70.0000	0.000000E+00
152	0	0	0	0	233.400	50.0000	0.000000E+00
153	0	0	0	0	233.400	30.0000	0.000000E+00
154	0	0	0	0	233.400	10.0000	0.000000E+00
155	0	0	0	0	11.6700	220.000	0.000000E+00
156	0	0	0	0	35.0100	220.000	0.000000E+00
157	0	0	0	0	58.3500	220.000	0.000000E+00
158	0	0	0	0	81.6900	220.000	0.000000E+00
159	0	0	0	0	105.030	220.000	0.000000E+00
160	0	0	0	0	128.380	220.000	0.000000E+00
161	0	0	0	0	151.710	220.000	0.000000E+00

162	0	0	0	0	175.050	220.000	0.000000E+00
163	0	0	0	0	198.390	220.000	0.000000E+00
164	0	0	0	0	221.730	220.000	0.000000E+00
165	0	0	0	0	11.6700	0.000000E+00	0.000000E+00
166	0	0	0	0	35.0160	0.000000E+00	0.000000E+00
167	0	0	0	0	58.3500	0.000000E+00	0.000000E+00
168	0	0	0	0	81.6900	0.000000E+00	0.000000E+00
169	0	0	0	0	105.030	0.000000E+00	0.000000E+00
170	0	0	0	0	128.380	0.000000E+00	0.000000E+00
171	0	0	0	0	151.710	0.000000E+00	0.000000E+00
172	0	0	0	0	175.050	0.000000E+00	0.000000E+00
173	0	0	0	0	198.390	0.000000E+00	0.000000E+00
174	0	0	0	0	221.730	0.000000E+00	0.000000E+00
175	0	0	0	0	11.6700	210.000	0.000000E+00
176	0	0	0	0	23.3400	210.000	0.000000E+00
177	0	0	0	0	35.0100	210.000	0.000000E+00
178	0	0	0	0	46.6800	210.000	0.000000E+00
179	0	0	0	0	58.3500	210.000	0.000000E+00
180	0	0	0	0	70.0200	210.000	0.000000E+00
181	0	0	0	0	81.6900	210.000	0.000000E+00
182	0	0	0	0	93.3600	210.000	0.000000E+00
183	0	0	0	0	105.030	210.000	0.000000E+00
184	0	0	0	0	116.700	210.000	0.000000E+00
185	0	0	0	0	128.370	210.000	0.000000E+00
186	0	0	0	0	140.040	210.000	0.000000E+00
187	0	0	0	0	151.710	210.000	0.000000E+00
188	0	0	0	0	163.380	210.000	0.000000E+00
189	0	0	0	0	175.050	210.000	0.000000E+00
190	0	0	0	0	186.720	210.000	0.000000E+00
191	0	0	0	0	198.390	210.000	0.000000E+00
192	0	0	0	0	210.060	210.000	0.000000E+00
193	0	0	0	0	221.730	210.000	0.000000E+00
194	0	0	0	0	11.6700	190.000	0.000000E+00
195	0	0	0	0	23.3400	190.000	0.000000E+00
196	0	0	0	0	35.0100	190.000	0.000000E+00
197	0	0	0	0	46.6800	190.000	0.000000E+00
198	0	0	0	0	58.3500	190.000	0.000000E+00
199	0	0	0	0	70.0200	190.000	0.000000E+00
200	0	0	0	0	81.6900	190.000	0.000000E+00
201	0	0	0	0	93.3600	190.000	0.000000E+00
202	0	0	0	0	105.030	190.000	0.000000E+00
203	0	0	0	0	116.700	190.000	0.000000E+00
204	0	0	0	0	128.370	190.000	0.000000E+00
205	0	0	0	0	140.040	190.000	0.000000E+00
206	0	0	0	0	151.710	190.000	0.000000E+00
207	0	0	0	0	163.380	190.000	0.000000E+00
208	0	0	0	0	175.050	190.000	0.000000E+00
209	0	0	0	0	186.720	190.000	0.000000E+00
210	0	0	0	0	198.390	190.000	0.000000E+00
211	0	0	0	0	210.060	190.000	0.000000E+00
212	0	0	0	0	221.730	190.000	0.000000E+00
213	0	0	0	0	11.6700	170.000	0.000000E+00
214	0	0	0	0	23.3400	170.000	0.000000E+00
215	0	0	0	0	35.0100	170.000	0.000000E+00
216	0	0	0	0	46.6800	170.000	0.000000E+00
217	0	0	0	0	58.3500	170.000	0.000000E+00
218	0	0	0	0	70.0200	170.000	0.000000E+00
219	0	0	0	0	81.6900	170.000	0.000000E+00
220	0	0	0	0	93.3600	170.000	0.000000E+00

221	0	0	0	0	105.030	170.000	0.000000E+00
222	0	0	0	0	116.700	170.000	0.000000E+00
223	0	0	0	0	128.370	170.000	0.000000E+00
224	0	0	0	0	140.040	170.000	0.000000E+00
225	0	0	0	0	151.710	170.000	0.000000E+00
226	0	0	0	0	163.380	170.000	0.000000E+00
227	0	0	0	0	175.050	170.000	0.000000E+00
228	0	0	0	0	186.720	170.000	0.000000E+00
229	0	0	0	0	198.390	170.000	0.000000E+00
230	0	0	0	0	210.060	170.000	0.000000E+00
231	0	0	0	0	221.730	170.000	0.000000E+00
232	0	0	0	0	11.6700	150.000	0.000000E+00
233	0	0	0	0	23.3400	150.000	0.000000E+00
234	0	0	0	0	35.0100	150.000	0.000000E+00
235	0	0	0	0	46.6800	150.000	0.000000E+00
236	0	0	0	0	58.3500	150.000	0.000000E+00
237	0	0	0	0	70.0200	150.000	0.000000E+00
238	0	0	0	0	81.6900	150.000	0.000000E+00
239	0	0	0	0	93.3600	150.000	0.000000E+00
240	0	0	0	0	105.030	150.000	0.000000E+00
241	0	0	0	0	116.700	150.000	0.000000E+00
242	0	0	0	0	128.370	150.000	0.000000E+00
243	0	0	0	0	140.040	150.000	0.000000E+00
244	0	0	0	0	151.710	150.000	0.000000E+00
245	0	0	0	0	163.380	150.000	0.000000E+00
246	0	0	0	0	175.050	150.000	0.000000E+00
247	0	0	0	0	186.720	150.000	0.000000E+00
248	0	0	0	0	198.390	150.000	0.000000E+00
249	0	0	0	0	210.060	150.000	0.000000E+00
250	0	0	0	0	221.730	150.000	0.000000E+00
251	0	0	0	0	11.6700	130.000	0.000000E+00
252	0	0	0	0	23.3400	130.000	0.000000E+00
253	0	0	0	0	35.0100	130.000	0.000000E+00
254	0	0	0	0	46.6800	130.000	0.000000E+00
255	0	0	0	0	58.3500	130.000	0.000000E+00
256	0	0	0	0	70.0200	130.000	0.000000E+00
257	0	0	0	0	81.6900	130.000	0.000000E+00
258	0	0	0	0	93.3600	130.000	0.000000E+00
259	0	0	0	0	105.030	130.000	0.000000E+00
260	0	0	0	0	116.700	130.000	0.000000E+00
261	0	0	0	0	128.370	130.000	0.000000E+00
262	0	0	0	0	140.040	130.000	0.000000E+00
263	0	0	0	0	151.710	130.000	0.000000E+00
264	0	0	0	0	163.380	130.000	0.000000E+00
265	0	0	0	0	175.050	130.000	0.000000E+00
266	0	0	0	0	186.720	130.000	0.000000E+00
267	0	0	0	0	198.390	130.000	0.000000E+00
268	0	0	0	0	210.060	130.000	0.000000E+00
269	0	0	0	0	221.730	130.000	0.000000E+00
270	0	0	0	0	11.6700	110.000	0.000000E+00
271	0	0	0	0	23.3400	110.000	0.000000E+00
272	0	0	0	0	35.0100	110.000	0.000000E+00
273	0	0	0	0	46.6800	110.000	0.000000E+00
274	0	0	0	0	58.3500	110.000	0.000000E+00
275	0	0	0	0	70.0200	110.000	0.000000E+00
276	0	0	0	0	81.6900	110.000	0.000000E+00
277	0	0	0	0	93.3600	110.000	0.000000E+00
278	0	0	0	0	105.030	110.000	0.000000E+00
279	0	0	0	0	116.700	110.000	0.000000E+00

280	0	0	0	0	128.370	110.000	0.000000E+00
281	0	0	0	0	140.040	110.000	0.000000E+00
282	0	0	0	0	151.710	110.000	0.000000E+00
283	0	0	0	0	163.380	110.000	0.000000E+00
284	0	0	0	0	175.050	110.000	0.000000E+00
285	0	0	0	0	186.720	110.000	0.000000E+00
286	0	0	0	0	198.390	110.000	0.000000E+00
287	0	0	0	0	210.060	110.000	0.000000E+00
288	0	0	0	0	221.730	110.000	0.000000E+00
289	0	0	0	0	11.6700	90.0000	0.000000E+00
290	0	0	0	0	23.3400	90.0000	0.000000E+00
291	0	0	0	0	35.0100	90.0000	0.000000E+00
292	0	0	0	0	46.6800	90.0000	0.000000E+00
293	0	0	0	0	58.3500	90.0000	0.000000E+00
294	0	0	0	0	70.0200	90.0000	0.000000E+00
295	0	0	0	0	81.6900	90.0000	0.000000E+00
296	0	0	0	0	93.3600	90.0000	0.000000E+00
297	0	0	0	0	105.030	90.0000	0.000000E+00
298	0	0	0	0	116.700	90.0000	0.000000E+00
299	0	0	0	0	128.370	90.0000	0.000000E+00
300	0	0	0	0	140.040	90.0000	0.000000E+00
301	0	0	0	0	151.710	90.0000	0.000000E+00
302	0	0	0	0	163.380	90.0000	0.000000E+00
303	0	0	0	0	175.050	90.0000	0.000000E+00
304	0	0	0	0	186.720	90.0000	0.000000E+00
305	0	0	0	0	198.390	90.0000	0.000000E+00
306	0	0	0	0	210.060	90.0000	0.000000E+00
307	0	0	0	0	221.730	90.0000	0.000000E+00
308	0	0	0	0	11.6700	70.0000	0.000000E+00
309	0	0	0	0	23.3400	70.0000	0.000000E+00
310	0	0	0	0	35.0100	70.0000	0.000000E+00
311	0	0	0	0	46.6800	70.0000	0.000000E+00
312	0	0	0	0	58.3500	70.0000	0.000000E+00
313	0	0	0	0	70.0200	70.0000	0.000000E+00
314	0	0	0	0	81.6900	70.0000	0.000000E+00
315	0	0	0	0	93.3600	70.0000	0.000000E+00
316	0	0	0	0	105.030	70.0000	0.000000E+00
317	0	0	0	0	116.700	70.0000	0.000000E+00
318	0	0	0	0	128.370	70.0000	0.000000E+00
319	0	0	0	0	140.040	70.0000	0.000000E+00
320	0	0	0	0	151.710	70.0000	0.000000E+00
321	0	0	0	0	163.380	70.0000	0.000000E+00
322	0	0	0	0	175.050	70.0000	0.000000E+00
323	0	0	0	0	186.720	70.0000	0.000000E+00
324	0	0	0	0	198.390	70.0000	0.000000E+00
325	0	0	0	0	210.060	70.0000	0.000000E+00
326	0	0	0	0	221.730	70.0000	0.000000E+00
327	0	0	0	0	11.6700	50.0000	0.000000E+00
328	0	0	0	0	23.3400	50.0000	0.000000E+00
329	0	0	0	0	35.0100	50.0000	0.000000E+00
330	0	0	0	0	46.6800	50.0000	0.000000E+00
331	0	0	0	0	58.3500	50.0000	0.000000E+00
332	0	0	0	0	70.0200	50.0000	0.000000E+00
333	0	0	0	0	81.6900	50.0000	0.000000E+00
334	0	0	0	0	93.3600	50.0000	0.000000E+00
335	0	0	0	0	105.030	50.0000	0.000000E+00
336	0	0	0	0	116.700	50.0000	0.000000E+00
337	0	0	0	0	128.370	50.0000	0.000000E+00
338	0	0	0	0	140.040	50.0000	0.000000E+00

339	0	0	0	0	151.710	50.0000	0.000000E+00
340	0	0	0	0	163.380	50.0000	0.000000E+00
341	0	0	0	0	175.050	50.0000	0.000000E+00
342	0	0	0	0	186.720	50.0000	0.000000E+00
343	0	0	0	0	198.390	50.0000	0.000000E+00
344	0	0	0	0	210.060	50.0000	0.000000E+00
345	0	0	0	0	221.730	50.0000	0.000000E+00
346	0	0	0	0	11.6700	30.0000	0.000000E+00
347	0	0	0	0	23.3400	30.0000	0.000000E+00
348	0	0	0	0	35.0100	30.0000	0.000000E+00
349	0	0	0	0	46.6800	30.0000	0.000000E+00
350	0	0	0	0	58.3500	30.0000	0.000000E+00
351	0	0	0	0	70.0200	30.0000	0.000000E+00
352	0	0	0	0	81.6900	30.0000	0.000000E+00
353	0	0	0	0	93.3600	30.0000	0.000000E+00
354	0	0	0	0	105.030	30.0000	0.000000E+00
355	0	0	0	0	116.700	30.0000	0.000000E+00
356	0	0	0	0	128.370	30.0000	0.000000E+00
357	0	0	0	0	140.040	30.0000	0.000000E+00
358	0	0	0	0	151.710	30.0000	0.000000E+00
359	0	0	0	0	163.380	30.0000	0.000000E+00
360	0	0	0	0	175.050	30.0000	0.000000E+00
361	0	0	0	0	186.720	30.0000	0.000000E+00
362	0	0	0	0	198.390	30.0000	0.000000E+00
363	0	0	0	0	210.060	30.0000	0.000000E+00
364	0	0	0	0	221.730	30.0000	0.000000E+00
365	0	0	0	0	11.6700	10.0000	0.000000E+00
366	0	0	0	0	23.3400	10.0000	0.000000E+00
367	0	0	0	0	35.0100	10.0000	0.000000E+00
368	0	0	0	0	46.6800	10.0000	0.000000E+00
369	0	0	0	0	58.3500	10.0000	0.000000E+00
370	0	0	0	0	70.0200	10.0000	0.000000E+00
371	0	0	0	0	81.6900	10.0000	0.000000E+00
372	0	0	0	0	93.3600	10.0000	0.000000E+00
373	0	0	0	0	105.030	10.0000	0.000000E+00
374	0	0	0	0	116.700	10.0000	0.000000E+00
375	0	0	0	0	128.370	10.0000	0.000000E+00
376	0	0	0	0	140.040	10.0000	0.000000E+00
377	0	0	0	0	151.710	10.0000	0.000000E+00
378	0	0	0	0	163.380	10.0000	0.000000E+00
379	0	0	0	0	175.050	10.0000	0.000000E+00
380	0	0	0	0	186.720	10.0000	0.000000E+00
381	0	0	0	0	198.390	10.0000	0.000000E+00
382	0	0	0	0	210.060	10.0000	0.000000E+00
383	0	0	0	0	221.730	10.0000	0.000000E+00
384	0	0	0	0	11.6700	200.000	0.000000E+00
385	0	0	0	0	35.0100	200.000	0.000000E+00
386	0	0	0	0	58.3500	200.000	0.000000E+00
387	0	0	0	0	81.6900	200.000	0.000000E+00
388	0	0	0	0	105.030	200.000	0.000000E+00
389	0	0	0	0	128.370	200.000	0.000000E+00
390	0	0	0	0	151.710	200.000	0.000000E+00
391	0	0	0	0	175.050	200.000	0.000000E+00
392	0	0	0	0	198.390	200.000	0.000000E+00
393	0	0	0	0	221.730	200.000	0.000000E+00
394	0	0	0	0	11.6700	180.000	0.000000E+00
395	0	0	0	0	35.0100	180.000	0.000000E+00
396	0	0	0	0	58.3500	180.000	0.000000E+00
397	0	0	0	0	81.6900	180.000	0.000000E+00

398	0	0	0	0	105.030	180.000	0.000000E+00
399	0	0	0	0	128.370	180.000	0.000000E+00
400	0	0	0	0	151.710	180.000	0.000000E+00
401	0	0	0	0	175.050	180.000	0.000000E+00
402	0	0	0	0	198.390	180.000	0.000000E+00
403	0	0	0	0	221.730	180.000	0.000000E+00
404	0	0	0	0	11.6700	160.000	0.000000E+00
405	0	0	0	0	35.0100	160.000	0.000000E+00
406	0	0	0	0	58.3500	160.000	0.000000E+00
407	0	0	0	0	81.6900	160.000	0.000000E+00
408	0	0	0	0	105.030	160.000	0.000000E+00
409	0	0	0	0	128.370	160.000	0.000000E+00
410	0	0	0	0	151.710	160.000	0.000000E+00
411	0	0	0	0	175.050	160.000	0.000000E+00
412	0	0	0	0	198.390	160.000	0.000000E+00
413	0	0	0	0	221.730	160.000	0.000000E+00
414	0	0	0	0	11.6700	140.000	0.000000E+00
415	0	0	0	0	35.0100	140.000	0.000000E+00
416	0	0	0	0	58.3500	140.000	0.000000E+00
417	0	0	0	0	81.6900	140.000	0.000000E+00
418	0	0	0	0	105.030	140.000	0.000000E+00
419	0	0	0	0	128.370	140.000	0.000000E+00
420	0	0	0	0	151.710	140.000	0.000000E+00
421	0	0	0	0	175.050	140.000	0.000000E+00
422	0	0	0	0	198.390	140.000	0.000000E+00
423	0	0	0	0	221.730	140.000	0.000000E+00
424	0	0	0	0	11.6700	120.000	0.000000E+00
425	0	0	0	0	35.0100	120.000	0.000000E+00
426	0	0	0	0	58.3500	120.000	0.000000E+00
427	0	0	0	0	81.6900	120.000	0.000000E+00
428	0	0	0	0	105.030	120.000	0.000000E+00
429	0	0	0	0	128.370	120.000	0.000000E+00
430	0	0	0	0	151.710	120.000	0.000000E+00
431	0	0	0	0	175.050	120.000	0.000000E+00
432	0	0	0	0	198.390	120.000	0.000000E+00
433	0	0	0	0	221.730	120.000	0.000000E+00
434	0	0	0	0	11.6700	100.000	0.000000E+00
435	0	0	0	0	35.0100	100.000	0.000000E+00
436	0	0	0	0	58.3500	100.000	0.000000E+00
437	0	0	0	0	81.6900	100.000	0.000000E+00
438	0	0	0	0	105.030	100.000	0.000000E+00
439	0	0	0	0	128.370	100.000	0.000000E+00
440	0	0	0	0	151.710	100.000	0.000000E+00
441	0	0	0	0	175.050	100.000	0.000000E+00
442	0	0	0	0	198.390	100.000	0.000000E+00
443	0	0	0	0	221.730	100.000	0.000000E+00
444	0	0	0	0	11.6700	80.0000	0.000000E+00
445	0	0	0	0	35.0100	80.0000	0.000000E+00
446	0	0	0	0	58.3500	80.0000	0.000000E+00
447	0	0	0	0	81.6900	80.0000	0.000000E+00
448	0	0	0	0	105.030	80.0000	0.000000E+00
449	0	0	0	0	128.370	80.0000	0.000000E+00
450	0	0	0	0	151.710	80.0000	0.000000E+00
451	0	0	0	0	175.050	80.0000	0.000000E+00
452	0	0	0	0	198.390	80.0000	0.000000E+00
453	0	0	0	0	221.730	80.0000	0.000000E+00
454	0	0	0	0	11.6700	60.0000	0.000000E+00
455	0	0	0	0	35.0100	60.0000	0.000000E+00
456	0	0	0	0	58.3500	60.0000	0.000000E+00

457	0	0	0	0	81.6900	60.0000	0.000000E+00
458	0	0	0	0	105.030	60.0000	0.000000E+00
459	0	0	0	0	128.370	60.0000	0.000000E+00
460	0	0	0	0	151.710	60.0000	0.000000E+00
461	0	0	0	0	175.050	60.0000	0.000000E+00
462	0	0	0	0	198.390	60.0000	0.000000E+00
463	0	0	0	0	221.730	60.0000	0.000000E+00
464	0	0	0	0	11.6700	40.0000	0.000000E+00
465	0	0	0	0	35.0100	40.0000	0.000000E+00
466	0	0	0	0	58.3500	40.0000	0.000000E+00
467	0	0	0	0	81.6900	40.0000	0.000000E+00
468	0	0	0	0	105.030	40.0000	0.000000E+00
469	0	0	0	0	128.370	40.0000	0.000000E+00
470	0	0	0	0	151.710	40.0000	0.000000E+00
471	0	0	0	0	175.050	40.0000	0.000000E+00
472	0	0	0	0	198.390	40.0000	0.000000E+00
473	0	0	0	0	221.730	40.0000	0.000000E+00
474	0	0	0	0	11.6700	20.0000	0.000000E+00
475	0	0	0	0	35.0100	20.0000	0.000000E+00
476	0	0	0	0	58.3500	20.0000	0.000000E+00
477	0	0	0	0	81.6900	20.0000	0.000000E+00
478	0	0	0	0	105.030	20.0000	0.000000E+00
479	0	0	0	0	128.370	20.0000	0.000000E+00
480	0	0	0	0	151.710	20.0000	0.000000E+00
481	0	0	0	0	175.050	20.0000	0.000000E+00
482	0	0	0	0	198.390	20.0000	0.000000E+00
483	0	0	0	0	221.730	20.0000	0.000000E+00

LIST OF PUBLICATIONS

Lim G.H., Ong J.H. and Penny J.E.T., 1997, "Vibration Analysis of a Printed Circuit Board Structure", *Proceedings of the Asia-Pacific Vibration Conference A-PVC'97*, 9-13 November, Kyongju, Korea, pp. 80-85.

Ong J.H. and *Lim G.H.,* 1999, "Dynamic Finite Element Model Improvement of a PCB Structure", *Journal of Vibration and Control*, Sage Science Press, Vol. 5, No. 1, January, pp. 57-74.

Lim G.H., Ong J.H. and Penny J.E.T., 1999, "Effect of Edge and Internal Point Support of a Printed Circuit Board Under Vibration", *Journal of Electronic Packaging*, Transactions of ASME, Vol. 121, No. 2, pp. 122-126.

Lim G.H. and Ong J.H., 1999, "On the Edge Supports of a Printed Circuit Board Under Vibration", *Proceedings of the Asia-Pacific Vibration Conference* A-PVC'99, 13-15 December, Singapore, pp. 99-105.

Ong J.H. and *Lim G.H.,* 2000, "A Simple Technique for Maximizing the Fundamental Frequency of Vibrating Structures", *Journal of Electronic Packaging*, Transactions of ASME, Accepted for Publication.